

Reconfiguration and Bifurcation in Flight Controls

A Thesis

Submitted to the Faculty

of

Drexel University

by

Suba Thomas

in partial fulfilment of the
requirements for the degree

of

Doctor of Philosophy

November 2004

Drexel University
Office of Research and Graduate Studies
Thesis Approval Form
(For Masters and Doctoral Students)

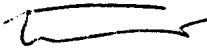
Hagerty Library will bind a copy of this form with each copy of your thesis/dissertation.

This thesis, entitled RECONFIGURATION AND BIFURCATION IN
FLIGHT CONTROLS


and authored by SUBA THOMAS, is hereby accepted and approved.

Signatures:

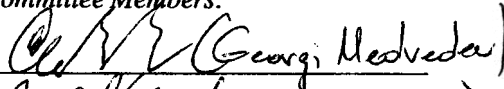
Chairman, Examining Committee



Supervising Professor:



Committee Members:

 (Georgi Medvedev) _____

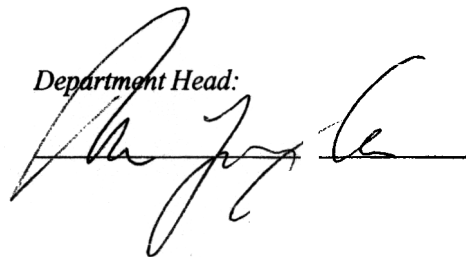
 (BRUCE D. KOTHMANN) _____

 _____

Program Advisor:



Department Head:



© Copyright 2004
Suba Thomas. All Rights Reserved.

Dedications

*To my parents,
for a legacy of faith, hope and love.*

Acknowledgements

*“There’s a divinity that shapes our ends,
rough-hew them how we will,”*

I am grateful to providence for enriching my life through the following people.

A world of thanks to my entire thesis committee. Dr. Chang introduced me to this wonderful research and provided constant support. It was a sheer delight to be working with Dr. Kwatny. I am yet to personally know a person with a more honed blend of serenity, productivity, intellect and knowledge. Dr. Medvedev was very encouraging and supportive. He was always willing to see me and share his very interesting thoughts on bifurcations. Dr. Kothmann was an ever present help in my moments of trouble with flight dynamics. I was amazed (and occasionally overwhelmed) by his extensive knowledge of the subject, keen mind and enthusiasm, that manifested itself in two-page-long emails and daunting questions. I’m better off for it. Also, thanks to Dr. Belta for his quiet support.

It would be remiss to omit the vital influence of my undergraduate advisor Dr. Ray. It was his guidance and nurturing that eventually paved the way for me to major in control systems. I am very grateful to him.

I thank Dr. Lau for being an exceptional and caring graduate advisor. Dr. Desai and Dr. Yousuff were also very kind and supportive during the past four years.

To my cherished friends, Eljen, Eric and Joanne, I owe a debt of gratitude. I thank Edoe for his support, and more relevantly, for proof reading my thesis. Thanks to Steven and Rares for helping me get around the annoying little beetles. I have benefitted greatly from my conversations with Gaurav, Karen, Murat, Carl and Nora. I also thank all my fellow graduate students at the PRISM Lab, Biomechanics Lab, Computer Aided Tissue Engineering Lab and the Hess Lab, for their acquaintance and for all that I learnt from them.

Special thanks to Kathie, Stephanie, Stephanos, Joanne and Jessica.

Thanks also to the wonderful folk at the New Testament Church, E & Allegheny. Heartfelt thanks to Bro. Matthew, Sis. Brenda, late Bro. Gary & Sis. Carolyn, Bro. Briant & Sis. Olga, Bro. Gershom and Sis. Sally, for their prayers, love, and encouragement. Thanks to Mrs. Michelle for her love and uplifting emails. For going out of their way in encouraging and helping me, I thank Mr. & Mrs. Bharadwaj, Mr. & Mrs. Thamburaj and Mr. & Mrs. Zechariah.

I am blessed, humbled and thankful beyond words to have the prayers and encouragement of late Mother Chellamma, Mother Ammini, Mr. & Mrs. Henry, Bro. Paul Mohan, late Pastor Chackochan, Pastor Chacko and Pastor Joshi, from the other side of the globe.

Above all, I thank my family for their unconditional love and support. My sister for her love and care. My father for his big thinking, and for never understanding why things could be impossible. My mother - whose mathematical bent I seem to have inherited - for standing by me in all my decisions and trying times, and for keeping me focused on the wonderful things in life.

Table of Contents

LIST OF TABLES	vii
LIST OF FIGURES	viii
ABSTRACT	xi
1 INTRODUCTION	1
1.1 Motivation.....	1
1.2 Literature survey	4
1.3 Problem formulation.....	8
1.4 Solution strategy.....	9
1.5 Contributions of the thesis	10
1.6 Organization of the thesis	15
2 RECONFIGURED CONTROLLER DESIGN	17
2.1 Regulator design	18
2.2 Estimator design	24
2.2.1 Preliminaries	24
2.2.2 Observers with linear error dynamics	27
2.2.3 Reduction to normal form	28
2.2.4 Computation via Lie transforms.....	31
2.2.5 Simulations.....	36
3 BIFURCATION ANALYSIS OF CONTROL SYSTEMS	40
3.1 Bifurcation analysis in dynamical systems	40
3.2 Control system bifurcations points	41
3.3 Obtaining bifurcation diagrams.....	44
4 THE F-16 AIRCRAFT	48
4.1 The nonlinear six degree of freedom F-16 model	48

4.2	Nominal controller design	52
5	BIFURCATION ANALYSIS OF THE F-16	55
5.1	Level flight bifurcation analysis.....	55
5.2	Coordinated turn bifurcation analysis.....	57
6	BIFURCATION ANALYSIS OF THE RECONFIGURED F-16	62
6.1	Left elevator failure.....	63
6.2	Right elevator failure	65
6.3	Aileron failure.....	67
6.4	Rudder failure.....	68
7	SIMULATION OF THE F-16's RECONFIGURATION	74
7.1	Left elevator failure.....	76
7.2	Right elevator failure	79
7.3	Aileron failure.....	80
7.4	Rudder failure.....	84
8	CONCLUDING REMARKS	89
8.1	Summary	89
8.2	Future research	94
	LIST OF REFERENCES	96
	APPENDIX A: THE F-16's EQUATIONS	102
	APPENDIX B: LIST OF SYMBOLS	105
	VITA	108

List of Tables

4.1	F-16 eigenvalues in the nominal level flight condition	52
5.1	Flying conditions of the nominal system at the bifurcation points associated with level flight.....	56
5.2	Flying conditions of the nominal system at the bifurcation points associated with a coordinated turn of radius 8018.2 ft	60
6.1	Flying conditions of the impaired system at the bifurcation points associated with level flight.....	71
6.2	Flying conditions of the impaired system at bifurcation points (B9 - B17) associated with a coordinated turn of radius 8018.2 ft	72
6.3	Flying conditions of the impaired system at bifurcation points (B18 - B22) associated with a coordinated turn of radius 8018.2 ft	73

List of Figures

2.1	The constant gain observer error response (solid) is compared with the 4 th -order normal form (identity) observer (long-short dashed) and the nonlinear output injection observer (long dashed) for initial conditions: $x_1(0) = 2$, $x_2(0) = .5$, $\hat{x}_1(0) = 0$, $\hat{x}_2(0) = 0$	37
2.2	The plots of Tanh and its approximations	38
2.3	Structure of the fault tolerant controller	39
5.1	Bifurcation diagrams of the nominal system in level flight	56
5.2	Dynamics of the open loop system at bifurcation point LA	57
5.3	Bifurcation diagrams of the nominal system in a coordinated turn of radius 8018.2 ft	60
5.4	Dynamics of the open loop system at bifurcation point TB	61
6.1	Bifurcation diagrams of the impaired system in level flight with a stuck left elevator.....	64
6.2	Bifurcation diagrams of the impaired system in a coordinated turn of radius 8018.2 ft with a stuck left elevator	65
6.3	Bifurcation diagrams of the impaired system in a coordinated turn of radius 8018.2 ft with a stuck right elevator	66
6.4	Bifurcation diagrams of the impaired system in level flight with a stuck aileron	67
6.5	Bifurcation diagrams of the impaired system in a coordinated turn of radius 8018.2 ft with a stuck aileron	68
6.6	Bifurcation diagrams of the impaired system in level flight with a stuck rudder	69
6.7	Bifurcation diagrams of the impaired system in a coordinated turn of radius 8018.2 ft with a stuck rudder.....	70
7.1	Plots of the regulated variables in the event of a left elevator failure in level flight. The left elevator is assumed stuck at -0.01 rad, and the switching time is set as 5 sec.....	77

7.2	Plots of the control inputs in the event of a left elevator failure in level flight. The left elevator is assumed stuck at -0.01 rad, and the switching time is set as 5 sec.....	78
7.3	Plots of the regulated variables in the event of a left elevator failure in a coordinated turn of radius 8018.2 ft. The left elevator is assumed stuck at -0.04 rad, and the switching time is set as 5 sec	78
7.4	Plots of the control inputs in the event of a left elevator failure in a coordinated turn of radius 8018.2 ft. The left elevator is assumed stuck at -0.04 rad, and the switching time is set as 5 sec.....	79
7.5	Plots of the regulated variables in the event of a right elevator failure in level flight. The right elevator is assumed stuck at -0.01 rad, and the switching time is set as 5 sec	81
7.6	Plots of the control inputs in the event of a right elevator failure in level flight. The right elevator is assumed stuck at -0.01 rad, and the switching time is set as 5 sec.....	81
7.7	Plots of the regulated variables in the event of a right elevator failure in a coordinated turn of radius 17598.7 ft. The right elevator is assumed stuck at -0.03 rad, and the switching time is set as 5 sec	82
7.8	Plots of the control inputs in the event of a right elevator failure in a coordinated turn of radius 17598.7 ft. The right elevator is assumed stuck at -0.03 rad, and the switching time is set as 5 sec	82
7.9	Plots of the regulated variables in the event of an aileron failure in level flight. The aileron is assumed stuck at -0.01 rad, and the switching time is set as 3 sec.....	83
7.10	Plots of the control inputs in the event of an aileron failure in level flight. The aileron is assumed stuck at -0.01 rad, and the switching time is set as 3 sec	84
7.11	Plots of the regulated variables in the event of an aileron failure in a coordinated turn of radius 8018.2ft. The aileron is assumed stuck at 0.02 rad, and the switching time is set as 3 sec.....	85
7.12	Plots of the control inputs in the event of an aileron failure in a coordinated turn of radius 8018.2ft. The aileron is assumed stuck at 0.02 rad, and the switching time is set as 3 sec	85
7.13	Plots of the regulated variables in the event of a rudder failure in level flight. The rudder is assumed stuck at 0.1 rad, and the switching time is set as 3 sec.....	86

- 7.14 Plots of the control inputs in the event of a rudder failure in level flight. The rudder is assumed stuck at 0.1 rad, and the switching time is set as 3 sec 87
- 7.15 Plots of the regulated variables in the event of a rudder failure in a coordinated turn of radius 8018.2ft. The rudder is assumed stuck at 0.05 rad, and the switching time is set as 3 sec..... 87
- 7.16 Plots of the control inputs in the event of a rudder failure in a coordinated turn of radius 8018.2ft. The rudder is assumed stuck at 0.05 rad, and the switching time is set as 3 sec 88

Abstract

Reconfiguration and Bifurcation in Flight Controls

Suba Thomas

Prof. Bor-Chin Chang &

Prof. Harry G. Kwatny

Numerous aviation accidents have been caused by stuck control surfaces. In most cases the impaired aircraft has sufficient redundancy to reconfigure the flight. However, the actions that the pilot needs to make could be counter intuitive, demanding and complicated. This is due to the drastic changes in the system's dynamics that are caused by the nonlinearities, the loss of control authority and the disturbance imposed by the stuck surface. The reconfiguration of the flight laws will alleviate the work load on the crew and give them a better leeway to safely land the aircraft. The fault tolerant scheme that is adopted here is a multiple model one with a finite number of reconfigured controllers. Each reconfigured controller consists of a nonlinear output regulator and a constant gain nonlinear observer. The guidelines available for designing the nominal stabilizer are not appropriate for the reconfigured systems.

The ability of the control law to reconfigure the aircraft is limited by saturation of the control surfaces, bifurcation points and stability limits. Identifying and characterizing these limitations is the first step in systematically improving the fault tolerant design. The computational results were obtained using a continuation method based on the Newton-Raphson and Newton-Raphson-Seydel methods. The numerous subtleties in employing these tools, when bifurcation points are clustered together, when many eigenvalues are near the origin or when the eigenvalues nearest the origin are complex, are addressed in this work. The reconfigured controller design for all possible single surface failures and the bifurcation analysis of the nominal and reconfigured systems was carried out on a real aircraft, namely the F-16. This was facilitated by the development of a unique, high fidelity, six degree of freedom, F-16 model.

CHAPTER 1: INTRODUCTION

All systems are prone to failures, in spite of regular maintenance. In flight control systems failures can be catastrophic, and in addition to loss of life, have economic ramifications and erode customer confidence. The failures can be structural, actuator, and/or sensor failures. This work deals with a special class of failures involving stuck actuators. In the event of a failure, the control law is reconfigured to accommodate the changes in the system. A bifurcation analysis is essential, to evaluate the reconfigured system for faults of varying severity and other parameters variations, and to improve the design and accommodate a larger flight envelope.

1.1 Motivation

“An airline pilot’s job involves countless hours of sheer boredom punctuated by moments of sheer terror”, is an old adage in commercial aviation [1]. At such crucial moments, pilots are more often than not at a loss to take the right decision. This can be attributed to a number of reasons. Failure scenarios are not encountered routinely by pilots who may be exposed to such environments only during the training period. Moreover, flight simulators currently used for pilot training are not truly representative of the flight conditions of the failed aircraft. The manufacturers either “hold the last value” or extrapolate to approximate the actual conditions. The dynamics of the crippled aircraft could wander into highly nonlinear regimes, depending on the severity of the fault and the conditions prior to the failure. Thus, the actions that need to be taken may be unfamiliar, counter intuitive, and complicated. Worse still, is the possibility that a failure could destabilize the system. It is desirable to at least stabilize the impaired system, and give the crew a fighting chance to safely land the aircraft.

Statistics reveal that aviation accidents resulting from loss of control account

for a substantial percentage of the total aviation accidents [2]. Prominent aircraft accidents that have been attributed to a stuck actuator caused by mechanical failure are reviewed below:

Boeing 747SR, August 12, 1985

On August 12, 1985 Japan Airlines flight 123, a Boeing 747SR, took off from Haneda, Tokyo and was headed to Osaka. Six minutes after take off, the control tower received a distress signal from JAL123 requesting permission to return to Haneda. Having granted permission, the controller observed that the aircraft was making a gradual turn of 50° to the right instead of a 177° turn. The aircraft was never able to make the maneuver and eventually crashed on the slopes of Mount Osutaka, killing the entire crew and 505 of the 509 passengers. This is the world's worst accident ever involving a single airliner. The cause for the crash was determined as the complete loss of the flying surfaces in the tail, and the control surfaces to a certain extent on the wings, as a result of an explosive decompression of its rear vertical tail plane. [3]

DC-10, July 19, 1989

On July 19, 1989 United Flight 232 was making a right turn in the skies over Iowa, when there was a loud bang from the rear of the aircraft, causing the entire aircraft to shudder. The DC-10 was enroute to Chicago from Denver. Instead of straightening out the aircraft continued to turn right and loose altitude. The inboard ailerons were sticking up and none of the controls seemed to be damaged or moving. Using mostly the port and starboard engine, and with brilliant airmanship the crew directed the aircraft to Sioux City and "managed" to land. Of the 285 passengers and 8 crew members, 185 people survived. It was later found that all the three hydraulics in the empennage was ruined from impact with fragments from the tail engine. The engine's fan disk was eventually recovered and pieced together. Two large fractures were found

in the disk, indicating overstress failure. The 17 year old disk had undergone routine maintenance and six times had been subjected to fluorescent penetration inspections. Investigators concluded that human error was responsible in improperly identifying the fatigued area before the accident. [4]

Boeing 737-300, September 8, 1994

An USAir Boeing 737-300 crashed at Aliquippa, 38km NW of Pittsburgh, Pennsylvania on September 8, 1994 killing all 5 crew members and 127 passengers. The pilot was positioning to land at the Greater Pittsburgh International Airport and was rolling out of a left turn when the aircraft suddenly entered the wake vortex of a Delta Airlines Boeing 727 that preceded it by about 69 seconds (4.2mls). This resulted in the aircraft continuing to roll left. The first officer manually overrode the autopilot without disengaging it by putting in a large right-wheel command at a rate of 150deg/sec. Control was not regained and the aircraft impacted the ground nose down. The National Transportation Safety Board (NTSB) determined the probably cause of the accident to have been a loss of control resulting from the movement of the rudder surface to its blowdown limit. The rudder most likely deflected in a direction opposite to that commanded by the first officer as a result of a jam of the main rudder PCU servo valve secondary slide to the servo valve housing offset from its neutral position and over travel of the primary slide. [5]

MD-83, January 31, 2000

On January 31, 2000 Alaska Airlines AL261, a McDonnell Douglas MD-83, was on flight from Lic Gustavo Diaz Ordaz International Airport, Puerto Vallarta, Mexico, to Seattle-Tacoma International Airport, with an intermediate stop planned at San Francisco International Airport. Near Los Angles the crew reported problems with the stabilizer trim, and mentioned that they were unable to control the pitch. Shortly

afterwards they claimed to have regained control and requested an emergency stop at Los Angeles International Airport. The last radio contact with the crew came as the aircraft passed 17,000 feet at an unusually slow speed of 119 knots. A park ranger, along with the pilots of a nearby aircraft, reported seeing the aircraft plunge into the Pacific Ocean in an inverted flight attitude. The NTSB determined that the in-flight failure of the horizontal stabilizer trim system jackscrew assembly acme nut threads resulted in the loss of the pitch control. The thread failure was caused by excessive wear resulting from Alaska Airlines insufficient lubrication of the jackscrew assembly. [6]

These examples attest that the debilitated aircraft does not crash on inception of the failure. Thanks to the inherent redundancy available in flight control systems, the safety of the impaired aircraft can almost always be maintained. Expecting the crew to capitalize on the redundancy, and ensure the safety of the flight in such circumstances, is a proposition that is left to chance with the odds heavily stacked against them. A systematic design and evaluation of a control system for the impaired system ensures higher survival capabilities and thus lower accident rates.

1.2 Literature survey

Fault tolerant control systems have generated a lot of interest and subsequently extensive research, especially in the context of flight control systems. The recovery strategies can be broadly categorized as passive or active. Passive fault tolerant control schemes are essentially robust control techniques in which structural failures are modelled as uncertainty regions around a nominal model. Although this approach can accommodate any failure within the stability radius, it is usually very conservative, and cannot guarantee that it can handle unanticipated and multiple failures. In the alternative active approach the fault is dealt with explicitly. The active approach is further classified as online and offline. In the online approach, the fault tolerant

control system adapts to the various faults in real time after the occurrence of the failure; while in the offline approach a set of controllers corresponding to various failure scenarios are pre-designed and stored on the in-flight computers, and are engaged on the occurrence of the corresponding failure. The online and offline fault-tolerant controllers are usually referred to as the restructured and reconfigured controllers respectively. It should be noted that this terminology has been used interchangeably. The online approach usually entails substantial computation power and lacks determinism and in some cases stability. A offline approach, on the other hand, is extensive, has rapid availability, guaranteed performance and may demand prodigious memory. Some of the well know fault tolerant schemes [7] are briefly discussed below.

A passive online scheme based on a neural network based adaptive control is investigated in [8] and [9]. In this design the nonlinear system is first feedback linearized, and the failure is cast as an inversion error. The control law is then formulated as the sum of a stabilizing linear compensator, the tracking signal, and an adaptive signal that is determined by the neural network to offset the inversion error. The control scheme was demonstrated on the Tailless Advanced Fighter Aircraft (TAFE) and the X-36. This approach can handle structural failures very well because of the neural network component in the control law, thus allowing for no assumptions to be made about the failure.

The Model Reference Adaptive Control (MRAC) approach [10] is an active online approach that formulates the fault tolerant control problem as a tracking problem, in which certain variables of the impaired system are required to track those from a reference model. The reconfigured law is constructed as a state feedback augmented with the reference signal. An input disturbance is also assumed. The goal is then to match the failed system dynamics with that of the reference model. Two approaches have been proposed for this, namely, indirect and direct. In the indirect approach, the control parameters are computed based on the plant estimates which are constantly

updated. In the direct approach, the control parameters are estimated directly. A reconfigurable scheme embodying the same philosophy is also proposed by Tao et al [11]. The ideas were extended to affine nonlinear systems [12], based on grouping of the healthy actuators. This increases the complexity of the adaptive scheme. The major drawback of these approaches is that they assume that the failed aircraft model can be determined online. This consumes a lot of memory and time, especially for aircrafts, and could compromise the safety of the flight before all the parameters are computed.

In [13], a multiple model, switching and tuning (MMST) scheme is adopted to achieve an offline fault-tolerant scheme. Models of various failure scenarios are envisioned and corresponding fixed or adaptive controllers are designed a priori. They admit that the fixed controller is preferable to an adaptive one. However, because their fixed models can represent only a fixed number of possible environments while there uncountable possible environments, they shy away from using an exclusively fixed model approach (which makes it an off line approach). In the event of a failure, switching is based on cost functions assigned to the various models and the controller corresponding to the closest model is chosen. If an adaptive controller is chosen then it tunes the parameters slowly over time to improve or achieve the desired performance.

In order to circumvent the need to model every failure scenario in the MMST scheme, the Interacting Multiple Model (IMM) scheme is proposed in [14], [15], and [16]. In this approach it is assumed that every possible failure can be modelled as a convex combination of models in a pre-determined model set. The specific combinations of models that make up a failure is determined online. Numerous techniques have been put forward to determine the control law once the failure is identified. The major shortcoming of IMM is that there is no guarantee that a failure can be represented in terms of the models in the model set. Also, there are no guidelines to define the model set.

In the Pseudo Inverse Method (PIM) [17], the feedback gain of the reconfigured controller is computed by equating the closed loop matrices of the nominal and failed systems. This involves computing the pseudo-inverse of the input matrix of the failed plant and hence the name. The major drawback of this method is that there is no guarantee that the system will be stable. Gao and Antsaklis [18] achieved stability by reformulating it as a constraint minimization problem. However, the solution loses its optimality when extended to the MIMO case. Another possible problem with the PIM is that it assumes that the nominal and failed plant matrices are accurately known. In the control mixer approach [19], which is based on the PIM, the control mixer module redistributes the signals in the closed loop systems so that the reconfigured system has the same or optimally approximate function as the nominal system. This method although attractive in terms of the ease in computation and implementation, was based on PIM and has no stability guarantees. Yang et. al. [20] proposed the Robust Control Mixer Module Method in which the stability, performance, and robustness can be considered simultaneously, but the mixer module increases becomes extremely complex due to the dynamic module.

Eigenstructure assignment for impaired aircrafts have been explored in [21] and [22]. The goal has been to match the characteristics of the impaired system to the original system, as much as possible. The biggest hindrance in this approach is that the best possible choice of eigenvalues and eigenvectors for failed aircraft dynamics is not yet understood. Moreover, all proposed designs are linear and based at the original equilibrium condition of the aircraft. In the event of a failure the aircraft dynamics could wander far away from the original conditions rendering the model on which the design is based irrelevant.

The concept of a Propulsion Controlled Aircraft (PCA) was developed at NASA Dryden Flight Research Center [23]. The idea is to use only engine thrust in the event of a complete failure of all control surfaces. Differential and symmetric throttle

inputs are used to control the roll and flight paths respectively. It was also found that it is very difficult to make a safe landing using just thrust control. This approach can be considered as a special case of the MMST scheme in which there is only one failure mode, namely that all the control surfaces are lost. It is also important to note that in all the tests the aircraft is in perfectly trimmed conditions before the reconfigured controller was engaged.

In [24] and [25], the problem of designing the reconfigured problem was treated as a disturbance rejection problem. It was recognized that the jammed actuator not only ceases to be an effective control input but also acts as a persistent disturbance on the impaired system. This is very important in flight control systems where unlike certain other systems, the impaired system dynamics cannot be just recast as the nominal system without the failed control input. The reconfigured controller was designed and simulated for a generic aircraft model, and it was observed that nonlinear terms in the control law provided a larger window of safety.

1.3 Problem formulation

Consider flight control systems of the form

$$\dot{\mathbf{x}} = \mathbf{f}(\mathbf{x}, \mathbf{u}_o)$$

$$\mathbf{y} = \mathbf{h}(\mathbf{x})$$

where $\mathbf{x} \in R^n$ is the set of states, $\mathbf{u}_o \in R^{p+1}$ is the set of control inputs, and $\mathbf{y} \in R^m$ are the measurements. During normal operations, suitable control laws ensure that the desired performance criteria are satisfied. Assume that, suddenly, one of the control surfaces is jammed. The dynamics of the system changes to

$$\dot{\mathbf{x}} = \mathbf{f}(\mathbf{x}, \mathbf{u}, \mu)$$

$$\begin{aligned}\dot{\mu} &= \mathbf{0} \\ \mathbf{y} &= \mathbf{h}(\mathbf{x})\end{aligned}\tag{1.1}$$

where μ is the failed surface and \mathbf{u} are the remaining effective control inputs. The failed surface not only ceases being an effective control input but also acts as persistent disturbances on the system. This renders the original controller - also referred to as the nominal controller - ineffective in sustaining the nominal performance, and can even cause the system to become unstable. We approach the problem by recognizing that in the event of a failure, via a stuck actuator, there is a considerable change in the structure of the system. With one of the control inputs unavailable and with the effect of the incessant disturbance it may not be possible for the performance of the debilitated system to be on par with the nominal system. However, we wish to design a controller that rejects the disturbance and also satisfies certain critical performance requirements. The reconfigured controller must respect the limitations imposed by the control bounds. It is also desirable that the reconfigured controller is valid for all stuck positions and doesn't need a priori information on the actual stuck position.

1.4 Solution strategy

The fault-tolerant flight control system that is adopted here is a multiple model switching scheme [13], [26], with predesigned controllers for all possible failure scenarios. Each controller is designed as a regulator with disturbance rejection capabilities as in [25]. In the event of a fault, it is assumed that a Fault Detection and Isolation (FDI) mechanism [27] identifies and isolates the failure and makes a switch to the appropriate controller. If there is substantial delay in this process the aircraft dynamics could become highly nonlinear. In the case of asymmetric failures the decoupling between the longitudinal and lateral dynamics is rendered untenable. Thus the reconfigured controller design should be based on a model that captures the es-

sential nonlinearities of the system. The reconfigured controller consists of a regulator and an estimator. The regulator achieves regulation of certain critical variables of the impaired aircraft while simultaneously negating the disturbance imposed by the failed control surface. The estimator/observer estimates the stuck actuator position, which is required by the regulator. Consequently, the reconfigured controller does not require the a priori knowledge of the stuck position. In this design strategy, we envision a particular reconfigured controller design to accommodate all failures arising from a specific stuck actuator or group of stuck actuator surfaces, and thus we have a fault tolerant system with a finite number of predesigned controllers and guaranteed performance.

The reconfigured aircraft encounters limitations that are imposed via lack of control authority, bifurcation points and stability boundaries. It is necessary to ascertain and understand these limitations in order to attempt to enlarge the safety envelope. The issues of saturation of control inputs and the occurrence of bifurcation points can be addressed by a feasible choice of regulated variables, that do not compromise flight safety. It would be desirable to steer clear of bifurcations; it may however not be an option in failure scenarios. At bifurcation points the linear system has degeneracies, and special controllers need to be implemented. The stability envelope can be enlarged by a design based on a better understanding of the aircraft dynamics and better reconfigured controller designs.

1.5 Contributions of the thesis

The thesis has four major contributions:

1. A set of mathematical and computer simulation models were developed for the F-16 aircraft. These high fidelity six degree of freedom models are indispensable in the design and evaluation of the nominal and fault-tolerant controllers, and

in carrying out the bifurcation analysis.

2. The bifurcation analyses of the F-16 in level flight and in coordinated turn conditions were carried out from a control systems perspective. The analysis was done for the nominal and various failure scenarios. This served two purposes:
 - a. It resulted in a better understanding of the F-16 in terms of the control issues at bifurcation points and the limitations associated with specific reconfigured control designs.
 - b. It helped in identifying numerical issues and subtleties associated with obtaining bifurcation diagrams. This knowledge would contribute greatly to automating the bifurcation analysis.
3. Normal form nonlinear observers - that estimate the stuck actuator positions - were constructed using a systematic and elegant method of transformation, namely, Lie transformation. This systematic approach is imperative for large systems and is also essential in automating the construction. The evaluation of several small systems using a coded *Mathematica* function showed that the constant gain observer is the most robust.
4. Controller designs:
 - a. A stability augmentation system for the nominal system was designed according to the guidelines in the literature. This is important in order to realistically evaluate the delay that reconfigured designs could accommodate.
 - b. Fault tolerant controllers were designed and evaluated for the various failure scenarios. The stabilizers were based on an LQR design with unit weighting on all the states and effective control variables. It was found

that this design was superior to the stabilizer designs based on the flying qualities of the nominal system.

Research on developing fault tolerant controllers has been ongoing for almost two decades, and yet, with the exception of the work done at NASA Dryden [23], none of the other approaches have been vetted and implemented on real aircrafts. This chasm between theory and practice in the flight safety community can be attributed to the want of the necessary mathematical models to verify and evaluate the proposed solutions. The vast majority of the examples involve other simpler physical systems or highly simplified aircraft models. A prominent contribution of this thesis has been the development of nonlinear six degree of freedom mathematical and computer simulation models for the F-16. This enables the development, verification, and evaluation of demonstrable fault tolerant flight control laws.

The mathematical models and computer simulation models of the nonlinear six degree of freedom F-16 aircraft were developed using the symbolic computing program *Mathematica* [28], supplemented with the modelling and control design package *TSi ProPac* [29]. While there are several simulation models available for the F-16, our process is unique in that we build a symbolic model that can be used for control system design (either linear or nonlinear) as well as a simulation model in the form of optimized C-code that compiles as a SIMULINK S-function. The symbolic model can be manipulated in various ways using standard *Mathematica* or specialized *ProPac* constructions. For example, linearized models can be derived or even parameter dependent linear families of models [30] can be obtained. In addition, the aerodynamic forces and moments, that are used in the model, are obtained using a global nonlinear parametric modelling technique [31], [32], which allows the model to be valid in a large flight envelope. Thus, these high fidelity models are relevant and useful in designing, simulating, validating, and assessing the various controllers and in investigating the limitations of the nominal and reconfigured F-16 vis-à-vis bifurcations, stability, and

available control authority.

The second contribution has been in the area of bifurcation analysis for flight control systems. Bifurcation analysis for dynamical systems is a well established field [33], [34]. There have also been numerous studies of bifurcations in aircraft dynamics [35], [36], [37], [38], [39]. Software packages like AUTO [40] have been developed to automate bifurcation analysis in dynamical systems. However bifurcation analysis for control systems is a nascent research area and is associated with trying to regulate the system's variables. The tools that are needed to carry out the analysis are well developed [41] and have been used in earlier works [42], [43]. In the analysis of the F-16 there were several issues in implementing these techniques because the aircraft had bifurcation points that clustered together and also had eigenvalues of an essential Jacobian that were in close proximity. These issues were ironed out and bifurcation analysis was carried out for the nominal and reconfigured aircrafts in level and coordinated turn conditions. This analysis is essential to assess and improve the reconfigured controller design methodologies.

Bifurcation analysis of the nominal system was carried out to provide a backdrop to the analysis of the reconfigured systems. The nominal F-16 had three bifurcation points each, in the level flight and coordinated turn conditions. The bifurcations are associated with regulation of the aircraft's speed, flight path, and orientation. The speed of the aircraft and the values of the longitudinal variables at which the bifurcations occur do not differ significantly between the two cases. At the bifurcation points in level flight, there is a transmission zero at the origin, the aircraft is uncontrollable and there are dependent inputs. In the bifurcations associated with the coordinated turn, the aircraft loses observability and has dependent outputs, in addition to reasons for the bifurcations in level flight. Most bifurcation points are associated with aircraft stall. Tumbling stall and an emergent spin that transitions to a roll departure was also observed.

A valuable application of the bifurcation analysis is the evaluation of the reconfigured system with respect to variations in the stuck control surface position. This helps in assessing the limitations of specific control formulations. Bifurcation analysis for the different reconfigured systems, namely, stuck, left elevator, right elevator, aileron, and rudder, was carried out in both level and coordinated flight. Bifurcation analysis with velocity as the parameter was also considered. The variables that are regulated are the aircraft's velocity and orientation. The reconfigured controller for the aileron failure is able to handle all stuck positions of the aileron. In the case of the left/right elevator and rudder failure, the reconfigured systems run out of aileron control. A failure of the elevator surface on the aircraft's side that is into the turn, is more difficult to manage than the one on the other side. In all, 22 bifurcation points were identified in the reconfigured systems. At the bifurcation points, there are dependent inputs, transmission zeros, the system becomes uncontrollable, unobservable, and in the majority of the cases have dependent outputs. Some bifurcation points are stable while others are not. The unstable bifurcation points are associated with aircraft stall.

The bifurcation diagrams obtained in this work will serve as a springboard and benchmark for automating bifurcation analysis for control systems. The diagrams were generated in *Mathematica* using Newton-Raphson and the Newton-Raphson-Seydel methods. In the vicinity of bifurcation points, the Newton-Raphson's method fail to converge and we must resort to Newton-Raphson-Seydel's method or a variation. Techniques to speed up the analysis are also outlined in the thesis.

In this work, avenues to improve the design proposed in [25] have been explored. The reconfigured controller in [25] had three components, namely a nonlinear regulator that annulled the disturbance, a linear stabilizer, and a linear observer that estimated the stuck actuator position. A natural idea was whether the design could be improved with a nonlinear observer gain. Normal form nonlinear observers were

constructed using a systematic and elegant method of transformation, namely, Lie transformation [34]. A methodology was developed in which the transformation, which is the solution of a Homological Equation, and the observer gain matrix, which is a series of matrix homogenous polynomials, can be sequentially computed. This approach is vastly more efficient than a brute force approach, especially for large systems. The process was automated as a *Mathematica* function. The automation helped us to quickly evaluate normal form nonlinear observers for numerous small systems, and it was concluded that the first order normal form observer is the most robust. Thus in this thesis the structure proposed in [25] is used in all the reconfigured designs. The observers that were implemented were constant gain observers that were designed using LQR theory.

A stabilizer for the nominal system was designed in accordance with the accepted standards, via eigenstructure assignment. This stabilizer was very robust in terms of variations in speed and turn radius. It was far superior to a stabilizer designed as a LQR regulator with unit weighting on all the states and control inputs; as can be expected because the former is based on well established results. However, when the two approaches were implemented on the impaired systems, it was found that the stabilizer designed using LQR theory with unit weighting on all the states and available control inputs performed much better. This suggested that the nominal system dynamics provide almost no guidelines in effectively stabilizing an impaired system.

1.6 Organization of the thesis

The rest of the dissertation is organized as follows. The theoretical framework in the development of the fault tolerant controller is detailed in Chapter 2. Bifurcation analysis in the context of control systems, the issues associated with obtaining the bifurcation diagrams, and identifying and characterizing bifurcation points and

discussed in Chapter 3. In Chapter 4, the development of the mathematical and symbolic models for the nonlinear six degree of freedom F-16 is presented. A stability augmentation system that was developed using eigenstructure assignment is also included. The Poincaré's equations for the aircraft are given in Appendix A. The bifurcation analysis of the nominal F-16 in level and coordinated turn conditions is explained in Chapter 5. The results of the bifurcation analysis for various failure scenarios of the F-16 in level and coordinated turn conditions are presented in Chapter 6. The reconfigured control laws and the simulation results of the reconfiguration of the F-16 for different failure scenarios and in level and turn flight conditions are shown in Chapter 7. The summary of the thesis and directions for further research are presented in Chapter 8. The list of symbols is tabulated in Appendix B.

CHAPTER 2: RECONFIGURED CONTROLLER DESIGN

In the event of a failure, via a stuck actuator, there is a drastic change in the dynamics of the system. The failed control surface not only becomes ineffective, but also imposes a persistent disturbance on the system. The severity of the failure, and delays in detecting and identifying the failure, could cause the nonlinearities in the dynamics to become relevant. The failure could also destabilize the system. The reconfigured controller is designed as a nonlinear regulator with disturbance rejection properties. Linear regulators based on disturbance estimates has been well developed and is detailed in [44], [45], [46]. The theoretical framework for the nonlinear regulator has been developed in [47] and was employed for reconfigured systems in [25]. The necessary and sufficient conditions for the existence of the control law is that the failed system be linearly controllable and that there are no bifurcation points in flight envelope. This design ensures that the failed system is stable while regulating certain critical variables and annulling the disturbance imposed by the failed actuator.

The regulator needs information on the stuck actuator position. The need for additional hardware can be obviated if the reconfigured controller is based on the original measurements. In addition it is not prudent to depend on information from a sensor that is physically at close proximity to the failed region. Normal form nonlinear observers, that rely on the original measurements and the healthy control inputs, are employed to estimate the stuck position. The normal form observers are constructed using Lie transformations. It was found that the constant gain nonlinear observer is the most robust. The necessary and sufficient condition for the construction of such observers is that the system be zero input linearly observable. The observer can also aid in the fault detection and isolation process.

The regulator and the observer together comprise an unit of the reconfigured controller. Different regulator-observer pairs are designed and stored online for the various failures. This is thus a multiple model scheme with a finite number of recon-

figured laws.

2.1 Regulator design

Consider the system

$$\dot{\mathbf{x}} = \mathbf{f}(\mathbf{x}, \mathbf{u}_o) \quad (2.1)$$

$$\mathbf{y} = \mathbf{h}(\mathbf{x}) \quad (2.2)$$

where $\mathbf{x} \in R^n$ is the set of states, $\mathbf{u}_o \in R^{p+1}$ is the set of control inputs, and $\mathbf{y} \in R^m$ are the measurements. Without any loss of generality we can assume that the equilibrium is at the origin, i.e., $\mathbf{f}(\mathbf{0}, \mathbf{0}) = \mathbf{0}$ and $\mathbf{h}(\mathbf{0}) = \mathbf{0}$. Moreover, we assume that a nominal controller ensures that the performance requirements of the nominal system (2.2) are met. Now consider a scenario when an actuator $\mu \in R$ is stuck. Its dynamics can be expressed as

$$\dot{\mu} = 0 \quad (2.3)$$

The set of control inputs $\mathbf{u} = \mathbf{u}_o \setminus \mu$, are the effective control inputs of the failed plant, and the stuck actuator acts on it as a disturbance with dynamics given by (2.3). Thus the dynamics of the impaired plant is given by

$$\begin{aligned} \dot{\mathbf{x}} &= \mathbf{f}(\mathbf{x}, \mathbf{u}, \mu) \\ \dot{\mu} &= 0 \\ \mathbf{y} &= \mathbf{h}(\mathbf{x}) \end{aligned} \quad (2.4)$$

In formulating the reconfigured controller problem, we acknowledge that it may not be possible to achieve the original performance; however, we still wish to regulate some very critical variables. Thus we can pose the problem as follows: Determine the

control law \mathbf{u} for the plant (2.4) having disturbances μ , so that the variables

$$\mathbf{z} = \mathbf{r}(\mathbf{x}) \quad (2.5)$$

have a prescribed steady state value. Let us assume that the reconfigured controller is given by the feedback law $\mathbf{u} = \mathbf{c}(\mathbf{x}, \mu)$. Thus the reconfigured controller is a *memoryless* system and is provided with the *full information* about the states and stuck actuator positions. The closed loop system is then described by the equations

$$\begin{aligned} \dot{\mathbf{x}} &= \mathbf{f}(\mathbf{x}, \mathbf{c}(\mathbf{x}, \mu), \mu) \\ \dot{\mu} &= 0 \end{aligned} \quad (2.6)$$

It is desirable that the equilibrium $\mathbf{x} = \mathbf{0}$ of

$$\dot{\mathbf{x}} = \mathbf{f}(\mathbf{x}, \mathbf{c}(\mathbf{x}, 0), 0) \quad (2.7)$$

is asymptotically stable in the first approximation. The property of asymptotic stability comes from the linear approximation of (2.7), namely

$$\dot{\mathbf{x}} = (A + BK)\mathbf{x} + (E + BJ)\mu + h.o.t \quad (2.8)$$

where the matrices A , B , K , E and P are defined as

$$A = \frac{\partial \mathbf{f}}{\partial \mathbf{x}}(\mathbf{0}, \mathbf{0}, \mathbf{0}), B = \frac{\partial \mathbf{f}}{\partial \mathbf{u}}(\mathbf{0}, \mathbf{0}, \mathbf{0}), K = \frac{\partial \mathbf{c}}{\partial \mathbf{x}}(\mathbf{0}, \mathbf{0}), E = \frac{\partial \mathbf{f}}{\partial \mu}(\mathbf{0}, \mathbf{0}, \mathbf{0}), P = \frac{\partial \mathbf{c}}{\partial \mu}(\mathbf{0}, \mathbf{0})$$

Thus asymptotic stability is guaranteed if all the eigenvalues of $(A + BK)$ have negative real parts. From pole placement we know that this can be achieved only if the pair (A, B) is stabilizable. Therefore (A, B) stabilizable is a sufficient but not necessary condition for solving the full information regulation problem. In flight

control problems this condition may not be stringent because of the redundant control surfaces on the aircraft.

The linearization of the closed loop system (2.6) can be expressed as

$$\dot{\mathbf{x}}_c = A_c \mathbf{x}_c \quad (2.9)$$

where $\mathbf{x}_c = [\mathbf{x}, \mathbf{u}_f]^T$ and $A_c = \begin{pmatrix} A + BK & E + BP \\ 0 & 0 \end{pmatrix}$. From fundamental linear algebra we know that the domain of the linear mapping A_c can be decomposed into three invariant subspaces, namely, the *stable subspace*, E^s , *unstable subspace*, E^u , and the *center subspace*, E^c , which are the eigenspaces containing the positive, negative and zero eigenvalues respectively. The equilibrium point is called hyperbolic if A_c has no zero eigenvalues, i.e, it has no center subspace. If A_c is hyperbolic, then Hartman-Grobman's theorem [33] establishes topological conjugacy between the nonlinear and linear systems, and many analysis of the nonlinear system can be carried out by considering only the linear system. From (2.9) we can see that the closed loop system has a center subspace which calls for a more detailed analysis using Center Manifold Theory. We start with a couple of definitions.

Definition 1.1 *Let U be a neighborhood of the origin. A C^r submanifold S of U is said to be locally invariant for (2.6) if for each \mathbf{x}_c^0 , there exists $t_1 < t < t_2$ with the property that the integral curve \mathbf{x}_c of (2.6) satisfying $\mathbf{x}_c(\mathbf{0}) = \mathbf{x}_c^0$ is such that $\mathbf{x}_c(t) \in S$ for all $t \in (t_1, t_2)$.*

Definition 1.2 *A manifold S passing through $\mathbf{x}_c = \mathbf{0}$ is said to be a center manifold for (2.6) at $\mathbf{x}_c = \mathbf{0}$, if it is locally invariant and the tangent space to S at $\mathbf{0}$ is exactly E^c .*

Definition 1.3 *Let U be a neighborhood of the origin. We define the local stable and*

unstable manifold of the equilibrium point $\mathbf{x}_c = \mathbf{0}$ as, respectively

$$W_{loc}^s = \{x_c \in U \mid \Psi_c(x_c, t) \rightarrow 0 \text{ as } t \rightarrow \infty \wedge \Psi_c(x_c, t) \in U \forall t \geq 0\}$$

$$W_{loc}^u = \{x_c \in U \mid \Psi_c(x_c, t) \rightarrow 0 \text{ as } t \rightarrow -\infty \wedge \Psi_c(x_c, t) \in U \forall t \leq 0\}$$

where $\Psi_c(x_c, t)$ is the flow generated by (2.6).

Theorem 1.4 (Center Manifold Theorem) Let $\mathbf{f}_c(\mathbf{x}_c)$ be a C^r vector field on R^{n+f} with $\mathbf{f}(\mathbf{0}) = \mathbf{0}$ and $A_c = \frac{\partial \mathbf{f}_c(\mathbf{0})}{\partial \mathbf{x}_c}$. Let the spectrum of A_c be divided into three sets $\sigma_s, \sigma_c, \sigma_u$ with

$$\text{Re } \lambda = \begin{cases} < 0 & \lambda \in \sigma_s \\ = 0 & \lambda \in \sigma_c \\ > 0 & \lambda \in \sigma_u \end{cases}$$

Let the (generalized) eigenspaces of σ_s, σ_c and σ_u be E^s, E^c, E^u , respectively. Then there exists C^r stable and unstable manifolds W^s and W^u tangent to E^s and E^u , respectively, at $\mathbf{x}_c = \mathbf{0}$ and a C^{r-1} center manifold W^c tangent to E^c at $\mathbf{x}_c = \mathbf{0}$. The manifolds W^s, W^c, W^u are all invariant with respect to the flow of $\mathbf{f}_c(\mathbf{x}_c)$. The stable and unstable manifolds are unique, but the center manifold need not be.

From (2.9) we can conclude that (2.6) has a stable manifold and a center manifold. The stable manifold is the hyperplane $\mu = 0$. The center manifold is tangent to $E^c = [\mathbf{0}_{(n \times n)}, 1]^T$ at the origin and its graph can be determined from the following theorem.

Theorem 1.5 There exist a neighborhood $\bar{V} \in R$ of $\mu = \mathbf{0}$ and a mapping $\mathbf{a} : \bar{V} \rightarrow R^n$ such that

$$\bar{S} = \{(\mathbf{x}, \mu) \in R^n \times \bar{V} : \mathbf{x} = \mathbf{a}(\mu)\} \quad (2.10)$$

is a center manifold for (2.6).

If a curve on the center manifold is a solution of (2.6) then we have by first differentiating (2.10)

$$\dot{\mathbf{x}} = \frac{\partial \mathbf{a}(\mu)}{\partial \mu} \dot{\mu} \quad (2.11)$$

and then from (2.6) and (2.10) the following is obtained

$$\mathbf{f}(\mathbf{a}(\mu), \mu, \mathbf{c}(\mathbf{x}, \mu)) = \mathbf{0} \quad (2.12)$$

Lemma 1.6 *Suppose (2.10) is a center manifold for (2.6) at $(\mathbf{0}, 0)$. Let $(\mathbf{x}(t), \mu)$ be a solution of (2.6). There exist a neighborhood U^0 of $(\mathbf{0}, 0)$ and real numbers $M_1 > 0$, $M_2 > 0$ such that, if $(\mathbf{x}(0), \mu(0)) \in U^0$, then*

$$\| \mathbf{x}(t) - \mathbf{a}(\mu(t)) \| \leq M_1 e^{-M_2 t} \| \mathbf{x}(0) - \mathbf{a}(\mu(0)) \| \quad (2.13)$$

This Lemma shows that if we start near the origin the trajectories eventually wind up on the center manifold and they do so exponentially. To achieve the desired regulation the following condition

$$\lim_{t \rightarrow \infty} \mathbf{r}(\mathbf{x}(t)) = \mathbf{0} \quad (2.14)$$

must be satisfied for each initial condition $(\mathbf{x}(0), \mu(0))$.

Lemma 1.7 *Assume that the closed loop system (2.6) is stabilized by some $\mathbf{c}(\mathbf{x}, \mu)$. Then, the condition (2.14) is also satisfied if and only if there exists a mapping $\mathbf{x} = \mathbf{a}(\mu)$, with $\mathbf{a}(0) = \mathbf{0}$, defined in the neighborhood of the origin, satisfying the conditions*

$$\mathbf{0} = \mathbf{f}(\mathbf{a}(\mu), \mu, \mathbf{c}(\mathbf{a}(\mu), \mu)) \quad (2.15)$$

$$\mathbf{0} = \mathbf{r}(\mathbf{a}(\mu)) \quad (2.16)$$

Proof : [47] ■

The first condition guarantees that the solution trajectories are in the center

manifold. The second chooses the trajectory on the center manifold along which the regulation is accomplished.

The necessary and sufficient condition to solve the Full Information Output Regulation Problem is given by the following theorem.

Theorem 1.8 *The Full Information Output Regulation Problem is solvable if and only if the pair (A, B) is stabilizable and there exists mappings $\mathbf{x} = \mathbf{a}(\mu)$ and $\mathbf{u} = \mathbf{b}(\mu)$, with $\mathbf{a}(0) = \mathbf{0}$ and $\mathbf{b}(0) = \mathbf{0}$, both defined in the neighborhood of the origin satisfying the conditions*

$$\begin{aligned}\mathbf{0} &= \mathbf{f}(\mathbf{a}(\mu), \mu, \mathbf{b}(\mu)) \\ \mathbf{0} &= \mathbf{r}(\mathbf{a}(\mu))\end{aligned}\tag{2.17}$$

Proof: [47] ■

A control law defined as

$$\mathbf{u} = \mathbf{b}(\mu) + K(\mathbf{x} - \mathbf{a}(\mu))\tag{2.18}$$

where K is a matrix that places the eigenvalues of $(A+BK)$ in the open left half plane, is a solution to the Full Information Regulator Problem. The number of variables \mathbf{z} that can be regulated is limited by the number of available control surfaces \mathbf{u} . The ability to regulate a specific variable is also dependent on the dynamics of the system. The choice of K dictates the transient response of the system. The mappings $\mathbf{x} = \mathbf{a}(\mu)$ and $\mathbf{u} = \mathbf{b}(\mu)$ can be considered as Taylor series expansions in μ

$$\begin{aligned}\mathbf{a}(\mu) &= \mathbf{a}'(0)\mu + \mathbf{a}''(0)\mu^2 + \mathbf{a}'''(0)\mu^3 + \dots \\ \mathbf{b}(\mu) &= \mathbf{b}'(0)\mu + \mathbf{b}''(0)\mu^2 + \mathbf{b}'''(0)\mu^3 + \dots\end{aligned}\tag{2.19}$$

and the unknown coefficients can be determined by substitution the expansion (2.19)

into (2.17).

Remark 1.9 *In order to ensure that the closed loop system has its equilibrium at $(\mathbf{0}, \mathbf{0})$ the control law approximated using (2.19) must satisfy the relation $\mathbf{c}(\mathbf{0}, \mathbf{0}) = \mathbf{0}$.*

Regulation occurs along the center manifold. If the initial states are on the stable manifold, then motion is along the hyperplane $\mu = 0$. As we move away from the origin, the flows have to wind up on the center manifold.

2.2 Estimator design

Investigation and development of observers with linear error dynamics has been in progress for over two decades. Krener and Isidori [48] and Krener and Respondek [49] considered the problem of synthesis of observers yielding error dynamics that are linear in transformed coordinates. However, the necessary conditions are quite restrictive. Kazantis and Kravaris [50] proposed the construction of normal form with linear dynamics based on Lyapunov's auxiliary theorem. The necessary conditions still pose undesirable restrictions because of the requirement that the eigenvalues of the linearized plant lie in the Poincaré domain. Krener and Xiao [51] extended the observer design method to the Siegel domain. The result can be applied to any real analytic zero-input linearly observable system. A method for constructing an observer with approximately linear error dynamics by polynomial approximation of the solution to the partial differential equation was outlined. For large systems a more systematic approach is needed.

2.2.1 Preliminaries

The impaired plant dynamics are given by

$$\dot{\mathbf{x}}_c = \mathbf{f}_c(\mathbf{x}_c, \mathbf{u})$$

$$\mathbf{y} = \mathbf{h}(\mathbf{x}) \quad (2.20)$$

where $\mathbf{x}_c = [\mathbf{x}, \mu]^T$.

Definition 2.10 *Let U be an open set in R^{n+1} . Two states x_1, x_2 are said to be U -distinguishable if there exists a control $\mathbf{u}(t)$, $t > 0$, whose trajectories from both x_1, x_2 remain in U , such that $\mathbf{y}(\cdot, x_1, \mathbf{u}) \neq \mathbf{y}(\cdot, x_2, \mathbf{u})$. Otherwise they are U -indistinguishable.*

Definition 2.11 *The system is said to be strongly locally observable at $x_0 \in R^{n+1}$ if for every neighborhood U of x_0 , every state in U other than x_0 is U -distinguishable from x_0 . The system is said to be strongly locally observable if it is strongly locally observable at x_0 for every $x_0 \in R^{n+1}$.*

Definition 2.12 *The plant is said to be locally observable at $x_0 \in R^{n+1}$ if there exists a neighborhood W of x_0 such that for every neighborhood U of x_0 contained in W every state in U other than x_0 is U -distinguishable from x_0 . It is said to be locally observable at x_0 if it is locally observable at x_0 for every $x_0 \in R^{n+1}$.*

In flight dynamics most of the states are measured we only have to estimate the stuck positions and thus the conditions for construction of the observer are easily satisfied.

Definition 2.13 *The system (2.20) is said to be exponentially detectable if there exists a function $\gamma(\boldsymbol{\xi}, \mathbf{y})$ defined on a neighborhood of $(\boldsymbol{\xi}, \mathbf{y}) = (\mathbf{0}, \mathbf{0})$ that satisfies:*

1. $\gamma(\mathbf{0}, \mathbf{0}) = \mathbf{0}$
2. $\gamma(\boldsymbol{\xi}, \mathbf{h}(\boldsymbol{\xi})) = \mathbf{f}_c(\boldsymbol{\xi})$
3. $\boldsymbol{\xi} = \mathbf{0}$ is an exponentially stable equilibrium point of $\dot{\boldsymbol{\xi}} = \gamma(\boldsymbol{\xi}, \mathbf{0})$

A system whose linearization is detectable is exponentially detectable. Exponential detectability implies that the system

$$\dot{\hat{\mathbf{x}}}_c = \boldsymbol{\gamma}(\hat{\mathbf{x}}_c, \mathbf{y}) \quad (2.21)$$

is a local observer for (2.20) in the sense that $\|\mathbf{x}_c(t) - \hat{\mathbf{x}}_c(t)\| \rightarrow 0$ as $t \rightarrow \infty$ provided $\mathbf{x}_c(t)$ remains sufficiently close to the origin, [29].

Lemma 2.14 *The system*

$$\dot{\mathbf{z}}_c = \boldsymbol{\eta}(\mathbf{z}_c, \mathbf{y}), \quad \mathbf{z}_c \in R^{n+1} \quad (2.22)$$

$$\hat{\mathbf{x}}_c(t) = \mathbf{T}(\mathbf{z}_c(t)) \quad (2.23)$$

is a full state exponential observer for (2.20) if $\boldsymbol{\eta}(\mathbf{0}, \mathbf{0}) = \mathbf{0}$, $\mathbf{z}_c = \mathbf{0}$ is an exponentially stable equilibrium point of (2.22) with $\mathbf{y} = \mathbf{0}$, and $\mathbf{T} : R^{n+1} \rightarrow R^{n+1}$ is a locally smooth, invertible mapping such that $\mathbf{x}_c(t) = \mathbf{T}(\mathbf{z}_c(t))$ for each $\mathbf{x}_c(\mathbf{0}) = \mathbf{T}(\mathbf{z}_c(\mathbf{0}))$ on a neighborhood of $\mathbf{x}_c = \mathbf{0}$.

Proof: Since

$$\dot{\mathbf{x}}_c = \left[\frac{\partial \mathbf{T}(\mathbf{z}_c)}{\partial \mathbf{z}_c} \boldsymbol{\eta}(\mathbf{z}_c, \mathbf{y}) \right]_{\mathbf{z}_c \rightarrow \mathbf{S}(\mathbf{x}_c), \mathbf{y} \rightarrow \mathbf{h}(\mathbf{x}_c)} = \mathbf{f}_c(\mathbf{x}_c)$$

where $\mathbf{z}_c(t) = \mathbf{S}(\mathbf{x}_c(t))$ is the inverse transformation of $\mathbf{x}_c(t) = \mathbf{T}(\mathbf{z}_c(t))$. It follows that the function

$$\boldsymbol{\gamma}(\mathbf{x}_c, \mathbf{y}) := \left[\frac{\partial \mathbf{T}(\mathbf{z}_c)}{\partial \mathbf{z}_c} \boldsymbol{\eta}(\mathbf{z}_c, \mathbf{y}) \right]_{\mathbf{z}_c \rightarrow \mathbf{S}(\mathbf{x}_c)} \quad (2.24)$$

satisfies the three conditions of Definition 2.13. ■

2.2.2 Observers with linear error dynamics

We seek an exponential observer of the type (2.22), (2.23) with linear dynamics, i.e.,

$$\dot{\mathbf{z}}_c = A_c \mathbf{z}_c - L_0 \mathbf{y}, \quad \mathbf{z}_c \in R^{n+1} \quad (2.25)$$

$$\hat{\mathbf{x}}_c(t) = \mathbf{T}(\mathbf{z}_c(t)) \quad (2.26)$$

Remark 2.15 *If such an observer exists, a simple calculation (see [50]) shows that the error dynamics are linear when expressed in the \mathbf{z}_c -coordinates, specifically*

$$\frac{d}{dt}(\mathbf{S}(\mathbf{x}_c) - \mathbf{S}(\hat{\mathbf{x}}_c)) = A_c(\mathbf{S}(\mathbf{x}_c) - \mathbf{S}(\hat{\mathbf{x}}_c))$$

We attempt to build an observer of the form (2.25) by direct construction. The formal Taylor series of (2.20) at $\mathbf{x}_c = \mathbf{0}$ is

$$\dot{\mathbf{x}}_c = \mathbf{F}\mathbf{x}_c + \mathbf{F}_2(\mathbf{x}_c) + \cdots + \mathbf{F}_r(\mathbf{x}_c) + O(|\mathbf{x}_c|^{r+1})$$

$$\mathbf{y} = \mathbf{H}\mathbf{x}_c + \mathbf{H}_2(\mathbf{x}_c) + \cdots + \mathbf{H}_r(\mathbf{x}_c) + O(|\mathbf{x}_c|^{r+1})$$

$\mathbf{F}_k(\mathbf{x}_c), \mathbf{H}_k(\mathbf{x}_c)$ are vector homogenous polynomials in the elements of \mathbf{x}_c of degree k .

The dynamics of (2.20) can be recast as

$$\dot{\mathbf{x}}_c = \mathbf{f}(\mathbf{x}_c) + \mathbf{L}(\mathbf{x}_c)\mathbf{h}(\mathbf{x}_c) - \mathbf{L}(\mathbf{x}_c)\mathbf{y}$$

where the matrix $L(\mathbf{x}_c)$ is the observer gain that has to be designed. We specify $L(\mathbf{x}_c)$ in the form

$$\mathbf{L}(\mathbf{x}_c) = [I + \mathbf{L}_1(\mathbf{x}_c) + \mathbf{L}_2(\mathbf{x}_c) + \cdots] \mathbf{L}_0$$

where the $\mathbf{L}_k(\mathbf{x}_c)$ are matrix homogenous polynomials of degree k in the elements of \mathbf{x}_c . Express $\mathbf{L}_k(\mathbf{x}_c)$ $k = 1, 2, \dots$ as matrix homogenous polynomials with unknown

coefficients. Using the expansions of f, h and L

$$\dot{\mathbf{x}}_c = A_c \mathbf{x}_c + \sum_{k \geq 1} \frac{\mathbf{f}_k(\mathbf{x}_c)}{k!} - \left[I + \sum_{k \geq 1} \mathbf{L}_k(\mathbf{x}_c) \right] \mathbf{L}_0 \mathbf{y} \quad (2.27)$$

where

$$A_c = F + \mathbf{L}_0 H$$

$$\frac{\mathbf{f}_k(\mathbf{x}_c)}{k!} = \mathbf{F}_{k+1}(\mathbf{x}_c) + \mathbf{L}_0 \mathbf{H}_{k+1}(\mathbf{x}_c) + \cdots + \mathbf{L}_k(\mathbf{x}_c) \mathbf{L}_0 H \mathbf{x}_c$$

The idea is to find a transformation $\mathbf{x}_c = \mathbf{T}(\mathbf{z}_c)$ of the form

$$\mathbf{x}_c = \mathbf{T}_0 \mathbf{z}_c + \mathbf{T}_1(\mathbf{z}_c) + \mathbf{T}_2(\mathbf{z}_c) + \cdots$$

such that nonlinear terms are eliminated from the transformed equations and result in an equation of the form (2.25).

2.2.3 Reduction to normal form

Definition 2.16 *An n -tuple $(\lambda_1, \dots, \lambda_n)$ of eigenvalues belongs to the Poincaré domain if the convex hull of the n points $(\lambda_1, \dots, \lambda_n)$ in the complex plane does not contain zero. An n -tuple of eigenvalues belong to the Siegel domain if zero lies in the convex hull of $(\lambda_1, \dots, \lambda_n)$.*

Definition 2.17 *The n -tuple $(\lambda_1, \dots, \lambda_n)$ of eigenvalues of a given $n \times n$ matrix A is said to be resonant if there exists a relation among the eigenvalues of the form*

$$\lambda_s = m_1 \lambda_1 + \cdots + m_n \lambda_n, \quad s \in \{1, \dots, n\}$$

$$m_k \geq 0, \quad \sum m_k \geq 2$$

Proposition 2.18 (*Poincaré-Siegel Theorem*) *Suppose the eigenvalues of A_c are non-resonant and the vector field $\mathbf{v}(\mathbf{x}_c)$ is given by the formal power series*

$$\mathbf{v}(\mathbf{x}_c) = A_c \mathbf{x}_c + \mathbf{v}_2(\mathbf{x}_c) + \mathbf{v}_3(\mathbf{x}_c) + \dots$$

Then $\mathbf{v}(\mathbf{x}_c)$ is reducible to the linear vector field

$$\mathbf{w}(\mathbf{z}_c) = A \mathbf{z}_c$$

by a near identity, formal power series change of variables. If, in addition, the eigenvalues of A_c belong to the Poincaré domain and the vector field is analytic, then the transformation is analytic (the series converges).

Proof: [52], Chapter 5. ■

Remark 2.19 *Since (F, H) is an observable pair there exists a matrix L_0 (indeed many) such that the matrix $A_c = F + L_0 H$ is asymptotically stable and its eigenvalues are nonresonant. Then, the above theorem can be used to establish the existence of a near identity transformation of (2.27) into (2.25). Furthermore, the analyticity requirement that the eigenvalues of A_c belong to the Poincaré domain can be eliminated if a stronger form of nonresonance is assumed.*

Definition 2.20 *A complex number λ is said to be of type (C, ν) with respect to the spectrum of $F = \sigma(F) = (\alpha_1, \dots, \alpha_n)$ if for any vector $m = (m_1, \dots, m_n)$ of nonnegative numbers, $|m| = \sum m_i > 0$, we have*

$$|\lambda - m \cdot \alpha| \geq \frac{C}{|m|^\nu}$$

where $C > 0, \nu > 0$ are constants.

Proposition 2.21 *Suppose all the eigenvalues of A_c are of type (C, ν) with respect to $\sigma(F)$. Then the transformation of Proposition 2.18 is analytic in some neighborhood of the origin.*

Proof: [52] ■

Proposition 2.22 *For each \mathbf{L}_0 that renders $A_c = F + \mathbf{L}_0 H$ asymptotically stable and nonresonant in the sense that*

$$\lambda_i \neq m_1 \alpha_1 + \cdots + m_{n+1} \alpha_{n+1}$$

$$i = 1, \dots, n+1, m_k \geq 0, \sum m_k \geq 2$$

where λ_i, α_i are respectively, the eigenvalues of A_c and F , there exists a formal power series change of variables $\mathbf{x}_c = \mathbf{T}(\mathbf{z}_c)$ such that

$$\dot{\mathbf{z}}_c = A_c \mathbf{z}_c - \mathbf{L}_0 \mathbf{y} \tag{2.28}$$

$$\hat{\mathbf{x}}_c(t) = \mathbf{T}(\mathbf{z}_c(t)) \tag{2.29}$$

is an exponential observer for (2.20).

Proof: This follows from direct application of the Poincaré-Siegel Theorem. See also [51]. ■

Remark 2.23 *Notice that observability of (F, H) is not required. Detectability is sufficient provided that nonresonance condition is satisfied.*

Remark 2.24 *The observer can be implemented as shown in Equations (2.28) and (2.29) or as an ‘identity’ observer:*

$$\dot{\hat{\mathbf{x}}}_c = \mathbf{f}_c(\hat{\mathbf{x}}_c) + \mathbf{L}(\hat{\mathbf{x}}_c)(\mathbf{y} - \mathbf{h}(\hat{\mathbf{x}}_c)) \tag{2.30}$$

Notice that because $\mathbf{L}(\mathbf{x}_c)$ is generated as a power series, we have a natural notion of observer ‘order’ associated with the degree of the terms retained in the expansion. The zeroth order observer, corresponding to $\mathbf{L}(\mathbf{x}_c) = \mathbf{L}_0$ is the frequently used ‘constant gain’ observer.

Remark 2.25 As suggested in [51] it may be advantageous to seek nonlinear output injection in the transformed system, i.e.,

$$\dot{\mathbf{z}}_c = A\mathbf{z}_c - \boldsymbol{\ell}(\mathbf{y}) \quad (2.31)$$

where $\boldsymbol{\ell}$ is smooth and of the form

$$\boldsymbol{\ell}(\mathbf{y}) = \mathbf{L}_0\mathbf{y} + h.o.t \quad (2.32)$$

This injects additional degrees of freedom (the coefficients of $\boldsymbol{\ell}$) that may be used to enlarge the domain of convergence of the transformation.

2.2.4 Computation via Lie transforms

Scale the state variables \mathbf{x}_c according to $\mathbf{x}_c \rightarrow \varepsilon\mathbf{x}_c$, where ε is a scalar parameter, so that (2.27) becomes

$$\dot{\mathbf{x}}_c = A_c\mathbf{x}_c + \sum_{k \geq 1} \frac{\mathbf{f}_k(\mathbf{x}_c)}{k!} \varepsilon^k - \frac{1}{\varepsilon} \left[I + \sum_{k \geq 1} \mathbf{L}_k(\mathbf{x}_c) \varepsilon^k \right] L_0\mathbf{y} \quad (2.33)$$

Now let $\mathbf{U}(\bar{\mathbf{T}}, \varepsilon)$ be a given ‘generating function’ and suppose the transformation $\mathbf{x}_c = \bar{\mathbf{T}}(\mathbf{z}_c, \varepsilon)$ is defined as the solution of the equation

$$\frac{\partial \bar{\mathbf{T}}}{\partial \varepsilon} = \mathbf{U}(\bar{\mathbf{T}}, \varepsilon), \quad \bar{\mathbf{T}}(\mathbf{z}_c, 0) = \mathbf{z}_c$$

In new coordinates the system equations are

$$\dot{\mathbf{z}}_c = A_c \mathbf{z}_c + \sum_{k \geq 1} \frac{\mathbf{g}_k(\mathbf{z}_c)}{k!} \varepsilon^k - \frac{1}{\varepsilon} \left[I + \sum_{k \geq 1} \mathbf{L}_k(\bar{\mathbf{T}}(\mathbf{z}_c, \varepsilon)) \varepsilon^k \right] \mathbf{L}_0 \mathbf{y}$$

where the components of \mathbf{g}_k are homogeneous polynomials in \mathbf{z}_c of degree $k + 1$.

Proposition 2.26 *Suppose that \mathbf{U} admits series expansion*

$$\mathbf{U}(\bar{\mathbf{T}}, \varepsilon) = \sum_{m=0}^{\infty} \mathbf{U}_m(\mathbf{z}_c) \varepsilon^m / m!$$

Define the sequence

$$f_i^{(m)}(\mathbf{x}_c), \quad i, m = 0, 1, 2, \dots,$$

by the recursive relations

$$\begin{aligned} f_i^m &= f_{i+1}^{(m-1)} - \sum_{0 \leq j \leq i} C_j^i \text{ad}_{f_{i-j}^{(m-1)}} \mathbf{U}_j \\ i &= 0, 1, 2, \dots \quad m = 1, 2, \dots \end{aligned} \tag{2.34}$$

$$f_i^{(0)} = f_i, \quad i = 0, 1, 2, \dots \tag{2.35}$$

where $C_j^i = i! / (j!(i-j)!)$ is the binomial coefficient. Then

$$\mathbf{g}_m = f_0^{(m)}, \quad m = 0, 1, 2, \dots \tag{2.36}$$

Proof: [33], Chapter 12 ■

Remark 2.27 *The computations can be organized according to the following triangle.*

$$\begin{array}{ccccccc}
 & & & & & & f_0^{(0)} \\
 & & & & & & f_1^{(0)} & f_0^{(1)} \\
 & & & & & & f_2^{(0)} & f_1^{(1)} & f_0^{(2)} \\
 & & & & & & f_3^{(0)} & f_2^{(1)} & f_1^{(2)} & f_0^{(3)} \\
 & & & & & & \vdots & \vdots & \vdots & \vdots & \ddots
 \end{array}$$

The i^{th} element of the m^{th} column of this triangle can be computed by knowing only the first $i + 2$ elements of the $(m - 1)^{\text{th}}$ column. The f_i 's are along the first column and the g_i 's are along the diagonal.

Our objective is to determine the generator $\mathbf{U}(\mathbf{x}_c, \varepsilon)$, from which we can obtain the transformation $\bar{\mathbf{T}}(\mathbf{z}_c, \varepsilon)$, that takes

$$\mathbf{f}(\mathbf{x}_c, \varepsilon) = A_c \mathbf{x}_c + \sum_{k \geq 1} \frac{\mathbf{f}_k(\mathbf{x}_c)}{k!} \varepsilon^k \quad (2.37)$$

into

$$g(\mathbf{z}_c, \varepsilon) = \sum_{m=0}^{\infty} g_m(\mathbf{z}_c) \varepsilon^m / m! = A \mathbf{z}_c \quad (2.38)$$

In particular, we require

$$\mathbf{g}_0(\mathbf{z}_c) = A_c \mathbf{z}_c, \quad \mathbf{g}_m(\mathbf{z}_c) = 0, \quad m \geq 1$$

Proposition 2.28 *The generator components \mathbf{U}_i for the transformation that takes the vector field (2.37) into (2.38) are given by*

$$\begin{aligned}
 ad_{A_c \mathbf{x}_c} \mathbf{U}_i &= \mathbf{f}_{i+1} - \sum_{0 \leq j \leq i-1} C_j^i ad_{\mathbf{f}_{i-j}} \mathbf{U}_j \\
 i &= 1, 2, \dots
 \end{aligned} \quad (2.39)$$

$$ad_{A_c \mathbf{x}_c} \mathbf{U}_0 = \mathbf{f}_1 \quad (2.40)$$

Proof: Let us compute the generator components U_j from (2.34) through (2.36), organizing the calculations in accordance with the table.

$$\begin{aligned}
f_0^{(0)} &= A_c \mathbf{x}_c = X(\text{say}) \\
f_1^{(0)} &= \mathbf{f}_1, \quad f_0^{(1)} = f_1^{(0)} - ad_{f_0^{(0)}} U_0 \\
&\Rightarrow ad_X \mathbf{U}_0 = \mathbf{f}_1 \\
f_2^{(0)} &= \mathbf{f}_2, \\
f_1^{(1)} &= f_2^{(0)} - C_0^1 ad_{f_1^{(0)}} \mathbf{U}_0 - C_1^1 ad_{f_0^{(0)}} \mathbf{U}_1, \\
f_0^{(2)} &= f_1^{(1)} = 0 \\
&\Rightarrow ad_X \mathbf{U}_1 = \mathbf{f}_2 - C_0^1 ad_{\mathbf{f}_1} \mathbf{U}_0 \\
f_3^{(0)} &= \mathbf{f}_3, \\
f_2^{(1)} &= f_3^{(0)} - C_0^2 ad_{f_2^{(0)}} \mathbf{U}_0 \\
&\quad - C_1^2 ad_{f_1^{(0)}} \mathbf{U}_1 - C_2^2 ad_{f_0^{(0)}} \mathbf{U}_2, \\
f_1^{(2)} &= f_2^{(1)} - C_0^1 ad_{f_1^{(1)}} \mathbf{U}_0 - C_1^1 ad_{f_0^{(1)}} \mathbf{U}_1, \\
f_0^{(3)} &= f_1^{(2)} = 0 \\
&\Rightarrow ad_X \mathbf{U}_2 = \mathbf{f}_3 - C_0^2 ad_{\mathbf{f}_2} \mathbf{U}_0 - C_1^2 ad_{\mathbf{f}_1} \mathbf{U}_1
\end{aligned}$$

In general, we obtain (2.39). To solve (2.39), (2.40) we need the following Lemma.

Lemma 2.29 *Consider the operator $ad_{A_c \mathbf{x}_c}$ that takes vector fields whose components are homogenous polynomials of degree m into the same linear vector space. If the eigenvalues of A_c are $\{\lambda_1, \dots, \lambda_{n+1}\}$ then the eigenvalues of $ad_{A_c \mathbf{x}_c}$ are given by*

$$\left\{ \sum_{i=1}^{n+1} m_i \lambda_i - \lambda_j \right\}$$

$$\sum_{i=1}^{n+1} m_i = m \quad j = 1, \dots, n+1$$

Moreover, if A_c is diagonal then the operator $ad_{A_c \mathbf{x}_c}$ is also diagonal on the space of homogenous vector-valued polynomials.

Proof: [52], Chapter 12. ■

Remark 2.30 *To solve the homological equation (2.39), (2.40) using the above Lemma we will first have to transform the system so that A_c is diagonal.*

Remark 2.31 L_0 should be chosen so that none of the eigenvalues of $ad_{A_c} \mathbf{x}_c$ are zero to ensure that the Homological equation has a unique solution.

Now that the generator \mathbf{U} is known, we wish to determine the transformation $\bar{\mathbf{T}}(\mathbf{z}_c, \varepsilon)$ that satisfies (9).

Proposition 2.32 *Define the sequence $p_i^{(m)}$, $i, m = 0, 1, 2, \dots$ by the recursive relations*

$$p_i^{(m)} = p_{i+1}^{(m-1)} + \sum_{0 \leq j \leq i} C_j^i L_{p_{i-j}^{(m-1)}} \mathbf{U}_j \quad (2.41)$$

$$i = 0, 1, 2, \dots, \quad m = 1, 2, \dots$$

If $p_i^{(0)} = \mathbf{U}_i$, $i = 0, 1, 2, \dots$, then $\bar{\mathbf{T}}_{m+1} = p_0^{(m)}$.

Proof: [33], Chapter 12. ■

Remark 2.33 *Notice that the computations of $p_0^{(m)}$ as given by (18) proceed along the same triangular structure as $f_0^{(m)}$. See Remark 13.*

$$\begin{array}{ccccccc} p_0^{(0)} & & & & & & \\ p_1^{(0)} & p_0^{(1)} & & & & & \\ p_2^{(0)} & p_1^{(1)} & p_0^{(2)} & & & & \\ p_3^{(0)} & p_2^{(1)} & p_1^{(2)} & p_0^{(3)} & & & \\ \vdots & \vdots & \vdots & \vdots & \ddots & & \end{array}$$

Remark 2.34 *Notice that in view of (8) f_m is a homogenous polynomial of degree $m + 1$. Hence (15) implies that \mathbf{U}_m is a homogenous polynomial of degree $m + 1$, and (18) implies that $\bar{\mathbf{T}}_m$ is a homogenous polynomial of degree $m + 1$.*

The k^{th} order transformation $\mathbf{x}_c = \bar{\mathbf{T}}_k(\mathbf{z}_c) = \mathbf{z}_c + \tilde{\mathbf{T}}_k$, where $\tilde{\mathbf{T}}_k = \mathbf{T}_1/1! + \dots + \mathbf{T}_k/k!$, thus obtained is in terms of the unknown polynomial coefficients of $\mathbf{L}(\mathbf{x}_c)$. The transformation transforms (7) into

$$\left\{ I + \frac{\partial \tilde{\mathbf{T}}_k}{\partial \mathbf{z}_c} \right\} \dot{\mathbf{z}}_c = A_c(\mathbf{z}_c + \tilde{\mathbf{T}}_k) + \sum_{j \geq 1} \frac{\mathbf{f}_j(\mathbf{z}_c + \tilde{\mathbf{T}}_k)}{j!} - \left[I + \sum_{j \geq 1} \mathbf{L}_j(\mathbf{z}_c + \tilde{\mathbf{T}}_k) \right] \mathbf{L}_0 \mathbf{y}$$

Retaining terms of order k we write

$$\begin{aligned} \left\{ I + \frac{\partial \tilde{\mathbf{T}}_k}{\partial \mathbf{z}_c} \right\} (A_c \mathbf{z}_c + \mathbf{L}_0 \mathbf{y}) &= A_c(\mathbf{z}_c + \tilde{\mathbf{T}}_k) + \sum_{j=1}^k \frac{\mathbf{f}_j(\mathbf{z}_c + \tilde{\mathbf{T}}_k)}{j!} - \left[I + \sum_{j=1}^{k-1} \mathbf{L}_j(\mathbf{z}_c + \tilde{\mathbf{T}}_k) \right] \mathbf{L}_0 \mathbf{y} \\ &\quad + O(|\mathbf{z}_c|^{k+1}) \end{aligned}$$

The transformation \mathbf{T}_k is constructed so that $\mathbf{f}_c(\mathbf{x}_c) \rightarrow A_x \mathbf{z}_c + O(|\mathbf{z}_c|^{k+1})$ or, equivalently, $ad_{A_c \mathbf{z}_c} \tilde{\mathbf{T}}_k = \sum_{j=1}^k \mathbf{f}_j/j!$. Thus, the unknown polynomial coefficients of $\mathbf{L}(\mathbf{x}_c)$ are determined from

$$\sum_{j=1}^{k-1} \mathbf{L}_j = \frac{\partial \tilde{\mathbf{T}}_k}{\partial \mathbf{z}_c}$$

Remark 2.35 *The observer gain matrix $\mathbf{L}(\mathbf{x}_c) = \partial \bar{\mathbf{T}} / \partial \mathbf{z}_c \big|_{\mathbf{z}_c \rightarrow \bar{\mathbf{T}}^{-1}(\mathbf{x}_c)}$ is real even if the eigenvalues of A_c are complex.*

2.2.5 Simulations

Numerous low order examples have been solved, including those in [50], [51] and [53] in order to verify the computations. Here is the Van der Pol system from [51].

$$\dot{x}_1 = x_2, \quad \dot{x}_2 = (1 - x_1^2)x_2 - x_1$$

We specify $L_0 = [-2, -4]^T$ which results in the eigenvalues $-0.5 \pm j 1.65831$. The transformation \mathbf{T} and its inverse are

$$\mathbf{T} = \begin{bmatrix} z_1 - 0.101852z_1^3 + 0.017789z_1^5 + 0.0277778z_1^2z_2 - 0.0132345z_1^4z_2 \\ +0.0277778z_1z_2^2 - 0.00547641z_1^3z_2^2 - 0.0185185z_2^3 + 0.0102185z_1^2z_2^3 \\ -0.00366901z_1z_2^4 + 0.00030489z_2^5 \\ -0.231481z_1^3 + 0.0997385z_1^5 + z_2 - 0.277778z_1^2z_2 + 0.0123547z_1^4z_2 \\ +0.222222z_1z_2^2 - 0.0931538z_1^3z_2^2 - 0.0648148z_2^3 + 0.0632284z_1^2z_2^3 \\ -0.0139039z_1z_2^4 + 0.00155164z_2^5 \end{bmatrix}$$

$$\mathbf{S} = \begin{bmatrix} x_1 - 0.101852x_1^3 + 0.00690236x_1^5 - 0.0277778x_1^2x_2 + 0.0214877x_1^4x_2 \\ -0.0277778x_1x_2^2 - 0.000696427x_1^3x_2^2 + 0.0185185x_2^3 + 0.0237321x_1^2x_2^3 \\ -0.0125347x_1x_2^4 + 0.00278153x_2^5 \\ 0.231481x_1^3 + 0.0352924x_1^5 + x_2 + 0.277778x_1^2x_2 - 0.00078059x_1^4x_2 \\ -0.222222x_1x_2^2 - 0.104377x_1^3x_2^2 + 0.0648148x_2^3 + 0.111154x_1^2x_2^3 \\ -0.0416517x_1x_2^4 + 0.00693601x_2^5 \end{bmatrix}$$

Typical responses are shown in Figure 2.1. Our experience indicates that observer

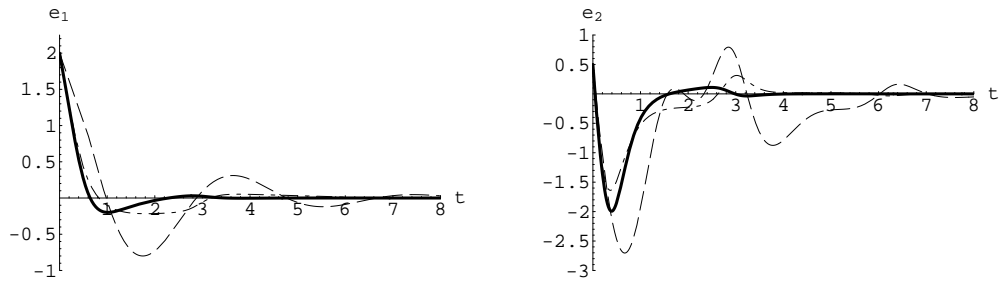


Figure 2.1: The constant gain observer error response (solid) is compared with the 4th-order normal form (identity) observer (long-short dashed) and the nonlinear output injection observer (long dashed) for initial conditions: $x_1(0) = 2$, $x_2(0) = .5$, $\hat{x}_1(0) = 0$, $\hat{x}_2(0) = 0$.

implementation in ‘identity’ form is by far the most reliable. The most surprising

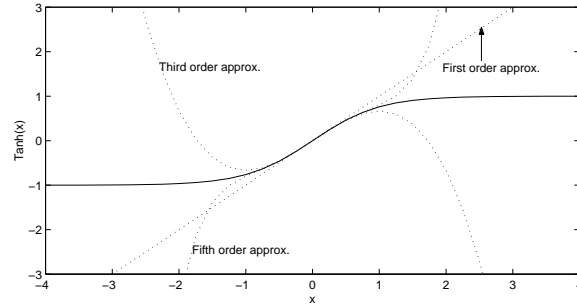


Figure 2.2: The plots of Tanh and its approximations.

result was the effectiveness of the constant gain observer. Any improvement by the higher order observers is marginal at best and often degrades if the series does not converge rapidly.

Fig. 2.2 is that of the tanh function and its series approximations of orders one, three and five. It is seen that at locations far from the origin, the approximations in fact diverge from the original function

$$\text{Tanh}[x] = \frac{e^x + e^{-x}}{e^x - e^{-x}}$$

Thus unless the hyperbolic tangent function is computed as series approximations to the exponential function it will diverge. Similarly it is our feeling that in the construction of the normal form observer the performance of the lower order observers will progressively improve only if the right hand side of (2.20) can be expressed in terms of appropriate functions. A very high order observer will be better than the constant gain observer, but given the performance of the latter we concluded that the computational demands vis-à-vis the performance for higher order observers were unjustifiable.

To summarize, we have a fault tolerant controller with multiple reconfigured controllers. The schematic of one of the reconfigured controllers is shown in Fig. 2.3.

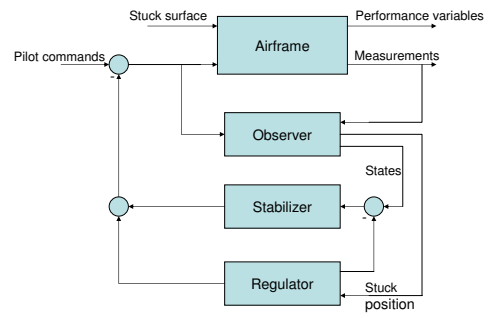


Figure 2.3: Structure of the fault tolerant controller.

CHAPTER 3: BIFURCATION ANALYSIS OF CONTROL SYSTEMS

The reconfigured system can encounter drastic changes in behavior at certain flight conditions and stuck control surface positions. The nominal system can also encounter sudden changes when the aircraft executes high performance maneuvers. In order to design control systems that encompass a large flight envelope and ensure that the demanding performance criteria are satisfied, we must be aware of the limitations of the system and understand the characteristics of the controlled aircraft when it approaches these limiting conditions. The limiting points include bifurcation points of the underlying mathematical model. Although bifurcations have been studied extensively from a dynamical perspective, those arising from a control system perspective have not received much attention. Bifurcations in control systems are associated with regulating certain variables of the system. At bifurcation points, the linearized system always has degeneracies in the zero dynamics. Software tools that analyze bifurcations from a control system perspective are also lacking.

3.1 Bifurcation analysis in dynamical systems

Bifurcation analysis of dynamical systems is a well established field, and consequently, powerful software tools like AUTO [40] have been developed to analyze bifurcations from a dynamical standpoint. Bifurcations in dynamical systems are associated with qualitative changes in the solutions of the equilibrium equations. In the analysis, the number of equilibrium equations is the same as number of variables. Control systems, which are essentially dynamical systems, have also been analyzed in a dynamical framework, with the goal of understanding nonlinear phenomena.

Nonlinear phenomena in aircraft, like stall, wing rock, and spin have been studied from a dynamical perspective. An investigation of the high angle of attack behavior of the same aircraft analyzed in this work, was conducted on the Langley differential

maneuvering simulator [54]. Various maneuvers were initiated to investigate issues like controllability and departure susceptibility. A pioneering work in the study of nonlinear phenomena by a continuation approach based on the aircraft's mathematical model is [35]. The authors were able to identify trim conditions corresponding to the onset of spin and wing rock. Further examples along this line of research can be found in [36] and [37]. The bifurcation analysis of the controller augmented aircraft was considered in [38] and [39]. The ultimate goal of all the above research is to design control systems that circumvent or alleviate the undesirable nonlinear phenomena.

As the bifurcation analysis of the mathematical models are carried out from a purely dynamical system perspective, the bifurcation parameters correspond to control surfaces positions. This analysis, may not correspond to what the aircraft encounters in practice and does not reveal control degeneracies that accompany the bifurcation. It will also be instructive to evaluate the impaired aircraft dynamics, with the stuck positions as the bifurcation parameter.

3.2 Control system bifurcations points

Consider a parameter dependent, nonlinear control system given by

$$\begin{aligned}
 \dot{\mathbf{x}} &= \mathbf{f}(\mathbf{x}, \mathbf{u}, \mu) \\
 \mathbf{y} &= \mathbf{h}(\mathbf{x}, \mu) \\
 \mathbf{z} &= \mathbf{r}(\mathbf{x}, \mu)
 \end{aligned} \tag{3.1}$$

where $\mathbf{x} \in R^n$ are the states, $\mathbf{u} \in R^p$ are the control inputs, $\mathbf{y} \in R^m$ are the measurements, $\mathbf{z} \in R^r$ are the regulated variables, and $\mu \in R$ is any parameter. The parameter could be a physical variables like the weight of the aircraft or the center of gravity location; or a regulated variable like velocity, flight path angle, altitude or roll angle; or a stuck control surface. This is a slight abuse of the notation, as μ is

not limited to denote the failed actuator. Equation (3.1) can represent either an open loop or closed loop system.

A triple $(\mathbf{x}^*, \mathbf{u}^*, \mu^*)$ is an *equilibrium* point of (3.1) if

$$\boldsymbol{\chi}(\mathbf{x}^*, \mathbf{u}^*, \mu^*) := \begin{pmatrix} \mathbf{f}(\mathbf{x}^*, \mathbf{u}^*, \mu^*) \\ \mathbf{r}(\mathbf{x}^*, \mu^*) \end{pmatrix} = \mathbf{0} \quad (3.2)$$

For an infinitesimally small change in the equilibrium value of the parameter μ from μ^* to $\mu^* + \Delta\mu^*$ the equilibrium point $(\mathbf{x}^*, \mathbf{u}^*, \mu^*)$ changes to $(\mathbf{x}^* + \Delta\mathbf{x}^*, \mathbf{u}^* + \Delta\mathbf{u}^*, \mu^* + \Delta\mu^*)$. Considering a first order Taylor series approximation of (3.2) at the new equilibrium point, we have

$$\begin{aligned} [D_{\mathbf{x}}\boldsymbol{\chi}(\mathbf{x}^*, \mathbf{u}^*, \mu^*) \quad D_{\mathbf{u}}\boldsymbol{\chi}(\mathbf{x}^*, \mathbf{u}^*, \mu^*)] \begin{pmatrix} \Delta\mathbf{x}^* \\ \Delta\mathbf{u}^* \end{pmatrix} \\ + D_{\mu}\boldsymbol{\chi}(\mathbf{x}^*, \mathbf{u}^*, \mu^*)\Delta\mu^* = \mathbf{0} \end{aligned} \quad (3.3)$$

Equation (3.3) can be solved for $\Delta\mathbf{x}^*$ and $\Delta\mathbf{u}^*$ only if $p \geq r$ and the Jacobian J is nonsingular. Since the number of controls can always be reduced we henceforth assume $p = r$. The Jacobian J is given by

$$J = [D_{\mathbf{x}}\boldsymbol{\chi}(\mathbf{x}^*, \mathbf{u}^*, \mu^*) \quad D_{\mathbf{u}}\boldsymbol{\chi}(\mathbf{x}^*, \mathbf{u}^*, \mu^*)] \quad (3.4)$$

Points where J is nonsingular are called *regular* points. A formal definition is given below.

Definition 2.36 [55] *An equilibrium point $(\mathbf{x}^*, \mathbf{u}^*, \mu^*)$ is regular if there is a neighborhood of μ^* on which there exist unique, continuously differentiable functions $\bar{\mathbf{x}}(\mu)$, $\bar{\mathbf{u}}(\mu)$ satisfying*

$$\boldsymbol{\chi}(\bar{\mathbf{x}}(\mu), \bar{\mathbf{u}}(\mu), \mu) = \mathbf{0} \quad (3.5)$$

From equations (2.17) it can be seen that at a regular point, the regulator problem

has a solution. If an equilibrium point is not a regular point it is a *static bifurcation point*. At a regular point the linear equivalent of (3.1) is such that

$$\det \begin{pmatrix} A & B \\ C & 0 \end{pmatrix} \neq 0 \Leftrightarrow \text{Im} \begin{pmatrix} A & B \\ C & 0 \end{pmatrix} = R^{n+r} \quad (3.6)$$

where A and B are the state and input matrices respectively and the matrix C is partial derivative of the regulated variables with respect to the states \mathbf{x} , evaluated at the equilibrium point. Then we have the following theorem for a static bifurcation point.

Theorem 2.37 *An equilibrium point $(\mathbf{x}^*, \mathbf{u}^*, \mu^*)$ is a static bifurcation point only if*

$$\text{Im} \begin{pmatrix} A & B \\ C & 0 \end{pmatrix} \neq R^{n+r} \quad (3.7)$$

Consequently we can conclude that at a static bifurcation point $\text{Im}P(\lambda = 0) \neq R^{n+r}$, where $P(\lambda) = \begin{pmatrix} \lambda I - A & B \\ -C & 0 \end{pmatrix}$ is the system matrix. Thus the occurrence of a bifurcation could be due to two possibilities:

1. The presence of invariant zeros at the origin. This is referred to as the *non-degenerate* case. The invariant zeros are comprised of the input decoupling zeros (uncontrollable modes), output decoupling zeros (unobservable modes) and the transmission zeros (remainder of the invariant zeros) [56].
2. The occurrence of dependent controls and/or dependent regulated variables. This is referred to as the *degenerate* case.

The *necessary* conditions for a static bifurcation point can be summarized as follows [43]:

Proposition 2.38 *The equilibrium point $(\mathbf{x}^*, \mathbf{u}^*, \mu^*)$ is a static bifurcation point of (3.1) only if one of the following conditions is true for its linearization:*

1. *there is a transmission zero at the origin,*
2. *there is an uncontrollable mode with zero eigenvalue,*
3. *there is an unobservable mode with zero eigenvalue,*
4. *it has insufficient independent controls,*
5. *it has redundant regulated variables.*

There is a fundamental difference between bifurcation analysis of dynamical systems and control systems. Software packages available for dynamical system bifurcation analysis are not amenable to the analysis of the problems at hand. As seen above, the behavioral aspects at the bifurcation points of control systems involve issues of system controllability, observability, et cetera, which are nonexistent for dynamical system bifurcation analysis. The results in this research have been generated manually using *Mathematica* [28], and will serve as a spring board and benchmark for automating the bifurcation analysis of control systems. The following section outlines the procedure employed to generate the bifurcation diagrams.

3.3 Obtaining bifurcation diagrams

To obtain the bifurcation diagrams, which is essentially a locus of the equilibrium points, we start at a known equilibrium condition and employ the Newton-Raphson (NR) method as a continuation process to the equilibrium equations (3.2). The NR algorithm is given by [57]

$$\begin{pmatrix} \mathbf{x}_{i+1} \\ \mathbf{u}_{i+1} \end{pmatrix} = \begin{pmatrix} \mathbf{x}_i \\ \mathbf{u}_i \end{pmatrix} - J^{-1} \boldsymbol{\chi}(\mathbf{x}_i, \mathbf{u}_i, \mu_{i+1})$$

As expected, it fails to converge as a bifurcation point is approached. To resolve this issue the NR method is replaced by the Newton-Raphson-Seydel (NRS) method

[41] at the point where the former breaks down. The NRS method is essentially the NR method applied to a modified set of equations, namely

$$\boldsymbol{\chi}(\mathbf{x}, \mathbf{u}, \mu) = \mathbf{0} \quad (3.8)$$

$$J \tilde{\mathbf{v}} = \lambda \tilde{\mathbf{v}} \quad (3.9)$$

$$\|\tilde{\mathbf{v}}\| = 1 \quad (3.10)$$

The idea is to evaluate the Jacobian at the point where the NR method fails and compute its eigenvalues and eigenvectors. The initial approximation of λ and $\tilde{\mathbf{v}}$ in (3.9) and (3.10) is chosen as the smallest eigenvalue of J and its corresponding eigenvector, respectively. In equations (3.8) - (3.10), λ is treated as a parameter and is made to approach zero. $\lambda = 0$ corresponds to a bifurcation point. Equations (3.9) and (3.10), with $\lambda = 0$, require that the Jacobian J be singular at the bifurcation point - a necessary condition for bifurcation. Once a bifurcation point is determined, the magnitude of λ must be increased, but with its sign opposite to that with which the bifurcation point was approached, to progress along the bifurcation curve. At points sufficiently far from any bifurcation points, the smaller set of NR equations can replace the NRS equations.

The above approach assumes that the smallest eigenvalue of the Jacobian, evaluated at the point where NR breaks down, is the one that eventually goes to zero at the bifurcation point. A dilemma occurs if there are two bifurcation points close to the origin. Also if the eigenvalues closest to the origin is a complex pair, the path they will take to the real axis so that one of them can eventually wind up at the origin, is not known a priori. In such instances it is advisable to choose an eigenvalue, whose locus is well established even if it is not approaching the origin, and its corresponding eigenvector. Sufficiently close to the bifurcation point, the smallest eigenvalue unambiguously approaches zero and can be used as the bifurcation parameter.

It should also be noted that an eigenvalue of the Jacobian may become small just by virtue of the proximity of the present point to a bifurcation point on another portion of the bifurcation curve. In such instances, allowing λ to converge to zero could result in a solution on the other branch of the curve. Also, in cases where there are two consecutive bifurcation points on the bifurcation curve, the smallest eigenvalue may move away from the origin and approach the origin from the same side, as we progress from the first to the second bifurcation point. In both these cases, as discussed above, it is better to work with an eigenvalue with a well established locus.

It is advisable to employ as the bifurcation parameter an eigenvalue that is far away from any other eigenvalue of the Jacobian matrix. Two specific cases have prompted this conclusion. First, if neighboring branches have eigenvalues that are in close proximity, the solutions obtained from the NRS equations could abruptly jump from one branch to the other. This could result in the curve being retraced or a bifurcation point being overlooked. Secondly, if the eigenvalue that is used as the bifurcation parameter collides with another eigenvalue, continued use of the same eigenvalue can only result in the bifurcation curve being retraced. The two real eigenvalues invariably become complex as the bifurcation curve unfolds.

Although the NRS equations are seemingly more involved than the NR equations, it was observed that the bifurcation curve could be generated faster with the former, with a judicious choice of the bifurcation parameter. The choice of a lone eigenvalue as the bifurcation parameter, enables us to progress much faster along the bifurcation curve than the NR equations, which may fail to converge for very large increments of the actual physical variables. The *Mathematica* function *FindRoot* was used to solve the NR and NRS equations. As a matter of fact, the entire bifurcation curve can be generated with such eigenvalues, and as the curve unfolds the regions where some other eigenvalue changes sign can be noted. These points can then be dealt

with later, and the bifurcation points identified.

An interesting case was encountered when two eigenvalues approached zero along the imaginary axis. The real part of these eigenvalues are not identically zero, but are offset infinitesimally from the origin. This gives a clue as to which eigenvalue approaches the origin, and how it progresses on the real axis as the bifurcation curve evolves. Another way is to observe the sign of the second smallest eigenvalue at the bifurcation point. The sign of this eigenvalue is the same as that of the infinitesimal real part of the complex eigenvalues.

As mentioned earlier, these techniques will aid in the developing software tools to automate the bifurcation analysis for control systems.

CHAPTER 4: THE F-16 AIRCRAFT

This chapter details the development of high fidelity six degree-of-freedom symbolic mathematical and simulation models, and the design of a stability augmentation system for the F-16. The choice of this specific aircraft is due to the extensive resources that already existed in terms of the aircraft's data, nondimensional coefficients and flying qualities. The aerodynamic force and moment coefficients are based on a multivariable polynomial formulation. This allows for the model to accommodate a large flight envelope. The development of the equations of motion is along conventional lines but it is automated in *Mathematica* using *Tsi Propac*. The resulting mathematical model is obtained as Poincaré's equations, from which the state equations are derived. The simulation model is a C-code which is compiled as a SIMULINK S-function. The six degree-of-freedom nonlinear model provides the perfect framework to see the coupling between the longitudinal and the lateral dynamics, to design and evaluate the various recovery designs, and to carry out the bifurcation analysis. A linear controller is designed, using eigenstructure assignment, following guidelines outlined in the literature.

4.1 The nonlinear six degree of freedom F-16 model

The aircraft is considered as a rigid body with a 6-DOF joint at the reference center of gravity location. The body fixed reference frame is located at the reference center of gravity location with the X, Y and Z axes in the forward, right wing and downward direction respectively. The position and orientation of this reference frame with respect to a earth fixed frame comprise the generalized coordinate vector $\mathbf{q} = [\phi, \theta, \psi, x, y, z]^T$, where (x, y, z) gives the position and (ϕ, θ, ψ) are the Euler angles. The joint velocities, comprising of the angular velocities (p, q, r) and the linear velocities (u, v, w) with respect to X, Y and Z respectively, define the joint velocity vector $\mathbf{p} = [p, q, r, u, v, w]^T$.

We considered a model with five control inputs, namely thrust T , left δ_{el} and right δ_{er} elevator, aileron δ_a and rudder δ_r . The terms left and right are designated based on the pilot's perspective. The control surface angles are limited as follows: elevators $|\delta_{er}|, |\delta_{el}| \leq 0.436$ rad (25°), aileron $|\delta_a| \leq 0.375$ rad (21.5°), and rudder $|\delta_r| \leq 0.524$ rad (30°). A positive δ_{el}/δ_{er} corresponds to the elevator surface moving up, while a positive δ_a signifies that the right aileron surface is moving up and the left surface is moving down. The movement of the rudder to the right corresponds to a negative δ_r .

The nondimensional aerodynamic force (C_x, C_y, C_z) and moment (C_l, C_m, C_n) coefficients are expressed as multivariate nonlinear functions and were adapted from [31] (see also [32] for background on polynomial aerodynamic formulation) .

$$\begin{aligned}
C_x &= \frac{1}{2}C_x(\alpha, \delta_{el}) + \frac{1}{2}C_x(\alpha, \delta_{er}) + C_{x_q}(\alpha)\tilde{q} \\
C_y &= C_y(\beta, \delta_a, \delta_r) + C_{y_p}(\alpha)\tilde{p} + C_{y_r}(\alpha)\tilde{r} \\
C_z &= \frac{1}{2}C_z(\alpha, \beta, \delta_{el}) + \frac{1}{2}C_z(\alpha, \beta, \delta_{er}) + C_{z_q}(\alpha)\tilde{q} \\
C_l &= C_l(\alpha, \beta) + C_{l_p}(\alpha)\tilde{p} + C_{l_r}(\alpha)\tilde{r} + C_{l_{\delta_a}}(\alpha, \beta)\delta_a + \frac{l_e}{2}((C_z)_{\delta_{er}=0} - (C_z)_{\delta_{el}=0}) \\
&\quad + C_{l_{\delta_r}}(\alpha, \beta)\delta_r \\
C_m &= \frac{1}{2}C_m(\alpha, \delta_{el}) + \frac{1}{2}C_m(\alpha, \delta_{er}) + C_{m_q}(\alpha)\tilde{q} + C_z(x_{cg_{ref}} - x_{cg}) \\
C_n &= C_n(\alpha, \beta) + C_{n_p}(\alpha)\tilde{p} + C_{n_r}(\alpha)\tilde{r} + C_{n_{\delta_a}}(\alpha, \beta)\delta_a + C_{n_{\delta_r}}(\alpha, \beta)\delta_r \\
&\quad - C_y(x_{cg_{ref}} - x_{cg})\left(\frac{\bar{c}}{b}\right)
\end{aligned}$$

where $\tilde{p} = pb/2V$, $\tilde{q} = q\bar{c}/2V$, $\tilde{r} = rb/2V$.

The following physical data was obtained from [58], [59] and [54]. $I_x = 9496 \text{ slug-ft}^2$, $I_y = 55814 \text{ slug-ft}^2$, $I_z = 63100 \text{ slug-ft}^2$, $I_{xz} = 982 \text{ slug-ft}^2$, $m = 637.14 \text{ slugs}$, $S = 299.992 \text{ ft}^2$, $b = 30 \text{ ft}$, $\bar{c} = 11.32 \text{ ft}$, $l_t = 0 \text{ ft}$, $l_e = 5.56 \text{ ft}$, $l_a = 6.39 \text{ ft}$.

The generalized force vector is $\bar{Q} = [L, M, N, X, Y, Z]^T$ where

$$L = \frac{1}{2}\rho V^2 SC_l, M = \frac{1}{2}\rho V^2 SC_m + l_t T, N = \frac{1}{2}\rho V^2 SC_n$$

$$X = \frac{1}{2}\rho V^2 SC_x + T, Y = \frac{1}{2}\rho V^2 SC_y, Z = \frac{1}{2}\rho V^2 SC_z$$

The model is then generated (see [29], [60] and [61] for more details) in the form of Poincaré's equations [29].

$$\dot{\mathbf{q}} = V(\mathbf{q})\mathbf{p} \quad (4.1)$$

$$M(\mathbf{q})\dot{\mathbf{p}} + C(\mathbf{p}, \mathbf{q})\mathbf{p} + Q(\mathbf{p}, \mathbf{q}, \mathbf{u}_o) = 0 \quad (4.2)$$

The function $Q(\mathbf{p}, \mathbf{q}, \mathbf{u}_o)$, the generalized force vector, contains the aerodynamics and the input vector is $\mathbf{u}_o = [T, \delta_{el}, \delta_{er}, \delta_a, \delta_r]^T$. We adjoin a set of output equations

$$\mathbf{y} = \mathbf{h}(\mathbf{p}, \mathbf{q}) = \begin{pmatrix} V \\ \alpha \\ \beta \\ \mathbf{p} \\ \mathbf{q} \end{pmatrix} \quad (4.3)$$

where $V = \sqrt{u^2 + v^2 + w^2}$ is the velocity, $\alpha = \arctan \frac{w}{u}$ is the angle of attack and $\beta = \arcsin \frac{v}{V}$ is the side-slip angle.

Finally Eqs. (4.1), (4.2) and (4.3) are automatically coded using *ProPac* (refer [29], [60] and [61] for more details). The output is a C file which can be compiled using any standard C compiler. We use Microsoft C to create a dll file that defines the SIMULINK S-function. The compilation is done from the Matlab command window with the command *mex*. We should note that differential equations of the form (4.2) require that the symmetric positive definite matrix $M(\mathbf{q})$ needs to be inverted at each

integration step. This is done efficiently using the Lapac routine *dvsop*. All required supporting subroutines are linked during the compilation process.

It is also possible to invert $M(\mathbf{q})$ symbolically and create the S-function for the resulting state space system. For the rigid airframe with relatively simple inertial dependencies on \mathbf{q} and parameters (like center of mass location), it is not clear which approach is more efficient. We have done both and they work very well. In the alternative approach we first convert from body to wind coordinates, i.e., $u, v, w \mapsto V, \alpha, \beta$, using the transformation

$$\begin{aligned} u &= V \cos \alpha \cos \beta \\ v &= V \sin \beta \\ w &= V \sin \alpha \cos \beta \end{aligned} \tag{4.4}$$

We do this mainly to show the flexibility of our tools. Then, we have the state space system

$$\dot{\mathbf{x}} = \mathbf{f}(\mathbf{x}, \mathbf{u}_o) \tag{4.5}$$

$$\mathbf{y} = \mathbf{h}(\mathbf{x}) \tag{4.6}$$

where $\mathbf{x} = [\phi \ \theta \ \psi \ x \ y \ z \ p \ q \ r \ V \ \alpha \ \beta]^T$. We construct the C file for (4.5) again using *ProPac* and then compile as before. It is also possible to find an equilibrium point for (4.5) and symbolically compute the required Jacobians to assemble a linear model. An equilibrium flight condition is $\phi = 0 \text{ rad}$, $\theta = 0.0872665 \text{ rad}$, $\psi = 0 \text{ rad}$, $p = 0 \text{ rad/s}$, $q = 0 \text{ rad/s}$, $r = 0 \text{ rad/s}$, $u = 349.897 \text{ ft/s}$, $v = 0 \text{ ft/s}$, $w = 30.612 \text{ ft/s}$, $T = 1595.46 \text{ lb}$, $\delta_{el} = -0.0267235 \text{ rad}$, $\delta_{er} = -0.0267235 \text{ rad}$, $\delta_a = 0 \text{ rad}$, $\delta_r = 0 \text{ rad}$, which corresponds to level flight at sea level with $\rho = 0.0023769 \text{ slug/ft}^3$, $g = 32.1302 \text{ ft/s}^2$ and the center of gravity location coinciding

Table 4.1: F-16 eigenvalues in the nominal level flight condition.

Phugoid (P)	$-0.01 \pm 0.0994987i$
Short Period (SP)	$-1.25 \pm 2.165060i$
Dutch-roll (DR)	$-0.50 \pm 1.936490i$
Spiral (S)	-0.01
Roll-subsidence (RS)	-5.00
Heading (H)	0

with the reference gravity position. This condition is denoted by LO in the bifurcation diagrams. The coordinated turn criterion at LO is trivially satisfied.

4.2 Nominal controller design

The aircraft's dynamics are inherently unstable and must be augmented with a stabilizing controller, viz, a Stability Augmentation System (SAS). The primary objective of the controller is to stabilize the system about its operating point, and also to have a degree of robustness to enable turns, and possess acceptable handling qualities. A linear controller, designed about the level flight equilibrium point, given in section 4.1, met all these criteria.

Eigenstructure assignment is used to obtain the SAS. Although this is not the most popular design strategy in flight control design, it has been explored and advocated [62]. The closed loop eigenvalues, listed in Table 4.1, are based on the guidelines provided in [63] and [64]. The multivariable nature of the system gives us some flexibility in choosing the eigenvectors as well [65], and it is desirable to decouple the longitudinal dynamics from the lateral. The examination of the linearization about the level flight condition reveals an inherent decoupling between the longitudinal and lateral dynamics. This was taken advantage of and the design was carried out independently for the longitudinal and lateral dynamics. The longitudinal and lateral states are $\{\theta, q, u, w\}$ and $\{\phi, \psi, p, r, v\}$ respectively. The longitudinal controls are

$\{\delta_{el}, \delta_{er}\}$ and the lateral ones are $\{\delta_a, \delta_r\}$. Alternatively, if the dynamics were not considered separately and the design was carried out along similar lines to achieve a decoupling in the dynamics, it was found that the controller is not robust and the system exhausts the available control authority even for very small turns. This is because the lateral terms in the resulting longitudinal control law demand that the ailerons have to sometimes provide additional rolling moment to counter the moment generated by the elevators.

The Dutch roll motion is a “flat” yawing/sideslipping motion in which rolling is suppressed [66]. Hence we ensure that ϕ is not excited in the Dutch roll mode. In both the spiral and the roll subsidence modes there is negligible sideslip and so in these modes the eigenvector is tailored not to affect v . The heading mode inherently does not influence p and r . Among the states it influences, namely ϕ , ψ and v , the eigenvector is designed so that in this mode only ψ is affected. The eigenvector assignment is summarized below:

$$\begin{array}{l}
 \phi : \\
 \theta : \\
 \psi : \\
 p : \\
 q : \\
 r : \\
 u : \\
 v : \\
 w :
 \end{array}
 \begin{array}{c}
 P \\
 SP \\
 DR \\
 S \\
 RS \\
 H
 \end{array}
 \begin{array}{c}
 \left[\begin{array}{c} 0 \\ \times \\ 0 \\ 0 \\ \times \\ 0 \\ \times \\ 0 \\ \times \end{array} \right] \\
 \left[\begin{array}{c} 0 \\ \times \\ 0 \\ 0 \\ \times \\ 0 \\ \times \\ 0 \\ \times \end{array} \right] \\
 \left[\begin{array}{c} 0 \\ 0 \\ \times \\ \times \\ 0 \\ \times \\ 0 \\ \times \\ 0 \end{array} \right] \\
 \left[\begin{array}{c} \times \\ 0 \\ \times \\ \times \\ 0 \\ \times \\ 0 \\ 0 \\ 0 \end{array} \right] \\
 \left[\begin{array}{c} \times \\ 0 \\ \times \\ \times \\ 0 \\ \times \\ 0 \\ 0 \\ 0 \end{array} \right] \\
 \left[\begin{array}{c} 0 \\ 0 \\ \times \\ \times \\ 0 \\ \times \\ 0 \\ 0 \\ 0 \end{array} \right]
 \end{array}$$

The thrust is left to the pilot. It was found that the closed loop system was very susceptible to becoming unstable if thrust was part of the feedback.

The SAS was implemented as a linear state feedback control law of the form

$$\mathbf{u}_o = K_o \mathbf{x} + \mathbf{v}_o \quad (4.7)$$

or more specifically as

$$T = T_c$$

$$\delta_{el} = \delta_{elc} - 1.3945 + 1.2722q + 0.3398\theta + 5.7944 \times 10^{-4}u + 3.7089 \times 10^{-2}w$$

$$\delta_{er} = \delta_{erc} - 1.3945 + 1.2722q + 0.3398\theta + 5.7944 \times 10^{-4}u + 3.7089 \times 10^{-2}w$$

$$\delta_a = \delta_{ac} + 6.4660p + 0.4058\phi - 3.1594r - 0.03101v$$

$$\delta_r = \delta_{rc} - 4.93p + 2.2151\phi - 25.4988r - 0.1877v$$

where $\mathbf{v}_o = [T_c \ \delta_{elc} \ \delta_{erc} \ \delta_{ac} \ \delta_{rc}]^T$ is the pilot's commanded inputs.

CHAPTER 5: BIFURCATION ANALYSIS OF THE F-16

In this chapter the bifurcation analysis of the nominal system in both level flight conditions and coordinated turn conditions are discussed. The bifurcations occur at low speeds, at which some high performance maneuvers are usually executed. Phenomena such as stall, tumbling and spin-roll departure were observed around bifurcation points. This work provides a basis for a formal understanding of how aircraft depart from controlled flight, it is a prerequisite for the systematic design of recovery strategies, and it will contribute to the design of reconfigurable control of impaired aircraft.

5.1 Level flight bifurcation analysis

In level flight, the body fixed frame has no rotational component with respect to the earth fixed frame and thus the roll ϕ , flight path angle Γ and heading Ψ are all zero. In this work, a positive ϕ and positive Ψ are along the positive X and positive Z_E directions respectively, while a positive Γ is in the negative Y_E direction. The subscript E is used to denote the earth fixed axis. The zero flight path angle specification is equivalent to a constant altitude condition, i.e. $\dot{z} = 0$. The latter condition can be obtained from the kinematics given by (4.1) and yields a much simpler expression than the one obtained from $\Gamma = 0$. The coordinated turn condition is trivially satisfied.

In level flight we are interested in regulating the velocity and orientation of the aircraft, i.e.,

$$\mathbf{r}(\mathbf{x}, \mu) = \{V, \phi, \Gamma, \Psi\}$$

The 4 regulated variables, together with the 9 state equations result in 13 equations. There are 14 variables, namely: $\phi, \theta, \psi, p, q, r, V, \alpha, \beta, T, \delta_{el}, \delta_{er}, \delta_a, \delta_r$. The velocity V is the parameter. In level flight, the variables $\phi, \psi, p, q, r, \beta, \delta_a, \delta_r$ are trivially zero. Also, $\delta_{el} = \delta_{er}$. Although the fold bifurcations can be observed in

Table 5.1: Flying conditions of the nominal system at the bifurcation points associated with level flight.

Bifurcation Point	LA	LB	LC
V (ft/s)	130.6755	132.5639	127.0139
$\alpha = \theta$ (rad)	0.8659	0.9349	0.8429
T (lb)	15064.2843	16387.6502	15254.9235
$\delta_{el} = \delta_{er}$ (rad)	0.0785	0.1621	0.3844
$\delta_{elc} = \delta_{erc}$ (rad)	-2.5619	-2.7626	-2.0736

the bifurcation diagrams of all the relevant non-trivial variables, only the bifurcation diagram of the left elevator is shown in Figure 5.1, due to space constraints. The flying conditions at the bifurcation points are given in Table 5.1.

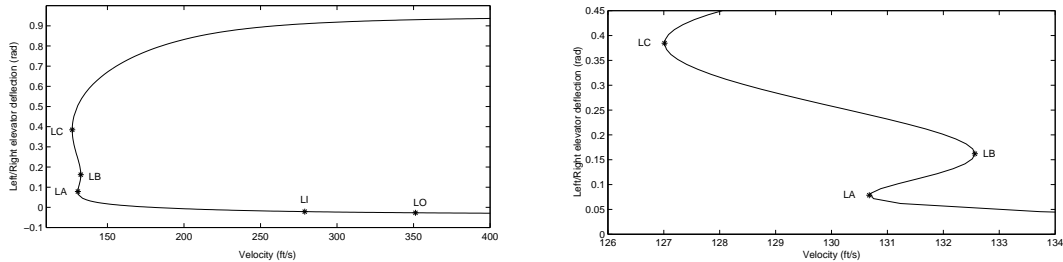


Figure 5.1: Bifurcation diagrams of the nominal system in level flight.

The closed loop bifurcation analysis is basically the same as that for the open loop case. The bifurcation curves of the pilot's commanded inputs, which hold no physical significance, can be determined from equation (4.2) once the open loop analysis is complete. However the analysis of stability and system characteristics at the bifurcation points are different for the open and closed loop cases.

It was found that at all three bifurcation points the open and closed loop systems are unstable. At the bifurcation points for both the open and closed loop case, the linear system has transmission zeros at the origin, is uncontrollable and has dependent inputs.

In level flight, at the bifurcation points, the aircraft usually stalls. This was true

of all the bifurcation points in both the open and closed loop configurations, except at bifurcation points LA and LB in the open loop scenario.

At bifurcation points LA and LB in the open loop configuration, the aircraft experiences the tumbling stall phenomenon. The dynamics are qualitatively similar at the two point and thus only the simulations for LA are shown in Figure 5.2. The aircraft is cartwheeling in addition to the tumbling motion as can be inferred from the plot of the pitch angle θ . Although the Euler angles are based on a 3-2-1 convention and could cause ambiguity when the aircraft is pointed vertically up or down [67], this is not the case here since both the roll angle ϕ and yaw angle ψ are zero.

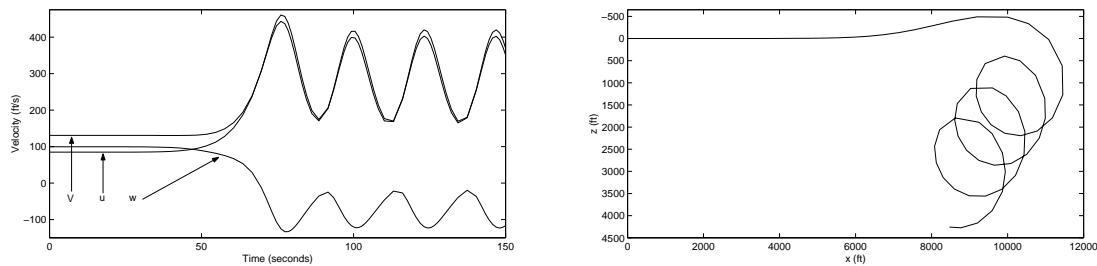


Figure 5.2: Dynamics of the open loop system at bifurcation point LA.

5.2 Coordinated turn bifurcation analysis

This section discusses the bifurcation analysis and characteristics of the F-16 in a *coordinated turn* of constant radius and at constant altitude.

A coordinated turn is one that satisfies the following two conditions [66]:

- C1. The angular velocity of the aircraft is constant and vertical.
- C2. The resultant of the gravity and centrifugal force at the center of gravity lies in the plane of symmetry (the x-z plane) of the aircraft.

Condition C1 implies that the angular velocity of the aircraft in the earth fixed frame is given by $\{0, 0, \omega\}$. This can be transformed into the body axes to yield the following relationships:

$$\begin{aligned} p &= -\omega \sin \theta \\ q &= \omega \cos \theta \sin \phi \\ r &= \omega \cos \theta \cos \phi \end{aligned} \quad (5.1)$$

The second condition C2 implies that the aerodynamic force should have no component in the Y direction . The force equation in the Y direction - from Eqn (4.2) - is

$$m x_{cg} \dot{r} + m \dot{v} + m p x_{cg} q + m r u - m p w - Y - g m \cos \theta \sin \phi = 0 \quad (5.2)$$

If the aircraft is in equilibrium while making the coordinated turn, with the center of gravity location coinciding with the reference location, then Eqn. (5.2) reduces to

$$m r u - m p w - g m \cos \theta \sin \phi = Y$$

For a coordinated turn we must have

$$\mathcal{L} := r u - p w - g \cos \theta \sin \phi = 0 \quad (5.3)$$

which guarantees that $Y = 0$. Alternatively we can also set $Y = 0$. While this is straightforward for the open loop case, where $C_y = 0$ would suffice, in the closed loop case care must be taken to ensure that the aerodynamic force Y also accounts for the feedback.

If we substitute Eqn (5.1) into the kinematic equations, we get $\{\dot{\phi}, \dot{\theta}, \dot{\psi}\} = \{0, 0, \omega\}$. This is because the angular velocity ω is about the vertical axis Z_E . It also explains the absence of ψ in Eqn (5.1). Thus in the present analysis it would suffice

to consider just the 6 dynamic equations in (4.2) with the angular rates p, q, r given by Eqn (5.1).

The constant altitude condition can be obtained, as discussed in Section 5.1, by equating the flight path angle Γ to zero, or from the constant altitude condition.

We obtain an equilibrium condition corresponding to a coordinated turn at level flight by starting at equilibrium point LO and employing the continuation approach. The 6 dynamic equations together with the coordinated turn and constant altitude condition result in 8 equilibrium equations. There are 12 variables, namely, $\phi, \theta, \psi, V, \alpha, \beta, T, \delta_{el}, \delta_{er}, \delta_a, \delta_r, \omega$. We hold $V, \psi, \delta_{el}, \delta_{er}$ fixed and vary ω , until we reached a radius ($R = V/\omega = -V \sin \theta/p$) of 8018.2 ft. The choice of the radius was arbitrary.

The regulated variables are

$$\mathbf{r}(\mathbf{x}, \mu) = \{V, \mathcal{L}, \Gamma, R\}$$

Again, the 6 dynamic equations together with the coordinated turn and constant altitude conditions result in 8 equilibrium equations. There are 10 variables namely: $\phi, \theta, V, \alpha, \beta, T, \delta_{el}, \delta_{er}, \delta_a$ and δ_r . We set $\delta_{el} = \delta_{er}$ and treat V as the parameter.

The bifurcation analysis was carried out for both the open and closed loop cases. As in the level flight scenario, there were three bifurcation points. At all three points the open and closed loop systems were unstable. At all the bifurcation points, the system was uncontrollable, unobservable, had dependent controls, dependent regulated variables and a transmission zero at the origin, for both the open and closed loop. The bifurcation diagram is shown in Figure 5.3.

As in the level flight case the aircraft stall at all bifurcation points in the coordinated turn case except at bifurcation point TB in the open loop scenario. At bifurcation point TB, initially the aircraft appears to enter a spin. However it grad-

Table 5.2: Flying conditions of the nominal system at the bifurcation points associated with a coordinated turn of radius 8018.2 ft.

Bifurcation Point	TA	TB	TC
V (ft/s)	130.851	133.175	127.046
α (rad)	0.8653	0.9399	0.8433
β (rad)	-0.002782	-0.001315	-0.002842
ϕ (rad)	0.1021	0.1162	0.09391
θ (rad)	0.8625	0.9366	0.8409
p (rad/s)	-0.01239	-0.01337	-0.0118
q (rad/s)	0.001082	0.00114	0.0009907
r (rad/s)	0.01056	0.009774	0.01051
T (lbs)	15077.5	16509.7	15300.2
$\delta_{el} = \delta_{er}$ (rad)	0.07208	0.1601	0.3882
δ_a (rad)	-0.04654	-0.09105	-0.03511
δ_r (rad)	0.006053	0.03262	0.001088

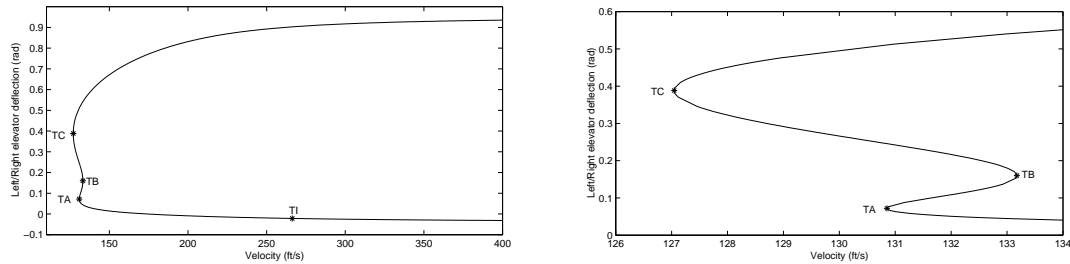


Figure 5.3: Bifurcation diagrams of the nominal system in a coordinated turn of radius 8018.2 ft.

usually deviates from the spin and comes down in a fast roll. The path taken by the vehicle is shown in Figure 5.4. It should be noted that the aircraft is constantly rolling about its axis. For the other bifurcation points the aircraft appears to stall. There is no indication of it entering into a spin motion.

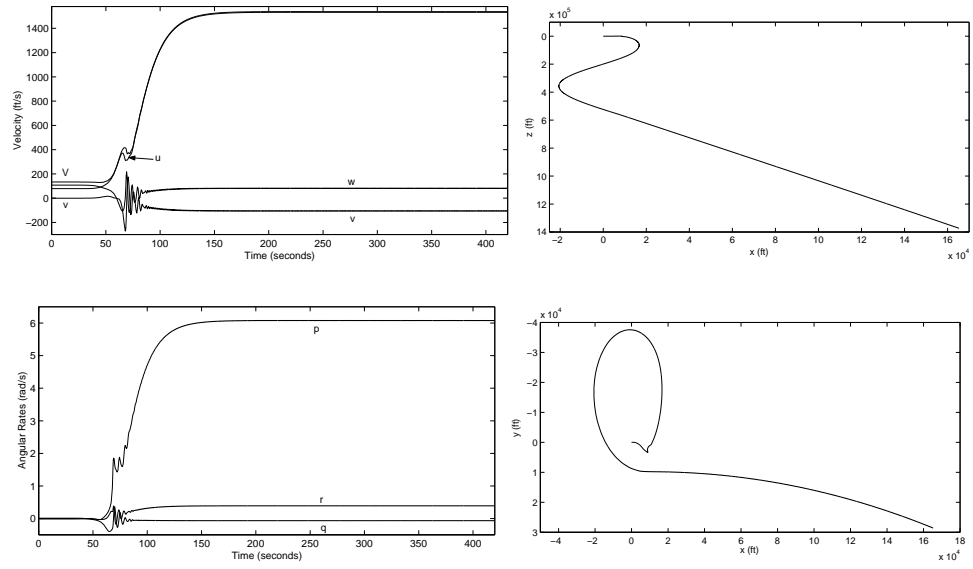


Figure 5.4: Dynamics of the open loop system at bifurcation point TB.

CHAPTER 6: BIFURCATION ANALYSIS OF THE RECONFIGURED F-16

The bifurcation analysis, of the different impaired systems, is imperative in assessing the stability, surface limitations and degeneracies of the reconfigured system. Of special significance is the analysis with the stuck surface as the bifurcation parameter. The bifurcation analysis was also carried out with velocity as the parameter. The techniques used in obtaining the bifurcation diagrams are outlined in Chapter 3. Most of the techniques were learnt in the process of analyzing the nominal and reconfigured systems.

In the reconfigured systems, the engine thrust was part of the feedback. The engine is modelled as a first order system given by equation (7.2). The analysis is carried out for the closed loop reconfigured system, and with the inclusion of T, the system has 10 states, namely, ϕ , θ , ψ , p, q, r, V, α , β , and T. The control laws for the various failures are given in Chapter 7. As in the previous chapter, the term stability is used in reference to the closed loop system.

For the analysis, we start with the 10 equilibrium equations corresponding to the 10 states. The angular rates, p, q and r, can be expressed in terms of the Euler angles, ϕ , θ and ψ , and the angular velocity, ω , of the aircraft, via equation (5.1). It should be noted that the level flight is a special case of the coordinated turn with $\omega = 0$. With the substitution of (5.1), the first three equilibrium equations corresponding to $\dot{\phi}$, $\dot{\theta}$, and $\dot{\psi}$ are trivially satisfied, and can be discarded in the analysis. If the first three equations are not dropped in the analysis, the *Mathematica* function *FindRoot* can handle only very small increments of the bifurcation parameter. Thus there are 7 equilibrium conditions along with the 13 variables, namely the 7 remaining states, the stuck surface, the remaining 4 healthy control inputs and the angular velocity ω .

As in the preceding chapter the regulated variables in the level and turn flight scenarios are given by equations (5.1) and (5.3) respectively.

In level flight conditions, we have, $\omega = 0$, $\phi = 0$, $\Gamma = 0$ and $\Psi = 0$. The constant altitude condition, $\dot{z} = 0$, which can be extracted from equation (4.1), is less involved computationally than $\Gamma = 0$. As ω and ϕ are trivial, they, along with the corresponding two equations, can be eliminated. Thus there are 9 equations and 11 variables. In the bifurcation analysis, either the stuck control surface can be held fixed and velocity treated as a parameter, or the velocity can be held fixed and the stuck position be treated as a parameter.

In the coordinated turn analysis, we have $\Gamma = 0$, (or the constant altitude condition) and $\mathcal{L} = 0$, given by equation (5.3). Thus there are 9 equations and 13 variables. First, omega is treated as a continuation parameter till the turn of desired radius is reached, and then holding the radius fixed either the velocity or the stuck position is treated as a parameter. The analysis is explained in greater detail for each case in what follows.

6.1 Left elevator failure

For the aircraft with a jammed left elevator in level flight, two bifurcation analysis were carried out. In the first analysis, the left elevator stuck is assumed stuck at its equilibrium position of -0.02672 rad, and the velocity is the bifurcation parameter; and in the second analysis, the velocity is held fixed at the equilibrium value of 351.233 ft/s, and the stuck position is treated as the bifurcation parameter. The bifurcation diagrams are shown in Figure 6.1.

At the two bifurcation points B1 and B2 (see Table 6.1) the failed system is unstable and is uncontrollable, unobservable, has dependent inputs and one transmission zero at the origin.

Starting from the stable operating point LO (351.233 ft/s), as the speed is decreased the system becomes unstable at S1 (214.283 ft/s). The upper aileron and rudder limits are reached at A1 (172.783 ft/s) and R1 (138.539 ft/s) respectively.

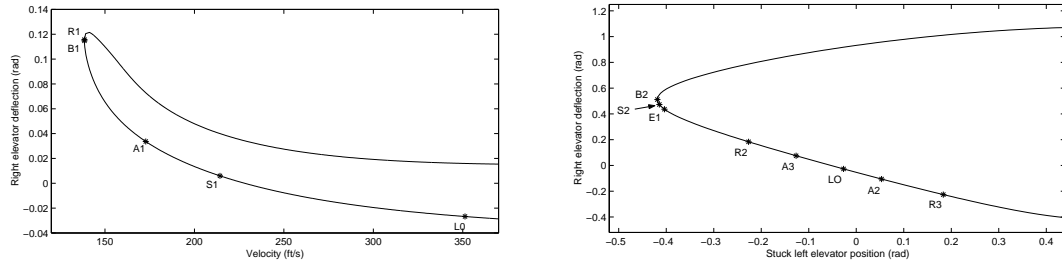


Figure 6.1: Bifurcation diagrams of the impaired system in level flight with a stuck left elevator.

In the bifurcation analysis with the stuck position as the parameter, and when the impaired aircraft's velocity and orientation is regulated, the system first runs out of aileron control: A2 (0.0532765 rad) and A3 (-0.126723 rad) correspond to the lower and upper aileron limits. Next it encounters the rudder limits: R2 (-0.226723 rad) is the lower limit and R3 (0.183277 rad) is the upper limit. The right elevator reaches its saturation point at E1 (-0.403723 rad). The stability boundary is S2 (-0.414523 rad).

In order to carry out the bifurcation analysis in a coordinated turn, the flying conditions at a coordinated turn need to be determined. This is accomplished by starting from the level flying conditions and varying ω till a turn radius of 8018.2 ft is reached. For this analysis we hold the stuck position at its equilibrium value, i.e., $\delta_{el} = -0.02672$ rad; assume no pilot input in the right elevator; and set $\psi = 0$. Once the radius is fixed there are 12 variables.

For the analysis with velocity as the parameter the stuck left elevator is held at its equilibrium value of -0.02672 rad and it is assumed that $\psi = 0$. The velocity is fixed for the analysis when the stuck position is the parameter. The bifurcation diagrams are shown in Figure 6.2.

At the bifurcation points, B9 through B12, all the conditions for the occurrence of a bifurcation point hold. They are all stable, except bifurcation point B12. The

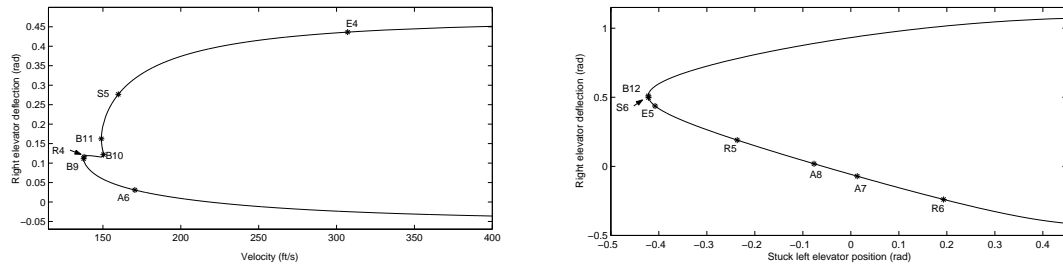


Figure 6.2: Bifurcation diagrams of the impaired system in a coordinated turn of radius 8018.2 ft with a stuck left elevator.

flying conditions at the bifurcation points are given in Table 6.2.

The occurrence of stable bifurcation points are unique to control systems. In the case of dynamical systems, bifurcation points are always associated with changes in the stability characteristics.

In the bifurcation analysis with the velocity as the parameter, S5 (159.8752 ft/s), A6 (170.4802 ft/s), R4 (137.8788 ft/s), and E4 (307.1252 ft/s) correspond to the stability boundary, aileron upper limit, the rudder upper limit, and the right elevator upper limit.

As in the level flight analysis, with the stuck position as the parameter the impaired system first runs out of aileron control: the lower and upper bounds are reached at A7 (0.01327 rad) and A8 (-0.07672 rad) respectively; then rudder control: R5 (-0.2367 rad) and R6 (0.1932 rad) correspond to the lower and upper bound respectively. The stability boundary is S6 (-0.4214 rad) and E5 (-0.4077 rad) is the right elevator upper limit.

6.2 Right elevator failure

The bifurcation analysis of the aircraft in level flight with the right elevator failure must be equivalent to the left elevator failure.

The analysis, when the aircraft is in a coordinated turn of radius 8018.2 ft, is

carried out along the lines of the left elevator failure, except that the left and right elevator terms are interchanged. The bifurcation curves with velocity as the parameter, and with the stuck position as the parameter are shown in Figure 6.3.

The results, however, do not correspond to the left elevator analysis, as the aircraft is considered in a coordinated turn to the right in both cases. The major distinction is that the entire plots in the right elevator cases are unstable. Thus the occurrence of right elevator failure while the aircraft is in a right turn is more severe than a left elevator failure, and vice versa; if we are trying to regulate the velocity and orientation of the aircraft.

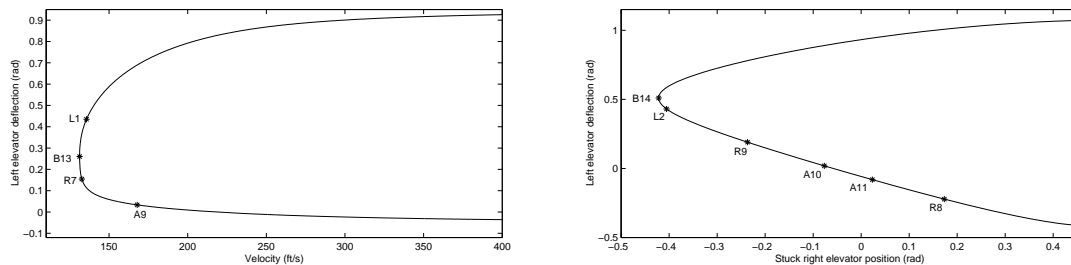


Figure 6.3: Bifurcation diagrams of the impaired system in a coordinated turn of radius 8018.2 ft with a stuck right elevator.

At the bifurcation points B13 and B14 (see Table 6.2) all the conditions for the occurrence of a bifurcation are valid.

In the analysis with velocity as the parameter, the aileron lower limit, the rudder upper limit, and the left elevator upper limit occur at A9 (167.903 ft/s), R7 (132.703 ft/s), and L1 (135.642 ft/s) respectively.

As in the left elevator's analysis, in the analysis with the stuck right elevator position as the parameter, the aileron limits (A10 and A11) are reached first, followed by the rudder (R8 and R9) and finally the left elevator (L2). The stuck position values at the limiting points are: A10 (-0.07672 rad), upper limit; A11 (0.02327 rad), lower limit; R8 (0.1733 rad), lower limit; R9 (-0.2367 rad), upper limit; and L2 (-0.4053

rad), upper limit.

6.3 Aileron failure

In the bifurcation analysis of the stuck aileron, with the velocity as the parameter and the aileron stuck at its equilibrium position of 0 rad, there are 3 bifurcation points. At all the three points, B3, B4, and B5, the reconfigured system has dependent inputs, is uncontrollable, unobservable and has two transmission zeros. The bifurcation point B3 is stable, while the other two are not. In Table 6.1 the flying conditions at the bifurcation points are tabulated. The bifurcation curves are given in Figure 6.4. At E2 (127.733 ft.s), the elevator upper limit is reached. No other control surface boundary is encountered. Stability is lost at S3 (132.412 ft/s). In the analysis with the stuck position as the parameter, the entire curve is stable and no bifurcation points or control limitations are encountered. This implies that the reconfigured design is adequate for any stuck position of the aileron, while in level flight.

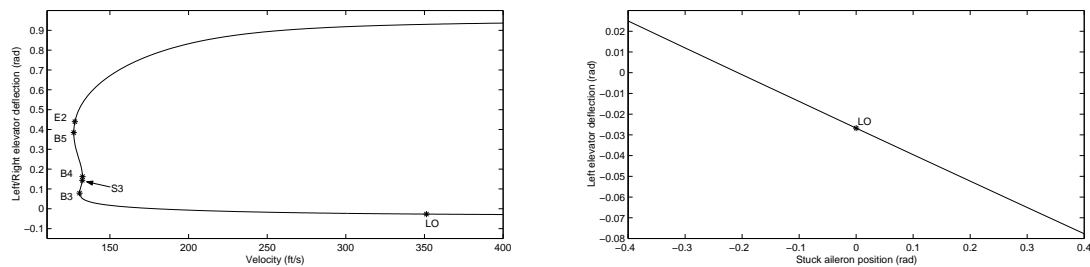


Figure 6.4: Bifurcation diagrams of the impaired system in level flight with a stuck aileron.

The flying conditions in a coordinated turn of radius 8018.2ft and the aileron stuck at 0 radians is determined as follows: A continuation in the angular velocity ω , is applied to the equilibrium equations, starting with the level flight conditions. It is assumed that the aileron is stuck at its equilibrium value of 0 rad, there is no pilot input to the rudder and that $\psi = 0$ radians. Once the flying conditions at the radius

of 8018.2 ft are determined, the bifurcation analysis for both the velocity and stuck position as parameter cases are carried out.

The bifurcation curves are shown in Figure 6.5. Although the bifurcation curves look similar to the level flight analysis there are differences in the actual numerical values. The stability boundary is S7 (132.829 ft/s) and the elevator limit is at E6 (128.087 ft/s). The bifurcation points B16 and B17 are unstable, while B15 is stable. At all the three bifurcation points, all the conditions for the occurrence of a bifurcation hold. From the bifurcation analysis with the stuck aileron position as the parameter, it can be seen that the reconfigured design can handle all stuck positions of the aileron.

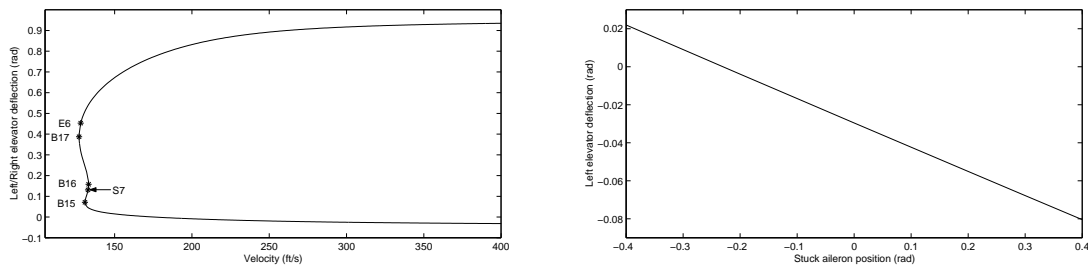


Figure 6.5: Bifurcation diagrams of the impaired system in a coordinated turn of radius 8018.2 ft with a stuck aileron.

6.4 Rudder failure

The level flight bifurcation analysis for the stuck rudder case, with the rudder stuck at its equilibrium value of 0 rad, and with the velocity as the bifurcation parameter (Fig 6.4), is numerically the same as that for the stuck aileron case with velocity as the parameter (Fig 6.6). This is because the aircraft is in level flight. The prominent difference is that the reconfigured system loses stability at a much higher velocity at S4 (197.091 ft/s). Thus at all the bifurcation points B6, B7, and B8 the reconfigured system is unstable. The upper elevator limit is encountered at E3 (127.733 ft/s).

At all three bifurcation points, B6, B7 and B8, the reconfigured system has dependent inputs, is uncontrollable, unobservable and has two transmission zeros.

In the level flight bifurcation analysis with the stuck rudder position as the parameter, the reconfigured system encounters the aileron's lower and upper limit at A4 (0.1 rad) and A5 (-0.1 rad) respectively.

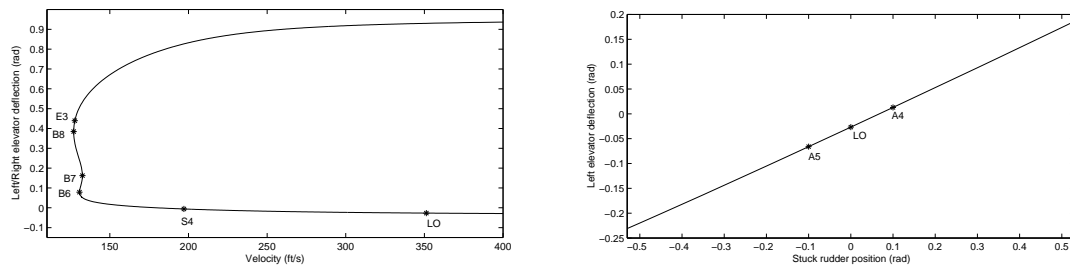


Figure 6.6: Bifurcation diagrams of the impaired system in level flight with a stuck rudder.

To obtain the coordinated turn conditions, the stuck rudder is held at its equilibrium position of 0 radians, and it is assumed that there are no pilot inputs to the left and right elevators. Then ω is varied till the radius of 8018.2 ft is attained. The bifurcation analysis is carried out with either the velocity or the stuck position as the parameter. The results are shown in Figure 6.7.

The analysis with the velocity as the bifurcation parameter reveals unexpected equilibrium surfaces. As the velocity is decreased, first the aileron lower limit is reached at A16 (231.942 ft/s), followed by the left elevator upper limit L5 (201.692 ft/s), the stability boundary S10 (192.692 ft/s), the bifurcation point B22, and the upper right elevator limit E9 (189.521 ft/s). There is another unexpected closed loop bifurcation curve with 4 other bifurcation points, namely, B18, B19, B20, B21. The curve is explained starting from the aileron upper limit A12 and in a counterclockwise manner. The points A12 (191.026 ft/s), A13 (132.442 ft/s), A14 (139.546 ft/s) and A15 (219.546 ft/s) correspond to the aileron's upper bound. The aileron is within

its bounds in the portion of the curve from A12 to A13 and from A14 to A15. L3 (128.555 ft/s) and L4 (218.026 ft/s) correspond to the left elevator's upper bound. The left elevator is within its bounds from L3 to L4. E7 (128.955 ft/s) and E8 (285.546 ft/s) correspond to the right elevator's upper limit. The right elevator is within its bounds from E7 to E8. The reconfigured system is stable from S8 (199.546 ft/s) to S9 (314.858 ft/s). Thus the feasible portion of the entire closed curve is the region between S8 and A15. At all the five bifurcation points all the conditions for the occurrence of a bifurcation are valid. They are all unstable.

In the analysis with the stuck position as the parameter, the system encounters elevator and aileron limits. The left elevator lower and upper limits occur at L6 (0.1 rad) and L7 (-0.12 rad); the right elevator lower and upper limits occur at E10 (-0.1 rad) and E11 (0.13 rad); and, the aileron lower and upper limits occur at A17 (-0.13 rad) and A18 (0.15 rad).

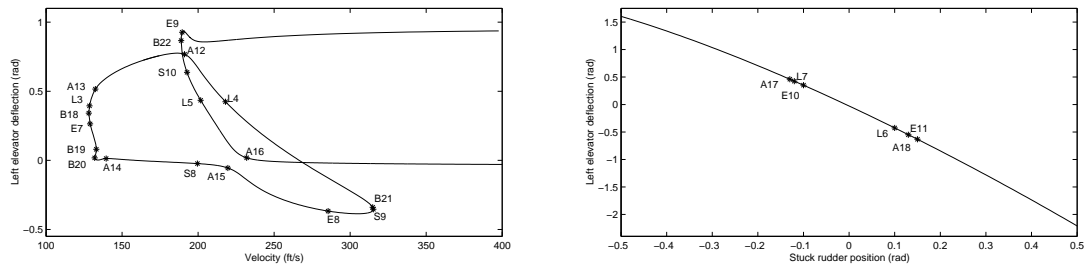


Figure 6.7: Bifurcation diagrams of the impaired system in a coordinated turn of radius 8018.2 ft with a stuck rudder.

Table 6.1: Flying conditions of the impaired system at the bifurcation points associated with level flight.

Bif. Pt.	B1	B2	B3	B4	B5	B6	B7	B8
V (ft/s)	138.5280	351.233	130.6754	132.5639	127.0139	130.6754	132.5639	127.0139
$\alpha = \theta$ (rad)	0.7344	0.07853	0.8659	0.9349	0.8429	0.8659	0.9349	0.8429
β (rad)	0.1813	0.01585	0	0	0	0	0	0
ψ (rad)	-0.1813	-0.01585	0	0	0	0	0	0
$T = T_c$ (lb)	12708.8856	4385.76	15064.2842	16387.6492	15254.9235	15064.2842	16387.6492	15254.9235
δ_{el} (rad)	-0.02672	-0.4186	0.0785	0.1621	0.3844	0.0785	0.1621	0.3844
δ_{er} (rad)	0.1146	0.5121	0.0785	0.1621	0.3844	0.0785	0.1621	0.3844
δ_a (rad)	2.4602	3.6404	0	0	0	0	0	0
δ_r (rad)	0.3643	-1.2228	0	0	0	0	0	0

Table 6.2: Flying conditions of the impaired system at the bifurcation points (B9 - B17) associated with a coordinated turn of radius 8018.2 ft.

Bif. Pt.	B9	B10	B11	B12	B13	B14	B15	B16	B17
V (ft/s)	137.599	150.29	149.004	354.43	131.257	354.642	130.851	133.174	127.046
α (rad)	0.7475	0.7647	0.8076	0.08796	0.8312	0.08775	0.8653	0.9399	0.8433
β (rad)	0.1770	0.4508	0.4678	0.02805	-0.1044	-0.01822	-0.001679	-0.001046	-0.001823
ϕ (rad)	0.09951	0.1130	0.1154	0.4555	0.09762	0.4553	0.1021	0.1161	0.09392
θ (rad)	0.7579	0.7997	0.8432	0.09133	0.8218	0.07085	0.8626	0.9366	0.8410
ψ (rad)	0	0	0	0	0	0	0	0	0
$T = T_c$ (lb)	12976.5	13111.6	13919.1	4688.5	14593.5	4690.16	15077.5	16509.4	15300.2
δ_{el} (rad)	-0.02672	-0.02672	-0.02672	-0.4218	0.2603	0.510127	0.07104	0.1582	0.3874
δ_{er} (rad)	0.1112	0.1218	0.1624	0.5101	-0.02672	-0.4217	0.07313	0.1620	0.3890
δ_a (rad)	2.4972	2.1968	1.9848	3.67286	-5.3704	-3.609	0	0	0
δ_r (rad)	0.3259	2.3465	2.5441	-1.1581	1.2461	1.1861	-0.003310	0.001143	-0.004671

Table 6.3: Flying conditions of the impaired system at the bifurcation points (B18 -B22) associated with a coordinated turn of radius 8018.2 ft.

Bif. Pt.	B18	B19	B20	B21	B22
V (ft/s)	128.12	133.047	131.979	315.279	188.852
α (rad)	0.8291	0.9166	0.8568	0.1161	0.3477
β (rad)	0.1210	0.1603	0.1363	0.2277	-0.1567
ϕ (rad)	0.09414	0.1126	0.1030	0.3651	0.1433
θ (rad)	0.8346	0.9245	0.8633	0.1899	0.3230
ψ (rad)	-0.9379	-0.9379	-0.9379	-0.9379	-0.9379
$T = T_c$ (lb)	15078.7	16098.7	14937.0	4870.71	7679.06
δ_{el} (rad)	0.3414	0.08012	0.0181	-0.353748	0.8666
δ_{er} (rad)	0.4497	0.2307	0.1363	0.629546	0.1648
δ_a (rad)	2.3266	3.0775	2.6196	4.31437	-3.0097
δ_r (rad)	0	0	0	0	0

CHAPTER 7: SIMULATION OF THE F-16's RECONFIGURATION

In the event of an actuator failure during flight, the nominal controller, more often than not, will be unable to stabilize the system. The handling qualities of the aircraft will invariably deteriorate, even if the nominal controller manages to maintain stability. It was observed that for the stability augmented F-16 that is developed in this work, the nominal controller is able to stabilize - but with much degraded performance - the failed system, only if the flying conditions are in a very small region about the trim condition. This agrees well with the experience of the crew of the DHL A300 that was hit by a hand held missile when taking off from Baghdad airport. [68] The pilots were able to land the aircraft with much difficulty, and sources concluded that, "having the trim set right when they were hit saved them." With the continued use of the nominal controller, the safety of the flight is highly dependent in the resourcefulness, skill and training of the crew. In the case of more severe faults the stability of the nominal system cannot be maintained, making the crew's job extremely demanding. A reconfigured controller, designed as outlined in Chapter 2, will be able to ensure superior performance.

In formulating the reconfigured controller problem, we recognize that it may not be possible to achieve the original performance; however, it is important that certain very critical variables be regulated. At the very least, the orientation of the impaired aircraft must be maintained. In addition, it is desirable that the velocity be regulated, in order to circumvent stall. Thus we have

$$\mathbf{r}(\mathbf{x}) = [\phi, \Gamma, \Psi, V]^T \quad (7.1)$$

which has a steady state value of $[0 \text{ rad}, 0 \text{ rad}, 0 \text{ rad}, 351.3 \text{ ft/s}]^T$ in level flight. The F-16 possesses sufficient redundancy to stabilize the system, and to regulate the variables given in equation (7.1), in the case of any single actuator surface failure,

namely, left elevator, right elevator, aileron or rudder.

The engine dynamics is modelled as a first order system with unit time constant, i.e.,

$$\dot{T} = T_c - T \quad (7.2)$$

where T_c is the commanded thrust and T is the actual thrust. The performance of the reconfigured system was evaluated, with and without thrust in the feedback, and no significant change was observed. In the simulations, thrust is also part of the feedback.

It was observed that the impaired system that is stabilized, so that its flying qualities mimicked those of the nominal system, is inferior to the system that is stabilized based on an LQR design with equal weighting on all states and healthy control inputs. It should be noted that in the latter design the longitudinal and lateral dynamics are coupled. The observer gain is also based on an LQR design, with equal weighting on all states and control inputs. It is felt that the design of the transients of the impaired system plays a crucial role in the robustness of the reconfigured system. This is a research area that needs to be explored. The computation of the reconfigured nonlinear control laws are facilitated by working in a symbolic computational environment. The control laws and the eigenvalues, for the various failures, are listed in the sections that follow. The reconfigured control law is a fourth order approximation in each case, because at the trim conditions it yielded the equilibrium values of the effective control inputs.

The simulations are carried out in SIMULINK. The relatively complex controllers are automatically coded, just as the model, producing separate SIMULINK S-functions that are integrated into a closed loop simulation. The bounds of each control surface is incorporated in the simulation. Also, each control surface is modelled as a first order system with a time constant of 0.05 seconds. The fault is modelled as a constant. The states of the aircraft, along with the observer's states and the control surfaces are

initialized at the appropriate flying conditions. The reconfiguration is demonstrated when the aircraft experiences a failure in level flight as well as in a coordinated turn.

The plots of the reconfiguration process for different actuator failures in level and turn flight conditions are shown in what follows. The failure occurs at $t = 0$ sec. The debilitated aircraft continues to operate with the nominal controller until the switch to the reconfigured controller is made by a FDI mechanism. An intervention by the pilot could improve or worsen the situation. In the simulations no pilot intervention is assumed. In the simulations for aircraft in a coordinated turn, the aircraft is at a radius of 8018.2 ft (this corresponds to a positive ω , which means that the aircraft is in a right turn), except for the right elevator failure.

7.1 Left elevator failure

The reconfigured control law for the left elevator failure is computed as:

$$\begin{aligned}
T_c &= 2270.3630 + 952.5891\delta_{el} + 17664.6249\delta_{el}^2 - 3913.7772\delta_{el}^3 + 1089.5586\delta_{el}^4 \\
&\quad + 0.06965q - 0.4142T + 0.2479\theta \\
\delta_{er} &= 273.1706 - 2.6825\delta_{el} + 16.4310\delta_{el}^2 - 0.6805\delta_{el}^3 + 15.3431\delta_{el}^4 - 0.3562p - \\
&\quad 0.3875\phi - 0.1376\psi + 46.0275q + 2.5082r + 118.1671\theta - 0.8526u \\
&\quad - 0.1584v + 0.5273w \\
\delta_a &= 27.9731 - 11.77\delta_{el} + 4.6942\delta_{el}^2 + 1.1815\delta_{el}^3 + 4.0632\delta_{el}^4 + 2.3075p \\
&\quad + 1.3263\phi + 0.9631\psi + 27.2358q - 1.8043r + 13.8271\theta - 0.08603u \\
&\quad - 0.2576v + 0.02449w \\
\delta_r &= -53.8823 - 12.343\delta_{el} + 5.0250\delta_{el}^2 + 5.1514\delta_{el}^3 - 2.6695\delta_{el}^4 - 3.1467p \\
&\quad - 2.8465\phi - 0.2310\psi - 18.0087q + 27.7184r - 23.6998\theta + 0.1660u \\
&\quad - 0.9341v - 0.09042w
\end{aligned} \tag{7.3}$$

The regulator eigenvalues are: $\{-13.5176 \pm 2.5769i, -4.7341, -2.1306, -1.4142, -0.7551 \pm 0.04935i, -0.1759 \pm 0.2078, -0.09191\}$, and the observer eigenvalues are: $\{-13.2472 \pm 13.2189i, -12.5935 \pm 12.543i, -4.0724 \pm 3.9497i, -1.4142, -1.2973, -1.2797 \pm 1.1939i, -1.0091\}$.

For the aircraft in level flight, the left elevator is assumed to be stuck at -0.01 radians. A delay of 5 seconds in the fault detection and isolation process is considered. The trajectories of the regulated variables and the healthy control inputs are shown in Figures 7.1 and 7.2 respectively.

In a coordinated turn of radius 8018.2 ft, the left elevator is assumed stuck at -0.04 radians, and a delay of 5 seconds is assumed in detecting and isolating the fault. The trajectories of the regulated variables and the healthy control inputs are shown in Figures 7.3 and 7.4 respectively.

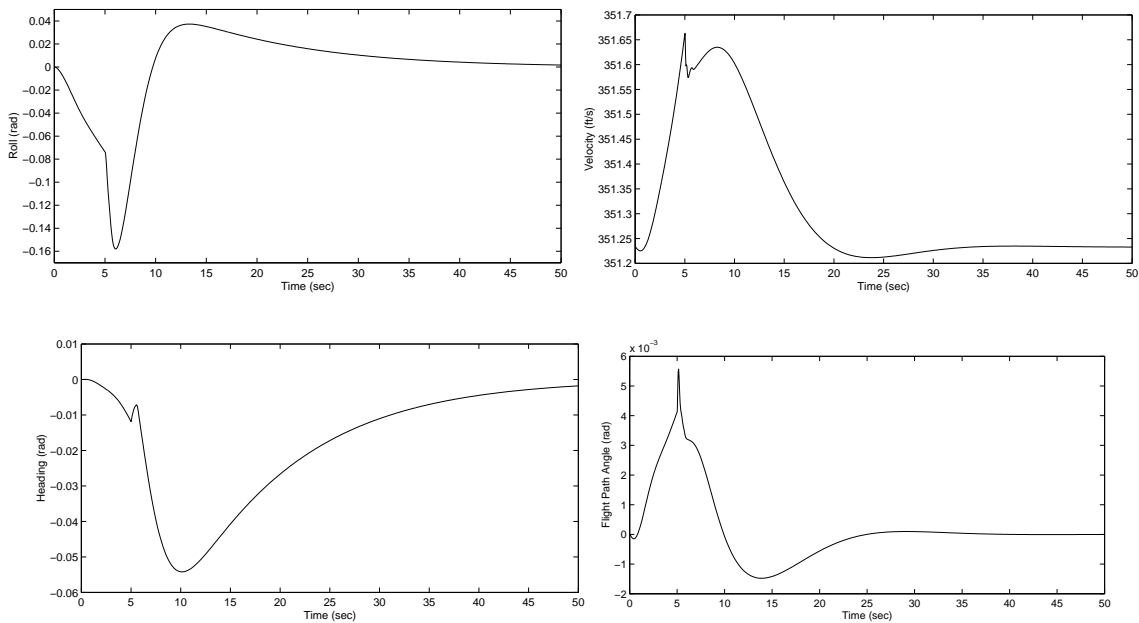


Figure 7.1: Plots of the regulated variables in the event of a left elevator failure in level flight. The left elevator is assumed stuck at -0.01 rad, and the switching time is set as 5 sec.

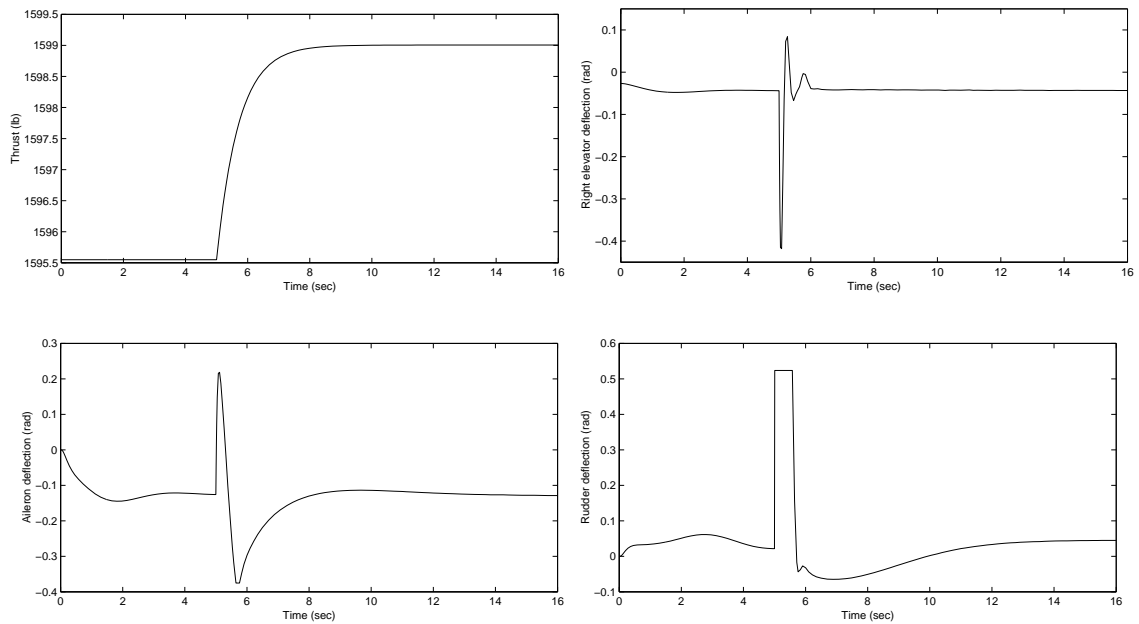


Figure 7.2: Plots of the control inputs in the event of a left elevator failure in level flight. The left elevator is assumed stuck at -0.01 rad, and the switching time is set as 5 sec.

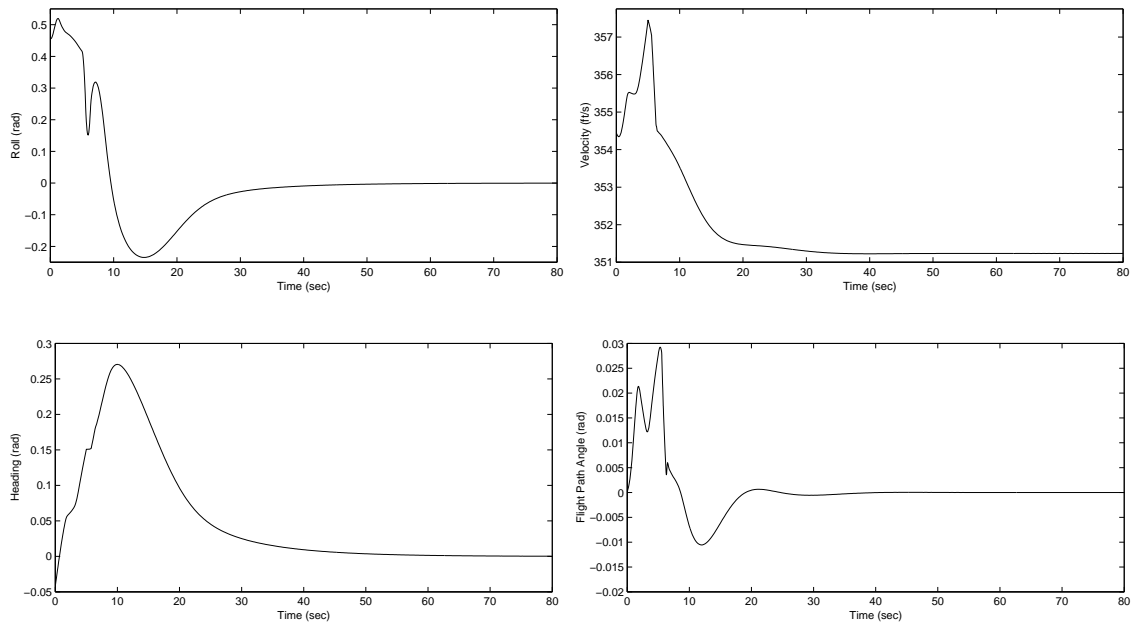


Figure 7.3: Plots of the regulated variables in the event of a left elevator failure in a coordinated turn of radius 8018.2 ft. The left elevator is assumed stuck at -0.04 rad, and the switching time is set as 5 sec.

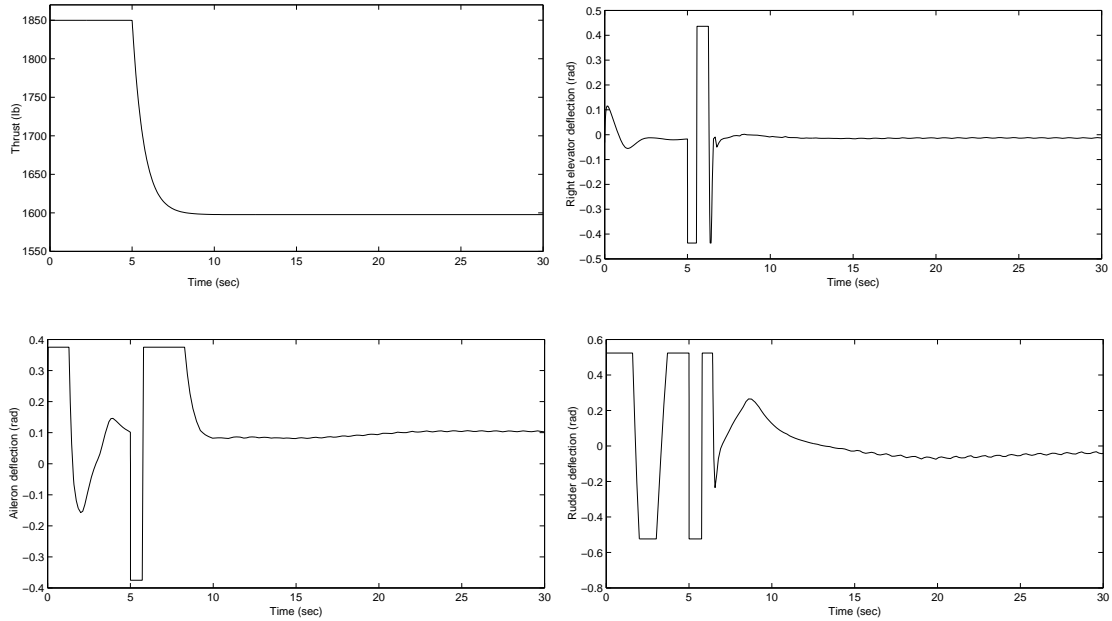


Figure 7.4: Plots of the control inputs in the event of a left elevator failure in a coordinated turn of radius 8018.2 ft. The left elevator is assumed stuck at -0.04 rad, and the switching time is set as 5 sec.

7.2 Right elevator failure

The reconfigured control law for the right elevator failure is computed as:

$$\begin{aligned} T_c = & 2270.3630 + 952.5891\delta_{er} + 17664.6248\delta_{er}^2 - 3913.7772\delta_{er}^3 + 1089.5586\delta_{er}^4 \\ & + 0.06965q - 0.4142T + 0.2479\theta \end{aligned}$$

$$\begin{aligned} \delta_{el} = & 273.1691 - 2.7914\delta_{er} + 14.3868\delta_{er}^2 - 0.7428\delta_{er}^3 + 16.2834\delta_{er}^4 + 0.3562p \\ & + 0.3875\phi + 0.1376\psi + 46.0275q - 2.5082r + 118.1671\theta - 0.8526u \\ & + 0.1584v + 0.5273w \end{aligned}$$

$$\begin{aligned} \delta_a = & -27.9706 + 11.9621\delta_{er} - 1.1345\delta_{er}^2 - 2.0771\delta_{er}^3 - 5.3979\delta_{er}^4 + 2.3075p \\ & + 1.3263\phi + 0.9631\psi - 27.2358q - 1.8043r - 13.8271\theta + 0.08603u \\ & - 0.2576v - 0.02449w \end{aligned}$$

$$\delta_r = 53.8909 + 12.9871\delta_{er} + 6.8998\delta_{er}^2 - 8.4647\delta_{er}^3 - 1.6709\delta_{er}^4 - 3.1467p$$

$$\begin{aligned}
& -2.8465\phi - 0.2311\psi + 18.0087q + 27.71849r + 23.6998\theta - 0.1661u \\
& - 0.9341v + 0.09042w
\end{aligned} \tag{7.4}$$

The regulator and the observer eigenvalues are the same as that for the reconfigured controller designed for the left elevator failure.

It is interesting to note that the reconfigured law for the right elevator is not a symmetrical counterpart of the left elevator failure. However the simulations of the reconfiguration for identical stuck positions and switching times result in identical responses, as expected. The reason the terms in the reconfigured control laws, (7.3) and (7.4), do not match up is because of the nonlinearities in the dynamics and due to the fact that the equilibrium is not at the origin. The plots for the right elevator are shown in Figures 7.5 and 7.6.

The reconfigured law cannot handle a right elevator failure in a coordinated turn of radius 8018.2 ft (the aircraft is turning to the right), and thus the reconfiguration is demonstrated, in Figures 7.7 and 7.8, at a much higher radius of 17598.7 ft.

7.3 Aileron failure

The reconfigured law for the failure involving the stuck aileron is computed as:

$$\begin{aligned}
T_c &= 2257.5885 + 295.8252\delta_a^2 - 1.3269\delta_a^3 - 0.03824\delta_a^4 + 0.0670q - 0.4142T \\
&\quad + 0.2442\theta - 3.5671 \times 10^{-3}u + 9.8206 \times 10^{-4}w \\
\delta_{el} &= 197.2237 - 0.6508\delta_a + 0.1554\delta_a^2 + 2.4921 \times 10^{-3}\delta_a^3 + 2.9196 \times 10^{-3}\delta_a^4 \\
&\quad + 1.7364p + 1.67\phi + 0.6579\psi + 29.2383q - 9.8851r - 6.2386 \times 10^{-4}T \\
&\quad + 85.1428\theta - 0.616u + 0.2532v + 0.3872w \\
\delta_{er} &= 197.2237 + 0.6508\delta_a + 0.2057\delta_a^2 - 5.0628 \times 10^{-3}\delta_a^3 + 2.6159 \times 10^{-3}\delta_a^4 \\
&\quad - 1.7364p - 1.67\phi - 0.6579\psi + 29.2383q + 9.8851r - 6.2386 \times 10^{-4}T
\end{aligned}$$

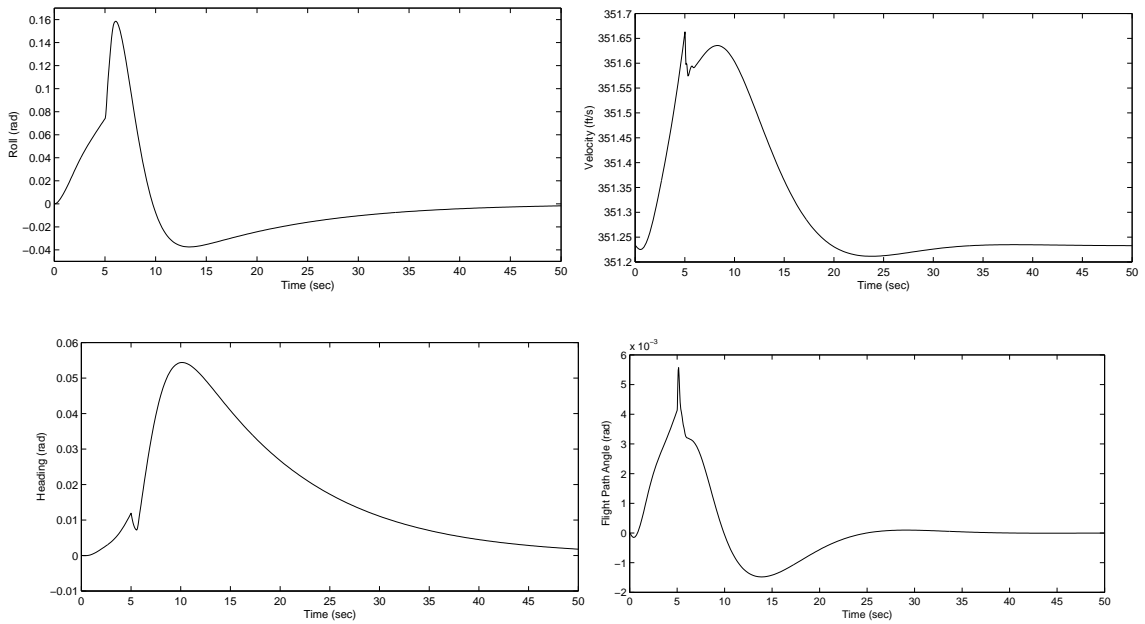


Figure 7.5: Plots of the regulated variables in the event of a right elevator failure in level flight. The right elevator is assumed stuck at -0.01 rad, and the switching time is set as 5 sec.

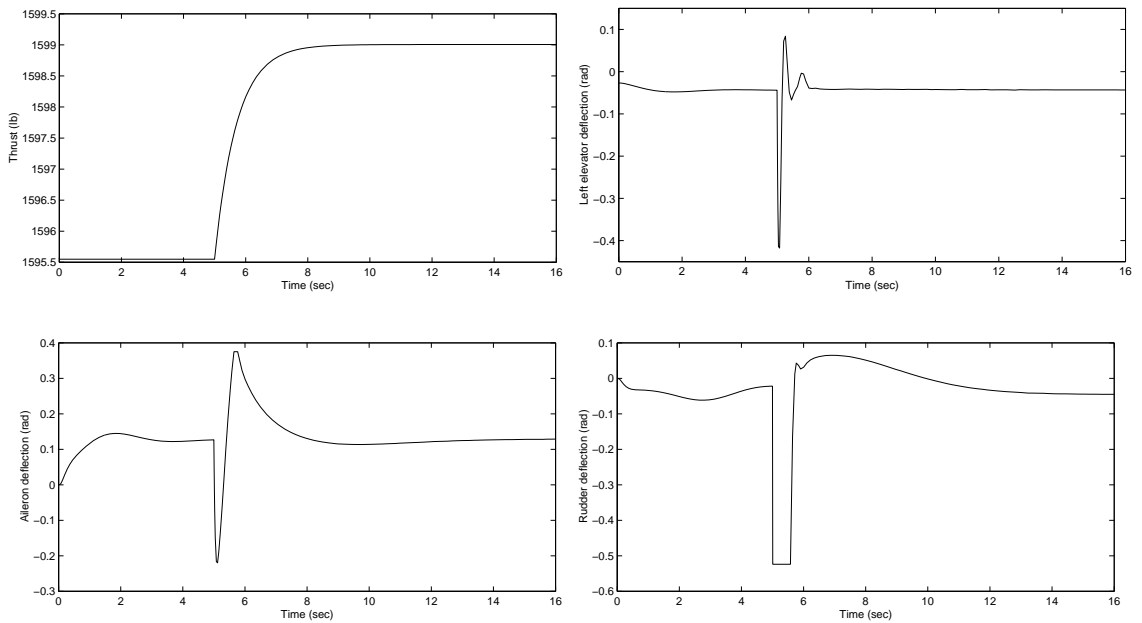


Figure 7.6: Plots of the control inputs in the event of a right elevator failure in level flight. The right elevator is assumed stuck at -0.01 rad, and the switching time is set as 5 sec.

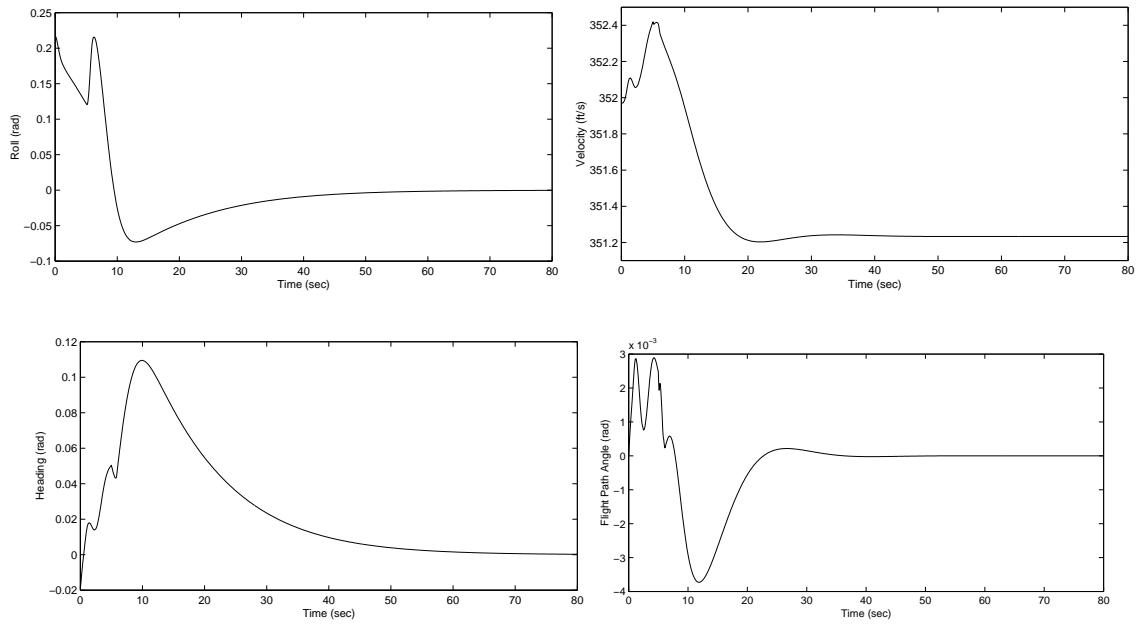


Figure 7.7: Plots of the regulated variables in the event of a right elevator failure in a coordinated turn of radius 17598.7 ft. The right elevator is assumed stuck at -0.03 rad, and the switching time is set as 5 sec.

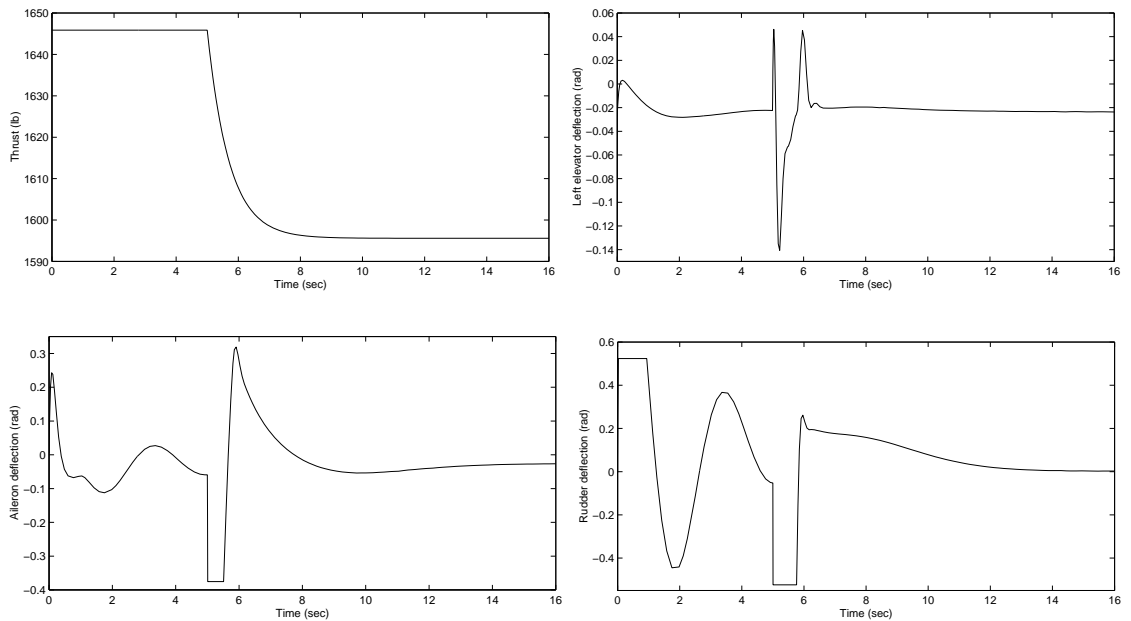


Figure 7.8: Plots of the control inputs in the event of a right elevator failure in a coordinated turn of radius 17598.7 ft. The right elevator is assumed stuck at -0.03 rad, and the switching time is set as 5 sec.

$$\begin{aligned}
& + 85.1428\theta - 0.616u - 0.2532v + 0.3872w \\
\delta_r = & 1.5790\delta_a + 0.09467\delta_a^2 - 0.014036\delta_a^3 - 5.7347 \times 10^{-4}\delta_a^4 - 1.6338p - 1.6654\phi \\
& + 0.3664\psi + 22.5465r - 0.9146v
\end{aligned}$$

The regulator eigenvalues are: $\{-20.6092, -9.5254 \pm 4.4484i, -5.2671, -1.4142, -1.3043, -0.5457, -0.1759 \pm 0.2078i, -0.09202\}$, and the observer eigenvalues are: $\{-13.248 \pm 13.219i, -12.587 \pm 12.5353i, -4.07014 \pm 3.94707i, -1.41421, -1.00643 \pm 0.532752i, -1.00186, -0.747952\}$.

The reconfiguration of the aircraft with an aileron failure is shown in Figures 7.9 and 7.10. The aileron is assumed stuck at -0.01 radians and a delay of 3 seconds is assumed.

The reconfiguration of the aircraft with an aileron failure in a coordinated turn of 8018.2 ft is shown in Figures 7.11 and 7.12. The aileron is assumed stuck at 0.05 radians and a delay of 3 seconds is assumed.

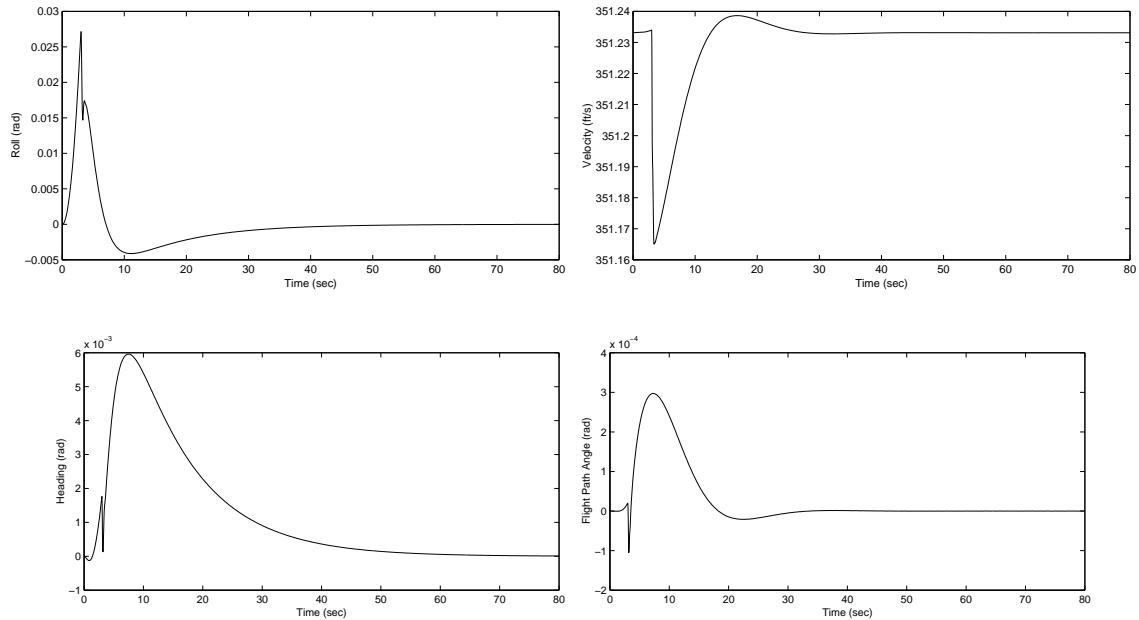


Figure 7.9: Plots of the regulated variables in the event of an aileron failure in level flight. The aileron is assumed stuck at -0.01 rad, and the switching time is set as 3 sec.

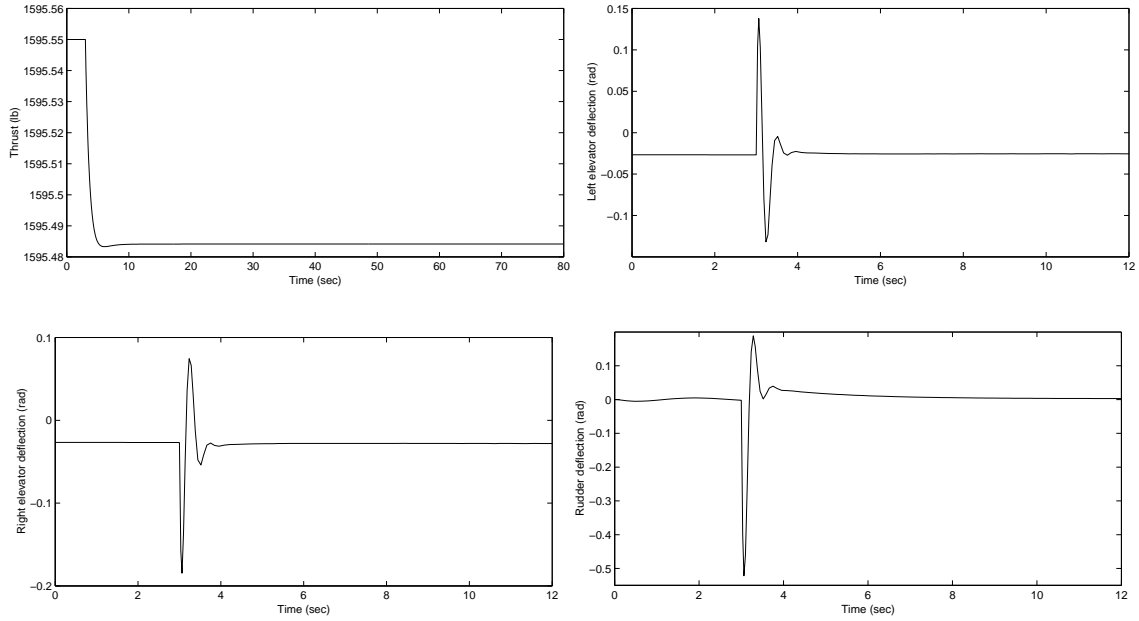


Figure 7.10: Plots of the control inputs in the event of an aileron failure in level flight. The aileron is assumed stuck at -0.01 rad, and the switching time is set as 3 sec.

7.4 Rudder failure

The reconfigured control law for the rudder failure is:

$$\begin{aligned} T_c = & 2257.5885 \delta_r + 2801.1416 \delta_r^2 - 67.9729 \delta_r^3 - 49.1732 \delta_r^4 + 0.06703q - 0.41421T \\ & + 0.2442\theta - 3.567 \times 10^{-3}u - 9.821 \times 10^{-4}w \end{aligned}$$

$$\begin{aligned} \delta_{el} = & 197.2237 + 4.3068\delta_r + 1.0453 \delta_r^2 - 0.3072\delta_r^3 + 0.2852\delta_r^4 + 3.0624p + 3.0263 \phi \\ & + 0.3292 \psi + 29.2383q - 28.0235 r - 6.2386 \times 10^{-4}T + 85.1428\theta - 0.616u \\ & + 0.6123v + 0.3872w \end{aligned}$$

$$\begin{aligned} \delta_{er} = & 197.2237 - 4.3068\delta_r + 2.3756\delta_r^2 + 0.2519\delta_r^3 + 0.1535\delta_r^4 - 3.0624p - 3.0263\phi \\ & - 0.3292\psi + 29.2383q + 28.0235r - 6.2386 \times 10^{-4}T + 85.1428\theta - 0.616u \\ & - 0.6123 v + 0.3872w \end{aligned}$$

$$\delta_a = -5.8723\delta_r + 0.5303\delta_r^2 + 0.2217\delta_r^3 - 0.05246\delta_r^4 - 0.7785p - 0.6912\phi +$$

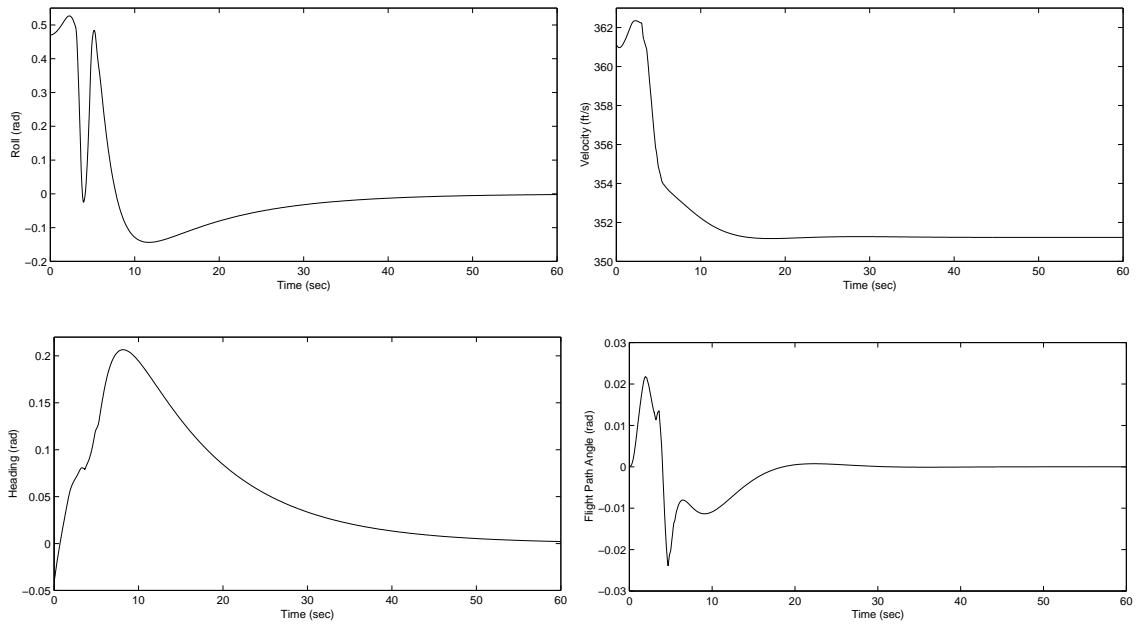


Figure 7.11: Plots of the regulated variables in the event of an aileron failure in a coordinated turn of radius 8018.2ft. The aileron is assumed stuck at 0.02 rad, and the switching time is set as 3 sec.

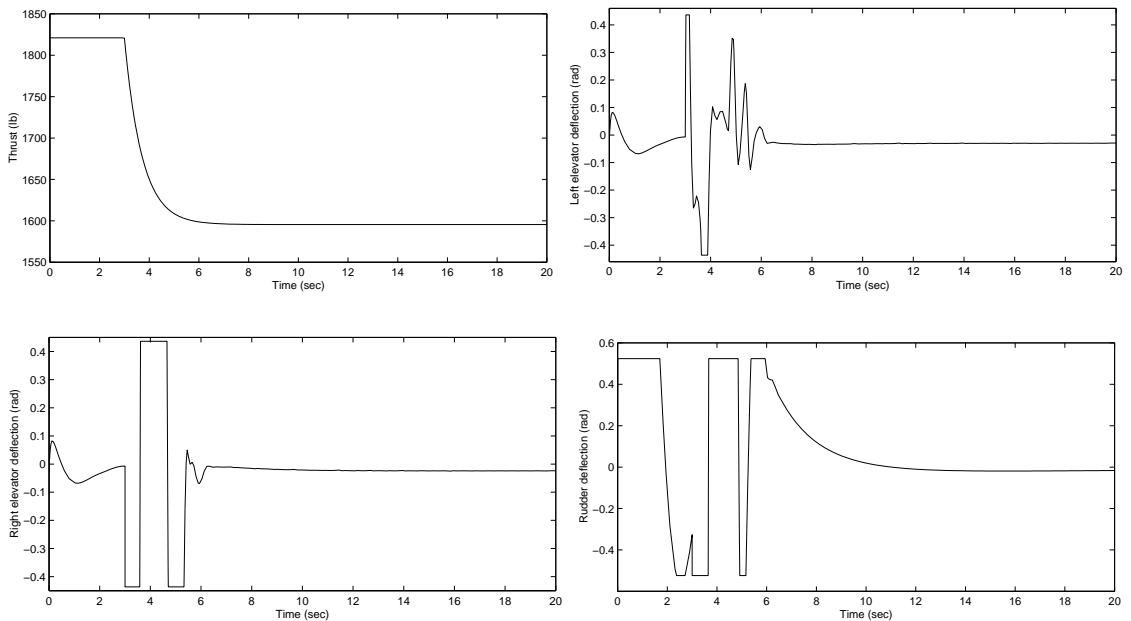


Figure 7.12: Plots of the control inputs in the event of an aileron failure in a coordinated turn of radius 8018.2ft. The aileron is assumed stuck at 0.02 rad, and the switching time is set as 3 sec.

$$0.8849\psi + 20.1680r - 0.4343v \quad (7.5)$$

The regulator eigenvalues are: $\{-20.6092, -7.6909 \pm 6.5933i, -5.2672, -1.4142, -1.2800, -0.1829, -0.1759 \pm 0.2078i, -0.1043\}$, and the observer eigenvalues are: $\{-13.251 \pm 13.222i, -12.587 \pm 12.5353i, -4.0701 \pm 3.9471i, -1.4142, -1.0995 \pm 0.4573i, -1.003, -0.1303\}$.

The reconfiguration of the aircraft in level flight, with a rudder failure at 0.1 radians and a delay of 3 seconds, is shown in Figures 7.13 and 7.14.

The reconfiguration of the aircraft in a coordinated turn of radius 8018.2 ft, with a rudder failure at 0.05 radians and a delay of 3 seconds, is shown in Figures 7.15 and 7.16.

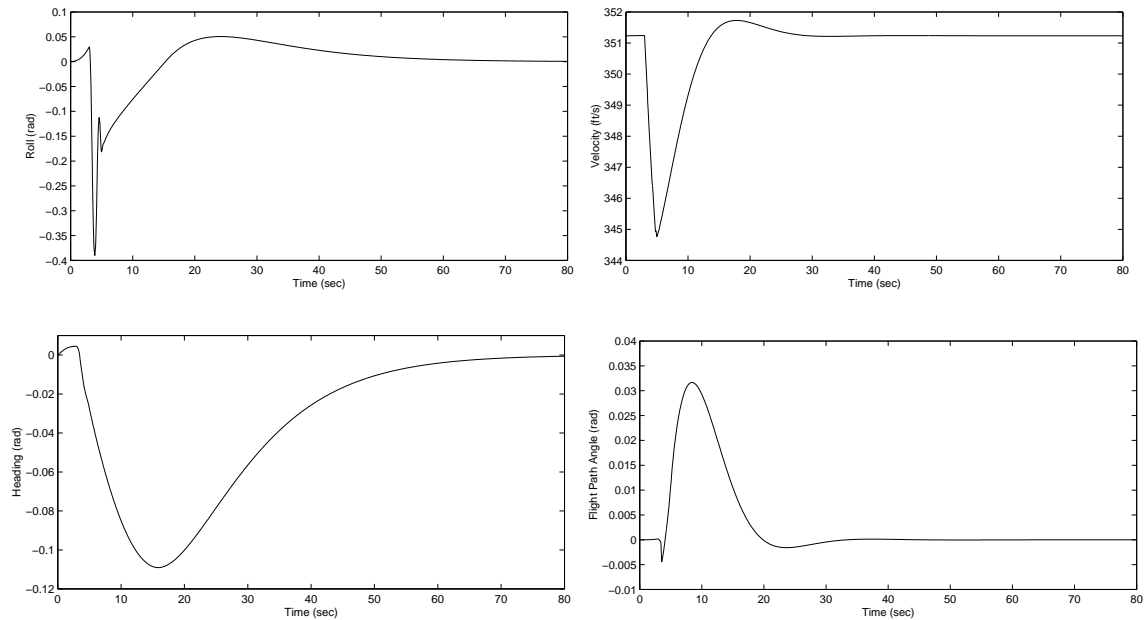


Figure 7.13: Plots of the regulated variables in the event of a rudder failure in level flight. The rudder is assumed stuck at 0.1 rad, and the switching time is set as 3 sec.

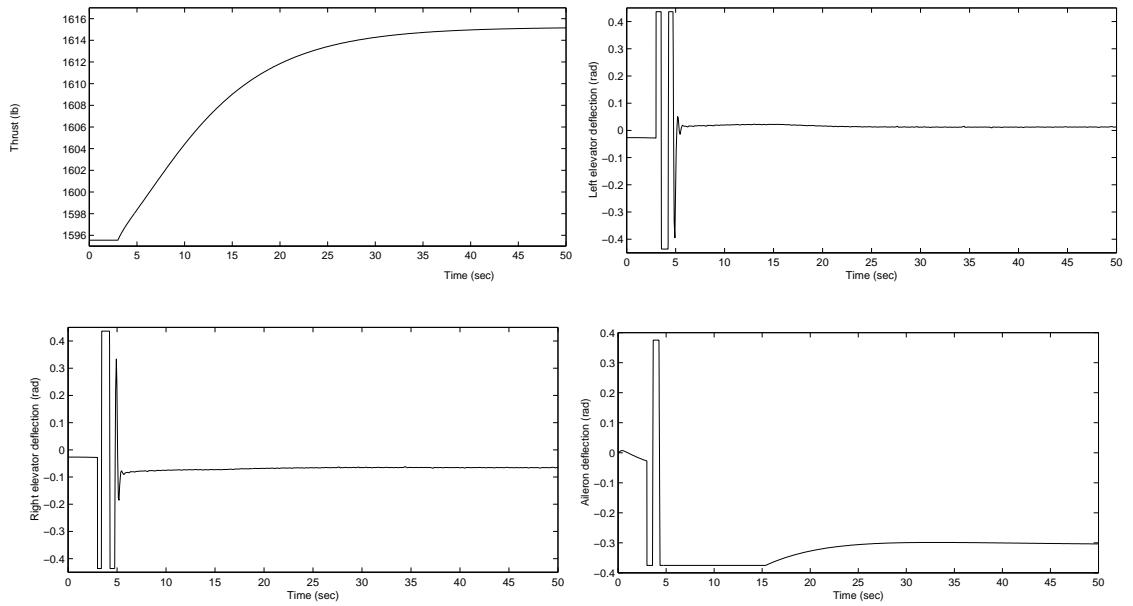


Figure 7.14: Plots of the control inputs in the event of a rudder failure in level flight. The rudder is assumed stuck at 0.1 rad, and the switching time is set as 3 sec.

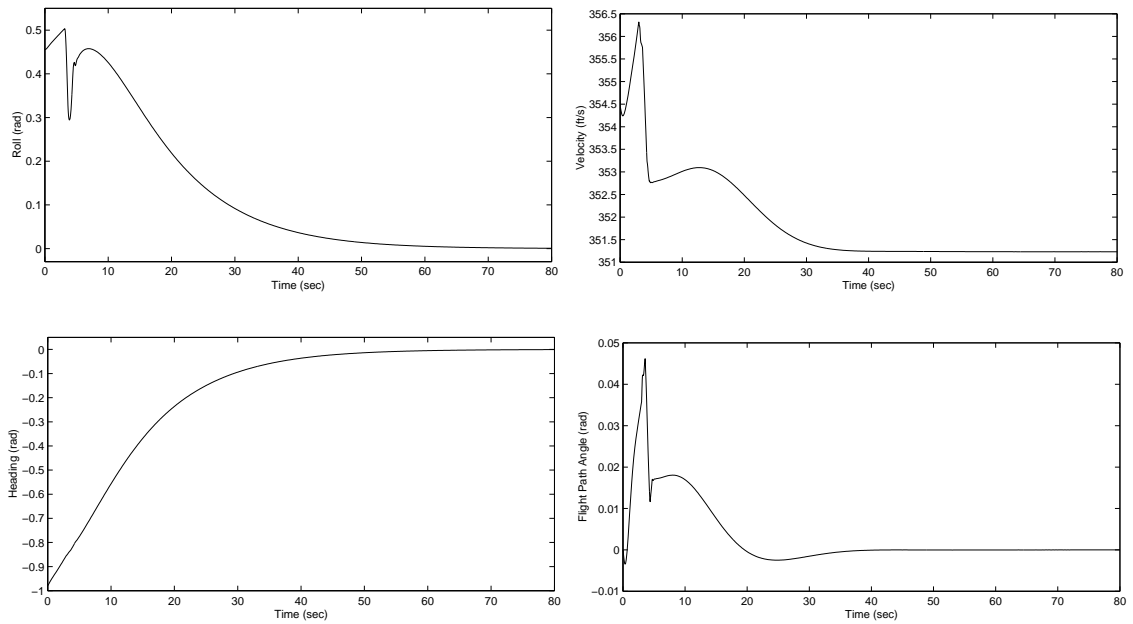


Figure 7.15: Plots of the regulated variables in the event of a rudder failure in a coordinated turn of radius 8018.2ft. The rudder is assumed stuck at 0.05 rad, and the switching time is set as 3 sec.

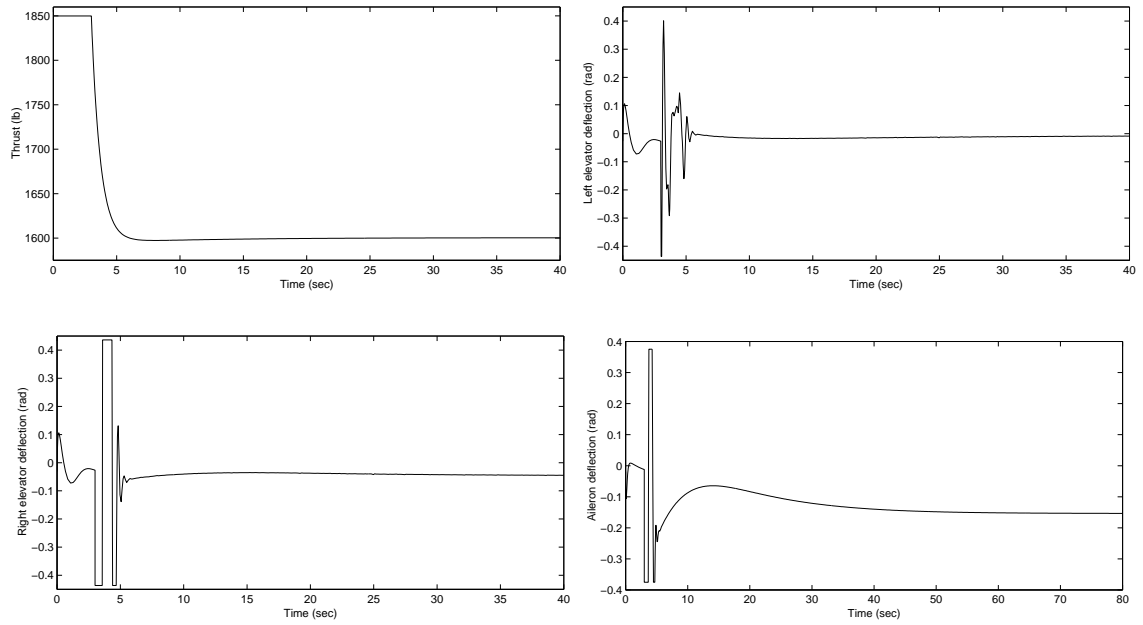


Figure 7.16: Plots of the control inputs in the event of a rudder failure in a coordinated turn of radius 8018.2ft. The rudder is assumed stuck at 0.05 rad, and the switching time is set as 3 sec.

CHAPTER 8: CONCLUDING REMARKS

This work has resulted in a few new kernels of knowledge, and has opened avenues for new areas of research. In this concluding chapter, the motivation for the thesis, the challenges entailing the problem, and the advancements made in obtaining the solution are summarized. Topics for future work are also outlined.

8.1 Summary

Actuator failures have been the cause of numerous fatal aircraft accidents. The flight control system, in most cases, has sufficient redundancy to reconfigure, so that the aircraft does not crash on the inception of the failure. Nonetheless, this redundancy has been successfully exploited by the crew in only a few cases. Even then, it was a daunting task to safely land the impaired aircraft. There are several reasons for the overwhelming challenges that the pilots face to reconfigure the aircraft. In the event of a failure, the aircraft dynamics could wander into nonlinear regimes and the operating point shifts from the nominal operation points. The nonlinearities are also important when the failure is asymmetric in nature. In such circumstances the response and feel of the aircraft could vastly differ from the pilot's experience and training. Thus, the actions that need to be taken may be unfamiliar, counter intuitive and complicated. In addition, the failed surface not only ceases to function as a viable input, but also morphs into a persistent disturbance on the system. The aircraft could also be destabilized, especially if the failure is severe. These are drastic changes in the dynamics of the system. As every failure scenario is different, the pilot's job becomes extremely challenging, if not impossible, even with the best training, unless there is a fault tolerant controller that explicitly factors these changes to the system. The reconfiguration of the flight laws will alleviate the work load on the pilot and give him a better leeway to safely land the aircraft.

The fault tolerant controller that was adopted in this work is a multiple model scheme [13], with a finite number of predesigned controllers that are stored on the system memory. In the event of a fault, a Fault Detection and Isolation (FDI) mechanism identifies and isolates the failure and makes the switch to the appropriate predesigned controller. Each controller, consisting of a regulator and an observer, is designed to accommodate the failure of a particular control surface or a set of control surfaces. This requires that each controller be robust. The regulator design problem is cast as a nonlinear output regulation problem [47], as in [25]. This design guarantees that the system is stable and that critical variables are regulated. The observer furnishes information about the failure to the regulator. The observer normal form computations based on Lie transforms were implemented in *Mathematica*, and it was concluded that the first order normal form observer, which is essentially a nonlinear constant gain observer, is the most robust. The constant gain observer can perform extremely well, if it is allowed to monitor the system well before the failure occurs. In this work a fault tolerant controller was implemented and analyzed on a real aircraft, namely the F-16, different failures involving stuck control surfaces of varying intensities.

To facilitate the design, analysis and simulation of the fault tolerant methodology on the F-16 fighter aircraft, high fidelity six degree of freedom mathematical and simulation models for the F-16 were developed. The aircraft's equations of motion was obtained using the automated tools available in *Tsi ProPac* and *Mathematica*. The aerodynamic forces and moments of the aircraft were based on a polynomial formulation [31], which allows the model to be valid in a large flight envelope. The mathematical model is obtained as Poincaré's equations, which can be converted to a state space model. The aircraft has five control inputs, namely, thrust, T , left and right elevator surfaces, δ_{el} , δ_{er} , aileron surface, δ_a and a rudder surface δ_r . There are 12 states namely, ϕ , θ , ψ , x , y , z , p , q , r , u , v and w . The model can be transformed to

wind coordinated by expressing the velocity components, u , v and w , in terms of V , α and β . The mathematical model is used in the design of nominal and reconfigured controllers and in the bifurcation analysis. A simulation model was obtained as an optimized C-code, which can be compiled as a SIMULINK S-function.

A nominal controller was designed using eigenstructure assignment, and flying qualities based on the guidelines in the literature. The stabilizing gain was designed so that the longitudinal and lateral dynamics were decoupled. Also in the design, the thrust was not part of the feedback.

The fault tolerant controller that accommodates all possible single surface failures, namely, left elevator, right elevator, aileron and rudder, was designed. The reconfigured laws were designed to regulate the orientation and velocity of the impaired aircraft. For all the single surface failures, the aircraft had sufficient redundancy to reconfigure the flight. The stabilizer gain was an optimal one, obtained with unit weighting on all the states and healthy control inputs. This is much superior to a stabilizer design that attempts to achieve the flying qualities of the nominal aircraft. The observer gain is also optimized with unit weighting on all the estimator states and the measurements. The fourth order approximation of the reconfigured law captures all the nonlinearities for the particular aircraft that was considered.

The simulations were carried out in SIMULINK. The nominal and reconfigured controllers were obtained as optimized C-codes using *Tsi ProPac*. This C-code is then compiled as an S-function. Flight reconfiguration for the various failures were carried out in both level and turn conditions. The position of the failed surface and the switching time were chosen arbitrarily. It was observed that the nominal controller could handle mild faults with degraded performance. The reconfigured controllers performed well when the stuck locations were close to the trim positions. In the event of severe faults the delay in the switching time was important in the ability of the reconfigured controller to succeed. It is interesting to note that the control

surfaces reach their final equilibrium values much earlier than the aircraft states. The control inputs of the healthy surfaces are such that the forces and moments they generate annul the disturbance of the stuck surface; and together with the thrust they sustain the impaired aircraft in level flight.

To ascertain the safety envelope, we need to be aware of the limitations of the failed system as the parameters vary. An important parameter is the stuck actuator position. The limitations include stability points, control saturation points and control system bifurcation points. The reconfigured controllers will positively fail at the control system bifurcation points. Thus such points that are feasible must be identified and characterized. Unlike bifurcation analysis in dynamical systems, the bifurcation analysis in control systems is not yet well developed. Bifurcation points in control systems is associated with trying to regulate certain variables. At bifurcation points, there can be loss of controllability, loss of observability, the presence of dependent inputs, dependent outputs or transmission zeros at the origin. Identifying and characterizing the limitations is the first step in enlarging the flight envelope.

As the currently available software packages are not suitable to carry out bifurcation analysis in control systems, the analysis was manually accomplished using a continuation approach. The continuation approach was based on the Newton-Raphson (NR) and the Newton-Raphson Seydel (NRS) methods. The NR method fails to converge near bifurcation points, because of the singularity in the Jacobian. Thus close to bifurcation points the NR algorithm must be replaced by the NRS method. An eigenvalue of the Jacobian is chosen as the bifurcation parameter. Although the choice of the smallest eigenvalue is mandatory in pinpointing the bifurcation point, the choice of another eigenvalue as the parameter is sometimes necessary in cases when the bifurcation points are clustered together and/or the eigenvalues are in close proximity. The bifurcation curve can be obtained faster using the NRS method, with a judicious choice of the continuation parameter, in spite of the fact that the NRS

method has more than twice the number of equations of the NR method. The bifurcation curve of the open loop and closed loop system are equivalent; they differ only in the analysis of control system properties and stability. Thus it may be easier to work with the open loop systems for both the nominal and reconfigured systems.

The bifurcations occurring in an F-16 in straight and level flight, and in a coordinated turn were identified and characterized. Three bifurcation points were identified in each case. The bifurcations are associated with the regulation of the aircraft's speed and orientation. The speeds at which the bifurcations occur do not differ substantially between the two cases. The longitudinal variables also do not show much difference. In straight and level flight, at the bifurcation points in both the compensated and uncompensated cases, there is loss of controllability, the presence of dependent inputs and a transmission zero at the origin. At the bifurcation points encountered in a coordinated turn or radius 8018.2 ft, the aircraft also loses observability and has redundant outputs. In most cases the bifurcations encountered were stalls. However, stall was followed by tumbling in one instance of a bifurcation in straight and level flight. During a coordinated turn the vehicle was observed to stall, enter a spin and then exit to roll divergence before the spin was fully developed.

The bifurcation analysis in both level flight and coordinated turn was carried out for each single control surface failure scenario, namely, stuck left elevator, stuck right elevator, stuck aileron and stuck rudder. The orientation and the velocity of the aircraft were the regulated variables. The analysis with the stuck position as the bifurcation parameter helped in ascertaining the range of stuck positions that the reconfigured controllers could accommodate. For the failures of the left elevator, right elevator and rudder the main issue is that the aircraft runs out of aileron control. The reconfigured controller was able to handle all stuck positions of the aileron. One bifurcation point was identified in each of the elevator failure cases. Bifurcation analysis was also carried out with the velocity as the parameter. The major issue

here was either loss of stability or the occurrence of a static bifurcation point; except for the case when the aircraft was in a coordinated turn with the rudder stuck at its equilibrium value. In that case the aircraft first ran out of aileron control. In all 20 bifurcation points were identified. Among them, 5 were stable. The existence of stable bifurcation points of the control system is a fundamental distinction from a dynamical system. In dynamical systems, bifurcation points are associated with a switch in the stability properties. It was found that the unstable bifurcation points are associated with aircraft stall. It is necessary to accurately identify the bifurcation point in order to characterize their control system properties. This analysis will help in the design of more robust fault tolerant controllers.

8.2 Future research

The performance of the reconfigured controller with a nonlinear regulator gain remains to be investigated. The regulator design approach adopted in this work is based on the estimates of the disturbance states. This framework provides no systematic method to design a nonlinear regulator gain. It should also be noted that the proposed control law is one of many viable solutions. A design based on error augmentation is proposed in [69], [70], [71]. In this framework, it is possible to design the regulator using nonlinear H_∞ theory. The necessary and sufficient conditions for the existence of solutions are the same in both the approaches.

It was learnt that if the guidelines used in the design of the nominal aircraft stabilizers are employed in the design of the stabilizers of the reconfigured system, the performance is much below par than that of a stabilizer designed based on LQR theory with uniform weighting on all the states and control inputs. This reflects the fact that fundamental changes in the dynamics of the system occur in the event of a fault. This calls for a more elaborate study of the dynamics of the failed systems.

As bifurcation analysis from a control system perspective provides valuable in-

sights into the dynamics of the system, software tools to carry out the bifurcation analysis efficiently and quickly must be developed. Some of the issues that need to be considered in automation of the process have been discussed in this thesis. The development of the software can also benefit from the earlier works such as, [40], [42] and [72]. Such a tool will help to quickly analyze the system from both a dynamical and control system perspective for different parameters.

The fault tolerant controller should be able to accommodate all possible failure scenarios. Multiple surface failures and engine failures have to be considered. The reconfigured controllers for flight conditions such as descent, climb and other special maneuvers must be investigated. The final reconfigured design should be able to accommodate as many failure scenarios as possible, as opposed to accommodating just a few very well.

The high fidelity six degree of freedom model of the F-16 developed in this work was essential in designing and analyzing the fault tolerant controllers. Such models needs to be assembled for other aircraft as well in order to develop effective fault tolerant controllers for them. These mathematical models should incorporate the other control surfaces of the aircraft like the flaps, spoilers, et cetera, that may be very useful in reconfiguring the impaired system.

In this work, the reconfiguration is assumed to be completely automated, and the pilot has not been considered in the reconfiguration process. In the event of a fault, there can be gradations in the level of automation. The reconfiguration could be fully automated in which the on board computers detects the faults and takes corrective measures; corrective measures could be triggered by a pilot activated panic button; the reconfigured system may just provide improved handling qualities and aid the pilot to land the craft; or a completely manual system that provides guidance to the pilots. It is believed that the synergy of a well designed fault tolerant system and a properly trained pilot can greatly enhance the fault imperviousness of future aircraft.

List of References

- [1] J. W. Croft, "NASA tackles loss of control," *Aerospace America*, March 2003.
- [2] (2004, May) Statistical summary of commercial jet airplane accidents. Worldwide operations 1959 - 2003. statsum.pdf. Boeing Commercial Airplanes. Seattle, WA. [Online]. Available: <http://www.boeing.com/news/techissues/pdf/statsum.pdf>
- [3] C. Kilroy. Special report: Japan airlines flight 123. [Online]. Available: <http://www.airdisaster.com/special/special-jal123.shtml>
- [4] ——. Special report: United airlines flight 232. [Online]. Available: <http://www.airdisaster.com/special/special-ua232.shtml>
- [5] ASN aircraft accident description 08 September 1994 Boeing 737-3B7 N513AU. [Online]. Available: <http://aviation-safety.net/database/1994/940908-0.htm>
- [6] (2002, December) Aircraft accident report NTSB/AAR-02/01. National Transportation Safety Board. Washington, D.C. [Online]. Available: <http://www.nts.gov/publictn/2002/AAR0201.pdf>
- [7] C. N. Jones, "Reconfigurable flight control," Department of Engineering, University of Cambridge, Tech. Rep., September 2002.
- [8] A. J. Calise, S. Lee, and M. Sharma, "Direct adaptive reconfigurable control of a tailless fighter aircraft," in *Guidance, Navigation and Control Conference*. AIAA, August 1998.
- [9] S. Sharma, A. J. Calise, and S. Lee, "Development of a reconfigurable flight control law for the X-36 tailless fighter aircraft," in *Guidance, Navigation and Control Conference*, no. 3940. Denver, CO: AIAA, August 2000.
- [10] M. Bodson and J. Groszkiewicz, "Multivariable adaptive algorithms for reconfigurable flight control," *IEEE Transactions on Control Systems Technology*, vol. 5, no. 2, pp. 217 – 229, March 1997.
- [11] G. Tao, S. M. Joshi, and X. Ma, "Adaptive state feedback and tracking control of systems with actuator failures," *IEEE Transactions on Automatic Control*, vol. 46, no. 1, pp. 78–95, January 2001.
- [12] X. Tang, G. Tao, and S. M. Joshi, "Compensation for nonlinear MIMO systems for uncertain actuator failures with an application to aircraft control," in *Conference on Decision and Control*, vol. 2. IEEE, December 2002, pp. 1245 – 1250.

- [13] K. S. Narendra and J. Balakrishnan, "Adaptive control using multiple models," *IEEE Transactions on Automatic Control*, vol. 42, no. 2, pp. 171 – 187, February 1997.
- [14] Y. Zhang and J. Jiang, "Integrated design of reconfigurable fault-tolerant control systems," *Journal of Guidance, Control and Dynamics*, vol. 24, no. 1, pp. 133–136, 2000.
- [15] P. S. Maybeck, "Multiple model adaptive algorithms for detecting and compensating sensor and actuator/surface failures in aircraft flight control systems," *International Journal of Robust and Nonlinear Control*, vol. 9, no. 14, pp. 1051 – 1070, December 1999.
- [16] S. Kanev, M. Verhaegen, and G. Nijssse, "A method for the design of fault-tolerant systems in case of sensor and actuator faults," in *European Control Conference*, September 2001.
- [17] A. Ostroff, "Techniques for accommodating control effector failures on a mildly statically unstable airplane," in *American Control Conference*. Boston, MA: IEEE, 1985, pp. 906 – 913.
- [18] Z. Gao and P. J. Antsaklis, "Stability of the pseudo-inverse method for reconfigurable control systems," *International Journal of Control*, vol. 53, no. 3, pp. 717 – 729, 1991.
- [19] Y. Zhenyu, S. Huazhang, and C. Zongji, "The frequency-domain heterogeneous control mixer module for control reconfiguration," in *International Conference on Control Applications*, vol. 2. IEEE, August 1999, pp. 1223 – 1228.
- [20] Z. Yang and M. Blanke, "The robust control mixer module method for control reconfiguration," in *American Control Conference*, vol. 5. IEEE, 2000, pp. 3407 – 3411.
- [21] I. K. Konstantopoulos and P. J. Antsaklis, "Eigenstructure assignment in reconfigurable control systems," *Interdisciplinary Studies of Intelligent Systems*, University of Notre Dame, IN, Tech. Rep. ISIS-96-001, January 1996.
- [22] A. I. Belkharraz and K. Sobel, "Fault tolerant flight control for a class of control surface failures," in *American Control Conference*, vol. 6. IEEE, June 2000, pp. 4209–4213.
- [23] F. W. Burcham Jr., C. G. Fullerton, and T. A. Maine, "Manual manipulation of engine throttles for emergency flight control," NASA Dryden Flight Research Center, Technical Report NASA/TM 2004-212045, May 2004.
- [24] B. C. Chang, G. Bajpai, and H. G. Kwatny, "A regulator design to address actuator failures," in *Conference on Decision and Control*, vol. 2. IEEE, December 2001, pp. 1454 – 1459.

- [25] G. Bajpai, “Reconfigurable control of aircraft undergoing sensor and actuator failure,” Ph.D. dissertation, Drexel University, Philadelphia, December 2002. [Online]. Available: <http://dspace.library.drexel.edu/handle/1860/19>
- [26] J. D. Boskovic and R. K. Mehra, “A multiple model-based reconfigurable flight control system design,” in *Conference on Decision and Control*, vol. 4. IEEE, December 1998, pp. 4503 – 4508.
- [27] J. Chen and R. J. Patton, *Robust Model-Based Fault Diagnosis for Dynamic Systems*. Norwell, MA: Kluwer Academic Publishers, 1999.
- [28] S. Wolfram, *The Mathematica Book, 4th ed.* Cambridge: Cambridge University Press, 1999.
- [29] H. G. Kwatny and G. L. Blankenship, *Nonlinear Control and Analytical Mechanics: a computational approach*, ser. Control Engineering. Boston: Birkhauser, 2000.
- [30] H. G. Kwatny and B. C. Chang, “Constructing linear families from parameter-dependent nonlinear dynamics,” *IEEE Transactions on Automatic Control*, vol. 43, no. 8, pp. 1143–1147, 1998.
- [31] E. A. Morelli, “Global nonlinear parametric modeling with application to F-16 aerodynamics,” in *American Control Conference*. Philadelphia: IEEE, 1998, pp. 997–1001.
- [32] —, “Global nonlinear aerodynamic modeling using multivariate orthogonal functions,” *Journal of Aircraft*, vol. 32, no. 2, pp. 270–277, 1995.
- [33] S. Chow and J. K. Hale, *Methods of Bifurcation Theory*. New York: SpringerVerlag, 1982.
- [34] J. Guckenheimer and P. Holmes, *Nonlinear Oscillations, Dynamical Systems, and Bifurcation of Vector Fields*. New York: SpringerVerlag, 1983.
- [35] J. V. Carrol and R. K. Mehra, “Bifurcation of nonlinear aircraft analysis,” *Journal of Guidance, Control and Dynamics*, vol. 5, no. 5, pp. 529–536, 1982.
- [36] C. C. Jahnke and F. E. C. Culick, “Application of bifurcation theory to high angle of attack dynamics of the F-14 aircraft,” *Journal of Aircraft*, vol. 31, no. 1, pp. 26–34, 1994.
- [37] D. C. Liaw, C. C. Song, Y. W. Liang, and W. C. Chung, “Two-parameter bifurcation analysis of longitudinal flight dynamics,” *IEEE Transactions on Aerospace and Electronic Systems*, vol. 39, no. 3, pp. 1103– 1112, July 2003.
- [38] G. Avanzini and G. de Matteis, “Bifurcation analysis of a highly augmented aircraft model,” *Journal of Guidance, Control and Dynamics*, vol. 20, no. 4, pp. 754–759, July 1997.

- [39] L. P. Gibson, N. K. Nichols, and D. M. Littleboy, “Bifurcation analysis of eigenstructure assignment control in a simple nonlinear aircraft model,” *Journal of Guidance, Control and Dynamics*, vol. 21, no. 5, pp. 792–798, September 1998.
- [40] E. J. Doedel, R. C. Paffenroth, A. R. Champneys, T. F. Fairgrieve, Y. A. Kuznetsov, B. E. Oldeman, B. Standstede, and X. Wang, “AUTO2000: Software for continuation and bifurcation problems in ordinary differential equations,” California Institute of Technology, Tech. Rep., June 2002.
- [41] R. Seydel, *Practical Bifurcation and Stability Analysis*. New York: Springer Verlag, 1994.
- [42] H. G. Kwatny, R. F. Fischl, and C. Nwankpa, “Local bifurcations in power systems: Theory, computation and application,” *Proceedings of the IEEE*, vol. 83, no. 11, pp. 1456–1483, November 1995.
- [43] H. G. Kwatny, B. C. Chang, and S. P. Wang, “Static bifurcation in mechanical control systems,” in *Chaos and Bifurcation Control: Theory and Applications*, G. Chen, Ed. Springer-Verlag, 2003.
- [44] B. A. Francis, “The linear multivariable regulator problem,” *SIAM Journal on Control and Optimization*, vol. 15, pp. 486–505, 1977.
- [45] H. G. Kwatny, J. P. McDonald, and K. C. Kalnitsky, “A class of multivariable controllers and its applications to power system control,” in *3th IFAC Symposium on Multivariable Technological Systems*, 1974.
- [46] H. G. Kwatny and K. C. Kalnitsky, “On alternative methodologies for the design of robust linear multivariable regulators,” *IEEE Transactions on Automatic Control*, vol. AC-23, no. 5, pp. 930–933, 1978.
- [47] A. Isidori, *Nonlinear Control Systems*, 3rd ed. London: Springer-Verlag, 1995.
- [48] A. J. Krener and A. Isidori, “Linearization by output injection and nonlinear observers,” *Systems and Control Letters*, vol. 3, p. 4752, June 1983.
- [49] A. J. Krener and W. Respondek, “Nonlinear observers with linearizable error dynamics,” *SIAM J. Control and Optimization*, vol. 28, no. 2, p. 197216, 1985.
- [50] N. Kazantzis and C. Kravaris, “Nonlinear observer design using lyapunov’s auxiliary theorem,” *Systems and Control Letters*, vol. 34, pp. 241–247, 1998.
- [51] A. J. Krener and M. Xiao, “Nonlinear observer design in the siegal domain through coordinate changes,” in *NOLCOS*, St Petersburg, 2001.
- [52] V. I. Arnold, *Geometrical Methods in the Theory of Ordinary Differential Equations*. New York: Springer-Verlag, 1983.

- [53] A. J. Krener and M. Xiao, "Observers for linearly unobservable nonlinear systems," in *American Control Conference*, vol. 1. Anchorage, AK: IEEE, May 2002, pp. 110 – 115.
- [54] L. T. Nguyen, M. E. Ogburn, W. P. Gilbert, K. S. Kibler, P. W. Brown, and P. L. Deal, "Simulator study of stall/post stall characteristics of a fighter aircraft with relaxed longitudinal stability," NASA Langley Research Center, Technical Paper 1538, December 1979.
- [55] H. G. Kwatny, W. H. Bennett, and J. M. Berg, "Regulation of relaxed stability aircraft," *IEEE Transactions on Automatic Control*, vol. AC-36, no. 11, pp. 1325–1323, 1991.
- [56] P. J. Antsaklis and A. N. Michel, *Linear Systems*. New York: McGraw-Hill, April 1997.
- [57] E. W. Weisstein. "Newton's method." from mathworld - a wolfram web resource. [Online]. Available: <http://mathworld.wolfram.com/NewtonsMethod.html>
- [58] F. R. Garza and E. A. Morelli, "A collection of nonlinear aircraft simulations in matlab," NASA Langley Research Center, Technical Report NASA/TM 2003-212145, January 2003.
- [59] M. C. Fox and D. K. Forrest, "Supersonic aerodynamic characteristics of an F-16 derivative aircraft configuration," NASA, Tech. Rep. TP 3355, 1993.
- [60] H. G. Kwatny and G. L. Blankenship, "Symbolic construction of models for multibody dynamics," *IEEE Transactions on Robotics and Automation*, vol. 11, no. 2, pp. 271–281, April 1995.
- [61] G. L. Blankenship, R. Ghanadan, H. G. Kwatny, C. LaVigna, and V. Polyakov, "Tools for integrated modeling, design, and nonlinear control," *IEEE Control Systems*, vol. 15, no. 2, pp. 65–79, April 1995.
- [62] L. F. Falerio, "The application of eigenstructure assignment to the design of flight control systems," Ph.D. dissertation, Loughborough University, Leicestershire, U.K., November 1998.
- [63] E. G. Rynaski, "Flight control synthesis using robust output observers," in *Guidance and Control Conference*. San Diego: AIAA, 1982, pp. 825–831.
- [64] B. N. Pamadi, *Performance, Stability, Dynamics, and Control of Airplanes*, ser. AIAA Education Series. Reston: AIAA, 1998.
- [65] B. C. Moore, "On the flexibility offered by state feedback in multivariable systems beyond closed loop eigenvalue assignment," *IEEE Transactions on Automatic Control*, vol. 21, no. 5, pp. 689–692, 1976.

- [66] B. Etkin and L. D. Reid, *Dynamics of Flight, Stability and Control*. New York: John Wiley and Sons, 1996.
- [67] P. C. Hughes, *Spacecraft Attitude Dynamics*. New York: J. Wiley and Sons, 1986.
- [68] D. Hughes and M. A. Dornheim, "DHL/EAT crew lands A300 with no hydraulics after being hit by missile," *Aviation Week & Space Technology*, August 2003.
- [69] E. J. Davison and H. W. Smith, "Pole assignment in linear time-invariant multi-variable systems with constant disturbances," *Automatica*, vol. 7, pp. 489 – 498, 1971.
- [70] E. J. Davison, "Optimal control of linear time-invariant systems with polynomial-type measurable disturbances," *IEEE Proceedings*, vol. 119, pp. 605–611, 1972.
- [71] M. Calovic, "Power systems load and frequency control using an optimum linear regulator with integral feedback," in *5th World IFAC Congress*, 1972.
- [72] Voltage Stability Toolbox. [Online]. Available: http://power.ece.drexel.edu/index_files/vst.htm

Appendix A: The F-16's Equations

In chapter 4, the model of the F-16 was obtained as Poincaré's equations,

$$\dot{\mathbf{q}} = V(\mathbf{q})\mathbf{p}$$

$$M(\mathbf{q})\dot{\mathbf{p}} + C(\mathbf{p}, \mathbf{q})\mathbf{p} + Q(\mathbf{p}, \mathbf{q}, \mathbf{u}_o) = 0$$

where, $\mathbf{q} = [\phi, \theta, \psi, x, y, z]^T$, $\mathbf{p} = [p, q, r, u, v, w]^T$, and $\mathbf{u}_o = [T, \delta_{el}, \delta_{er}, \delta_a, \delta_r]^T$.

The matrices V, M, C, Q are given by

$$V(\mathbf{q}) = \begin{pmatrix} V_{11} & 0_{3 \times 3} \\ 0_{3 \times 3} & V_{22} \end{pmatrix}$$

with

$$V_{11} = \begin{pmatrix} 1 & \sin\phi \tan\theta & \cos\phi \tan\theta \\ 0 & \cos\phi & -\sin\phi \\ 0 & \sec\theta \sin\phi & \cos\phi \sec\theta \end{pmatrix}$$

$$V_{22} = \begin{pmatrix} \cos\psi \cos\theta & -\cos\phi \sin\psi + \cos\psi \sin\phi \sin\theta & \sin\phi \sin\psi + \cos\phi \cos\psi \sin\theta \\ \cos\theta \sin\psi & \cos\phi \cos\psi + \sin\phi \sin\psi \sin\theta & -\cos\psi \sin\phi + \cos\phi \sin\psi \sin\theta \\ -\sin\theta & \cos\theta \sin\phi & \cos\phi \cos\theta \end{pmatrix}$$

$$C(\mathbf{p}, \mathbf{q}) = \begin{pmatrix} C_{11} & C_{12} \\ 0_{3 \times 3} & C_{22} \end{pmatrix}$$

with

$$C_{11} = \begin{pmatrix} -982q & -55814r & 63100q \\ 982p + 9496r & 0 & -63100p - 982r \\ -9496q & 55814p & 982q \end{pmatrix}$$

$$C_{12} = \begin{pmatrix} 0 & -637.14w & 637.14v \\ 637.14w & 0 & -637.14u \\ -637.14v & 637.14u & 0 \end{pmatrix}$$

$$C_{22} = \begin{pmatrix} 0 & -637.14r & 637.14q \\ 637.14r & 0 & -637.14p \\ -637.14q & 637.14p & 0 \end{pmatrix}$$

$$M(\mathbf{q}) = \begin{pmatrix} M_{11} & 0_{3 \times 3} \\ 0_{3 \times 3} & M_{22} \end{pmatrix}$$

with

$$M_{11} = \begin{pmatrix} 9496 & 0 & -982 \\ 0 & 55814 & 0 \\ -982 & 0 & 63100 \end{pmatrix}$$

$$M_{22} = \begin{pmatrix} 637.14 & 0 & 0 \\ 0 & 637.14 & 0 \\ 0 & 0 & 637.14 \end{pmatrix}$$

and

$$Q(\mathbf{p}, \mathbf{q}, \mathbf{u}_o) = \begin{pmatrix} -L \\ -M - l_t T \\ -N \\ -T - X + 20471.4 \sin\theta \\ -Y - 20471.4 \cos\theta \sin\phi \\ -Z - 20471.4 \cos\phi \cos\theta \end{pmatrix}$$

The partitioning of the matrices is due to space limitations. The matrices correspond to flight conditions at sea level ($\rho = 0.0023769 \text{ slug}/ft^3$, $g = 32.1302 \text{ ft}/s^2$), with the center of gravity coinciding with the reference center of gravity location.

The flight path angle Γ and the heading Ψ are given by

$$\Gamma = \tan^{-1} \left[\frac{w \cos\phi \cos\theta + v \cos\theta \sin\phi - u \sin\theta}{u \cos\psi \cos\theta + w(\sin\phi \sin\psi + \cos\phi \cos\psi \sin\theta) + v(-\cos\phi \sin\psi + \cos\psi \sin\phi \sin\theta)} \right]$$

$$\Psi = \sin^{-1} \left[\frac{u \cos\theta \sin\psi + w(-\cos\psi \sin\phi + \cos\phi \sin\psi \sin\theta) + v(\cos\phi \cos\psi + \sin\phi \sin\psi \sin\theta)}{\sqrt{u^2 + v^2 + w^2}} \right]$$

In level flight, a positive Γ signifies that the aircraft is losing altitude, and a positive Ψ signifies that the aircraft is heading towards the right. The expressions are obtained from the velocity components of the aircraft in the earth fixed frame.

Appendix B: List of Symbols

The dissertation has employed numerous symbols and the list in this appendix is not exhaustive. All the symbols pertaining to the aircraft have been collated below. Those used in explaining the theory have been omitted, as they have been explained in their local contexts. Care has been taken to ensure that there are no conflicts.

α	angle of attack, <i>rad</i>
β	side slip angle, <i>rad</i>
δ_a	aileron control surface deflection, <i>rad</i>
δ_{ac}	aileron pilot input, <i>rad</i>
δ_{el}	left elevator control surface deflection, <i>rad</i>
δ_{elc}	left elevator pilot input, <i>rad</i>
δ_{er}	right elevator control surface deflection, <i>rad</i>
δ_{erc}	right elevator pilot input, <i>rad</i>
δ_r	rudder control surface deflection, <i>rad</i>
δ_{rc}	rudder pilot input, <i>rad</i>
ϕ	Euler roll angle, <i>rad</i>
Γ	flight path angle, <i>rad</i>
θ	Euler pitch angle, <i>rad</i>
μ	bifurcation parameter
ρ	atmospheric density, <i>slug/ft³</i>
ψ	Euler yaw angle, <i>rad</i>
Ψ	heading, <i>rad</i>
ω	angular velocity of the aircraft in the positive Z direction, <i>rad/s</i>
b	wing span, <i>ft</i>
\bar{c}	mean aerodynamic chord, <i>ft</i>

C_l	non-dimensional rolling moment coefficient
C_m	non-dimensional pitching moment coefficient
C_n	non-dimensional rolling moment coefficient
C_x	non-dimensional X body-axis force coefficient
C_y	non-dimensional Y body-axis force coefficient
C_z	non-dimensional Z body-axis force coefficient
g	earth gravitational acceleration, ft/s^2
I_x	X body-axis moment of inertia, $slug - ft^2$
I_{xz}	X-Z body-axis product of inertia, $slug - ft^2$
I_y	Y body-axis moment of inertia, $slug - ft^2$
I_z	Z body-axis moment of inertia, $slug - ft^2$
l_a	horizontal distance from the aileron center of mass location to the center of gravity, ft
l_e	horizontal distance from the elevator center of mass location to the center of gravity, ft
l_t	vertical distance from the engine thrust location to the center of gravity, ft
m	aircraft mass, $slugs$
p	X body-axis angular velocity component, rad/s
\mathbf{p}	joint velocity vector ($= [p, q, r, u, v, w]^T$)
q	Y body-axis angular velocity component, rad/s
\mathbf{q}	generalized coordinated vector ($= [\phi, \theta, \psi, x, y, z]^T$)
r	Z body-axis angular velocity component, rad/s
R	radius of the turn, ft
S	wing reference area, ft^2
T	engine thrust, lb
T_c	commanded thrust, lb
u	X body-axis translational velocity component, ft/s

u	set of healthy inputs of the impaired system
u_o	set of original inputs
v	Y body-axis translational velocity component, <i>ft/s</i>
v_o	set of original pilot command inputs
V	airspeed, <i>ft/s</i>
w	Z body-axis translational velocity component, <i>ft/s</i>
x	X body-axis position, <i>ft</i>
x	state vector
y	Y body-axis position, <i>ft</i>
y	measurements (= h (x , μ))
z	Z body-axis position, <i>ft</i>
z	regulated variables (= r (x , μ))
L	coordinated turn condition C2

Vita

SUBA THOMAS

EDUCATION

Doctor of Philosophy, Mechanical Engineering, Drexel University, December 2004

Master of Science, Mechanical Engineering, Drexel University, June 2003

Bachelor of Technology, Mechanical Engineering, Indian Institute of Technology, Guwahati, India, April 1999

RESEARCH INTERESTS

Flight safety, Linear and nonlinear control, Flight mechanics, Bifurcations, Dynamical systems, Robotics, Applied mathematics.

RESEARCH EXPERIENCE

Research Assistant, September 2000 - December 2004

Systems and Controls Group, Department of Mechanical Engineering and Mechanics, Drexel University.

Undergraduate Project Research, July 1998 - May 1999

Mechanical Engineering Department, Indian Institute of Technology, Guwahati, India.

TEACHING EXPERIENCE

Adjunct Instructor, January 1st 2004 - March 31st 2004

Goodwin College of Professional Studies, Drexel University

Course: Performance Enhancement of Dynamical Systems

Teaching Assistant, September 2000 - December 2004

Department of Mechanical Engineering and Mechanics, Drexel University

Teaching assistant for several courses, namely, Introduction to Controls, Performance Enhancement of Dynamical Systems, Mechanical Engineering and Mechanics Laboratory I & II, Dynamic Systems Laboratory

MAJOR PUBLICATIONS

S. Thomas, H. G. Kwatny, and B. C. Chang, "Nonlinear reconfiguration for asymmetric failures in a six degree-of-freedom F-16," in *American Control Conference*. Boston, MA: IEEE, June/July 2004, pp. 1823 - 1829.

S. Thomas, H. G. Kwatny, and B. C. Chang, "Lie transform construction of exponential normal form observers," in *4th IFAC Symposium on Robust Control Design*, vol. WM01-2, Milano, Italy, June 2003.

